EFFECTS OF SOME TRANSITION METAL SALTS ON THE SYNTHESIS OF MESOPOROUS SILICA

A THESIS

SUBMITTED TO THE DEPARTMENT OF CHEMISTRY

AND THE INSTITUTE OF ENGINEERING AND SCIENCES

OF BILKENT UNIVERSITY

IN PARTIAL FULFILLMENT OF THE REQUIREMENTS

FOR THE DEGREE OF

MASTER OF SCIENCE

By

AHMET FAİK DEMİRÖRS

July 2005

I certify that I have read this thesis and in my opinion it is fully adequate, in scope and in quality, as a thesis of the degree of Master of Science

_____

Assoc. Prof. Dr. Ömer DAĞ

I certify that I have read this thesis and in my opinion it is fully adequate, in scope and in quality, as a thesis of the degree of Master of Science

_____

Prof. Dr. Şefik SÜZER

I certify that I have read this thesis and in my opinion it is fully adequate, in scope and in quality, as a thesis of the degree of Master of Science

_____

Assoc. Prof. Dr. Margarita KANTCHEVA

I certify that I have read this thesis and in my opinion it is fully adequate, in scope and in quality, as a thesis of the degree of Master of Science

_____

Asst. Prof. Ayşen YILMAZ

I certify that I have read this thesis and in my opinion it is fully adequate, in scope and in quality, as a thesis of the degree of Master of Science

_____

Asst. Prof. Dönüş TUNCEL

Approved for the Institute of Engineering and Sciences

_____

Prof. Dr. Mehmet BARAY

Director of Institute of Engineering and Sciences

ABSTRACT

EFFECTS OF SOME TRANSITION METAL SALTS ON THE SYNTHESIS OF MESOPOROUS SILICA

AHMET FAİK DEMİRÖRS

M.S. in Chemistry
Supervisor: Assoc. Prof. Dr. Ömer DAĞ
July 2005

True Liquid Crystal (TLC) templating approach has been extensively used to produce mesostructured silica films and monoliths. It is known that nonionic surfactants (C_nEO_m) are suitable templates for this purpose. In this work, we have introduced various transition metal salts into mesostructured silica materials through TLC approach. The work has two aims; one is to introduce large quantities of metal ions into the silica channels and second is to study the effect of the metal cation and the counter anion to the structure of the mesophase. Current understanding about the solubility of non-ionic surfactants in aqueous media is that, the solubility decreases upon dehydration. Salting-out ions (according to the Hofmeister series) that cause dehydration will decrease the solubility of surfactants. Due to the solubility change the concentration and the type of salt will affect the structure of the LC template and as a result the mesostructured silica. The total charge (ionic strength) of the system has also a principal role on the structure of the mesophase. High ionic strength will decrease the solubility and influence the assembly of the surfactant molecules into LC mesophases. Although an alkaline metal perchlorate anion makes the surfactant more soluble than nitrate anion in a water:surfactant system, the transition metal perchlorates are harder to dissolve compared to nitrate salts in a salt:surfactant system. This fact is due to the coordination of the nitrate ion to the metal cation. Upon coordination the ionic strength decreases and this

increases the solubility of transition metal nitrates. However the perchloriate ion does not coordinate to a transition metal cation.

In this thesis, the structural changes in the transition metal salt (TMS):C_nEO_m:silica systems were investigated using diffraction (XRD), microscopy (POM) and spectroscopy (FTIR and micro-Raman) techniques. The $[Co(H_2O)_6](NO_3)_2$ salt silica systems are hexagonal up to 1.2 salt/$C_{12}EO_{10}$ mole ratio and over this concentration the mesophase is cubic. Usage of a surfactant with longer alkyl chain ($C_{18}EO_{10}$) increases this phase change over 2.0 mole ratio. However, the $[Co(H_2O)_6](ClO_4)_2$ salt:silica systems have cubic structures at very low salt/$C_{12}EO_{10}$ mole ratios (above 0.2 mole ratio), whereas they are hexagonal when no perchlorate salt is added.

It has been demonstrated that the LC mesophases of the TMS:Pluronic(triblock copolymer surfactant family) systems exist with a very rich structural chemistry. The TMS:Pluronic systems have lamella, hexagonal, various types of cubic and a tetragonal mesophases. The TMS:P65 and TMS:P123 systems are ordered and well structured. The hexagonal mesophase in the $[Zn(H_2O)_6](NO_3)_2$:P65 systems and the tetragonal and cubic LC mesophases in the $[Zn(H_2O)_6](NO_3)_2$:P123 systems were identified. The LC mesophases of TMS:Pluronics can be used as templating agents for the synthesis of stable mesostructured silica. The lamella mesostructured silica obtained using $[Zn(H_2O)_6](NO_3)_2$:P123 LC mesophase transforms to 2D hexagonal structure upon calcinations (goes from layered structure to long channel hexagonal tubes).

Keywords: Lyotropic liquid crystals, mesophases, transition metal aqua complexes, non-ionic surfactants, Pluronics, mesoporous materials, Hofmeister effect.

ÖZET

BAZI GEÇİŞ METALİ TUZLARININ MEZO-YAPILI SİLİKA SENTEZİ ÜZERİNE ETKİLERİ

AHMET FAİK DEMİRÖRS

Kimya Bölümü Yüksek Lisans Tezi

Tez Yöneticisi: Doç. Dr. Ömer DAĞ

Temmuz 2005

Sıvı kristal kalıplama (SKK) yöntemi mezoyapılı silika film ve monolit sentezinde sıkça kullanılmaktadır. İyonik olmayan yüzey-aktiflerin(C_nEO_m) bu amaçla kullanılmaya müsait kalıplar olduğu bilinmektedir. Bu çalışmamızda SKK yöntemi ile çeşitli geçiş metali tuzlarının silika materyal yapıya katılımını sağladık. Bu çalışmanın iki amacı vardır, birisi mezoyapılı silika içerisine büyük miktarlarda metal iyonu hapsetmek, ikincisi ise geçiş metal katyon ve anyonlarının mezoyapıya etkisini araştırmaktır. İyonik olmayan yüzey-aktiflerin sulu çözeltilerdeki çözünürlüğünün yüzey-aktifin sudan arındırılmasıyla azaldığı düşünülmektedir. Hofmeister serisine göre tuzlanmayı artırıcı (salting-out) olarak sınıflandırılan anyonlar, yüzey-aktiflerinin kurumasına (dehydration) neden olur ve yüzeyaktifin çözünürlüğünü azaltırlar. Çözünürlükteki değişiklikler nedeniyle geçiş metali tuzlarının derişimi ve çeşidi SK kalıbın yapısını ve sonuç olarak da mezoyapılı-silikanın yapısında değişikliklere neden olmaktadır. Sistemdeki tuzlardan kaynaklanan toplam elektrik yükünün de (ionik direncin) mezofazın yapısında önemli rolü vardır. Yüksek iyonik direnç, yüzey-aktifin çözünürlüğünü azaltır ve yüzey-aktiflerin kendilerini SK mezofaza organize etmelerini etkiler. Su:yüzey-aktif sistemlerinde, alkali metal perklorat anyonunun yüzey-aktiflerin çözünürlüğünü nitratlara göre artırıyor olmasına rağmen, geçiş metal perklorat tuzlarının nitrat tuzlarına göre daha zor çözülür. Bu durum nitrat iyonunun metal katyonuna koordinasyonun bir sonucudur.

Koordinasyon sonucunda sistemin toplam elektrik yükü azalır ve böylece geçiş metali tuzunun çözünürlüğü artar. Halbuki perklorat iyonu metal katyonuna koordine olma özelliği yoktur.

Bu tezde geçiş metali tuzları (GMT):C_nEO_m:silika sistemindeki yapısal değişiklikler kırınım (XRD), mikroskopi (POM) ve spektroskopi (FT-IR ve mikro-Raman) teknikleri ile tetkik edilmiştir. $[Co(H_2O)_6](NO_3)_2$:silika sistemleri 1,2 tuz/$C_{12}EO_{10}$ mol oranına kadar hegzagonal yapıda iken, bu derişimin üzerinde mezoyapı kübiktir. Daha uzun alkil zincirli yüzey-aktiflerin kullanımı bu faz değişimini 2,0 mol oranının üzerine taşır. Perklorat tuzu eklenmemiş sistemler hegzagonal yapıda olmalarına rağmen. $[Co(H_2O)_6](ClO_4)_2$:silika sistemi çok düşük tuz/$C_{12}EO_{10}$ mol oranlarında (0,2 mol oranı ve üzerinde) dahi kubik yapıdadır.

GMT:Pluronik sıvı kristal mezofazlarının çok zengin yapısal kimyaya sahip olduğu gösterilmiştir. GMT:Pluronik sistemler lamella, hegzagonal, değişik kübik ve tetragonal yapılara sahiptir. GMT:P65 ve GMT:P123 sistemleri düzenli ve oldukça güzel yapılıdır. $[Zn(H_2O)_6](NO_3)_2$:P65 sistemlerinde hegzagonal, $[Zn(H_2O)_6](NO_3)_2$:P123 sistemlerinde tetragonal ve kübik SK mezofazlar tayin edilmiştir. GMT:Pluronik SK mezofazları, mezoyapılı silika sentezinde kalıp olarak kullanıbilinir. Tuz:Pluronik kullanılarak elde edilen mezoyapılı silika filimler ve/veya monolitler genelde lamela yapıdadır. $[Zn(H_2O)_6](NO_3)_2$:P123 SK mezofazı kalıp olarak kullnıldığında lamela mezoyapılı olmasına rağmen, yüksek sıcaklıklarda yakılmasıyla 2D hegzagonal yapıya dönüşür (katmanlı yapıdan, uzun tünelli hegzagonal tüblere geçer).

Anahtar kelimeler: Liyotropik sıvı kristaller, mezofazlar, geçiş metal sulu kompleksleri, iyonik olamayan yüzey-aktifler, Pluronikler, mezogözenekli malzemeler, Hofmeister etkisi.

ACKNOWLEDGEMENT

I would like to express my deep gratitude to Assoc. Prof. Dr. Ömer DAĞ for his encouragement and supervision throughout my studies.

I am very thankful to Nesibe CINDIR, Olga SAMARSKAYA, Yaşar AKDOĞAN, Oğuzhan ÇELEBİ, Anıl AĞIRAL, Korcan DEMİROK, Mehtap KÜYÜKOĞLU, and my home mates Mesut ŞAHİN, Süleyman TEK , Hüseyin ACAN, Aşkın KOCABAŞ and all present and former members of Bilkent University Chemistry Department for their kind helps and supports during all my study.

I wish to thank to Bekir ESER for his help in preparation of some of the samples.

TABLE OF CONTENTS

LIST OF TABLES

LIST OF FIGURES

1. INTRODUCTION

1.1 Mesoporous Inorganic Materials

According to IUPAC definition Inorganic solids with pore diameter sizes in the range of 20 to 500 Å are called mesoporous materials. Examples of mesoporous materials such as M41S family (Family of well defined mesostructures synthesized by the Mobil Research group), aerogels (dry gels), and pillared layered structures are listed in Table 1.1 [1]

Table 1.1 Nomenclature of Porous Inorganic Materials according to their pore sizes.

Pore Size	Definition	Example	Actual size range
Macroporous	> 500 Å	Glasses	> 500 Å
Mesoporous	20-500 Å	Aerogels	> 100 Å
		Pillared layered clays	10 Å, 100 Å
		M41S	16-100 Å
Microporous	< 20 Å	Zeolites, zeotypes	< 14.2 Å
		Activated carbon	6 Å

Mesoporous materials are used extensively as heterogeneous catalysts and adsorption media along with microporous materials. The function of these materials, in their microstructures is to permit molecules access to large internal surfaces and cavities.

Large internal surfaces and cavities are the important keywords for catalytic activity and adsorptive capacity. A major subclass of the microporous materials is molecular sieves. The most known example for molecular sieves is zeolites. Zeolites are aluminosilicates which have micropores (< 14.2 Å in pore size) that are regular arrays of uniformly-sized channels. Zeolites are crystalline solids and they exhibit an extremely narrow pore size distribution. Due to these properties zeolites are very important in size selective catalysis [2], ion exchange [3], desiccation and sorption [3] reactions. Zeolites are also used as nanoreactors for host-guest chemistry [4].

Typical mesoporous materials known are amorphous or paracrystalline solids, such as silicas[5] or transitional aluminas[6] or modified layered materials such as pillared clays and silicates[7-11]. These materials generally have irregularly spaced pores, broadly distributed in size [8]. Due to this fact there has been a significant effort to synthesize materials within the mesoporous range with well defined properties and a regular structure. Before the pioneering work of Mobil researchers [12], the investigations of mesoporous materials were not that significant because they were not actually in mesoporous range. Cacoxenite, a natural ferroaluminophosphate with 14 Å channels nearly in mesoporous size range was characterized [13] and $A1P0_4$-8,[14] ,VPI-5,[15]: and cloverite [16] which have pore diameters within the 8-13 Å range were synthesized. Common property for many of these materials is their lack of thermal or hydrothermal stability. In 1990`s the researchers at Mobil-Oil-Corporation used long chained alkyl-ammonium ions $[CH_3(CH_2)_nN(CH_3)_3^+]$ in an attempt to increase the pore size of zeolites [12]. Note that he amphiphilic molecules with a hydrocarbon chain length of n less than eight are normally too small to self assemble (and for the supramolecular templating) in an aqueous solution and would be expected to behave as molecular templating agents (as in zeolite synthesis). Here the deriving force for the self-assembly is the tendency of organic tails to stay together in an aqua solution.

Navrotsky et al [17] have found that MCM-41, which is the mesoporous silica with 2D hexagonal structure and zeolites are thermodynamically only slightly less stable than the stable phase of silica, α-quartz. This means that the synthesis of mesoporous silica

with desired porosity and size is thermodynamically available if the appropriate kinetic pathway is used.

For the first time the mobil researchers [12] achieved to synthesize mesoporous molecular sieves with regular, well-defined channels in a variety of pore sizes, ranging from 15 to 120 Å (designated as M41S). Especially one of the members of the family, MCM-41, is extensively investigated. It has a hexagonal arrangement of uniform mesopores with well defined, tunable pore sizes. These materials with larger pore sizes have high surface areas above 700 m^2/g and hydrocarbon sorption capacities of 0.7 cc/g and greater. The Mobil researchers proposed the liquid crystal templating mechanism (LCT) for the M41S family.The liquid crystal structures formed by the surfactant molecules serve as organic templates for assembly of the mesostructured silica. The MCM-41, 2D hexagonal mesoporous phase is the first reported example of mesoporous silica materials [12]. The surfactant templating has also been applied to synthesize materials in cubic, MCM-48 and lamella, MCM-50 forms additional to hexagonal, MCM-41 silica materials, see Figure 1.1

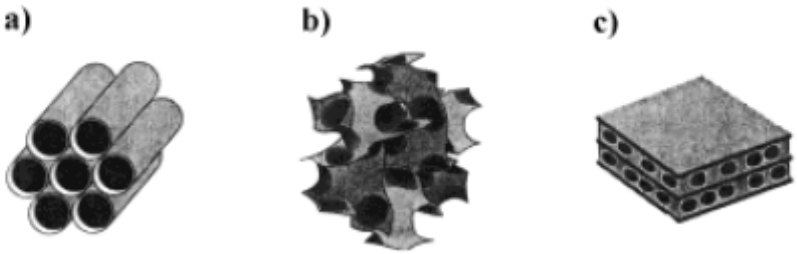

Figure 1.1 Illustrations of mesoporous M41S materials: a) MCM-41, b) MCM-48, and c) MCM-50 [18].

In general, the M41S family of mesoporous molecular sieves was synthesized by combining appropriate amounts of a silica source (e.g. tetraethylorthosilicate (TEOS), fumed silica, sodium silicate), an alkyltrimethylammonium halide surfactant (e.g. cetyltrimethylammonium bromide (CTAB)), a base (e.g. sodium hydroxide or tetramethylammonium hydroxide (TMAOH)), and water. This mixture,

aged at temperatures usually over 100° C for 24 to 144 hours, resulted in a solid precipitate. The organic-inorganic mesostructured product was then filtered, and washed with water, and air-dried. The product was calcined at about 500 °C under a flowing gas. At this temperature the surfactant burns off and the mesoporous inorganic material is left. Note that the templates used in these approachs are ionic alkyltrimethylammonium halide surfactants with a long alkyl chain. It is known that the small alkyl chain quaternary directing agents were used for zeolite synthesis, see Figure 1.2. The benefit of the ionic alkyltrimethylammonium halide surfactant with a long alkyl chain is that they assemble into micelle structures whereas the small alkyl chain quaternary agents were templating the zeolites (alone) in the molecular level, see Figure 1.2. The key feature of the MCM family is the ability to modify the structure and the ability to control the pore size (20-100 Å) by changing the synthesis conditions (e.g. surfactant chain length, addition of auxiliary organics)

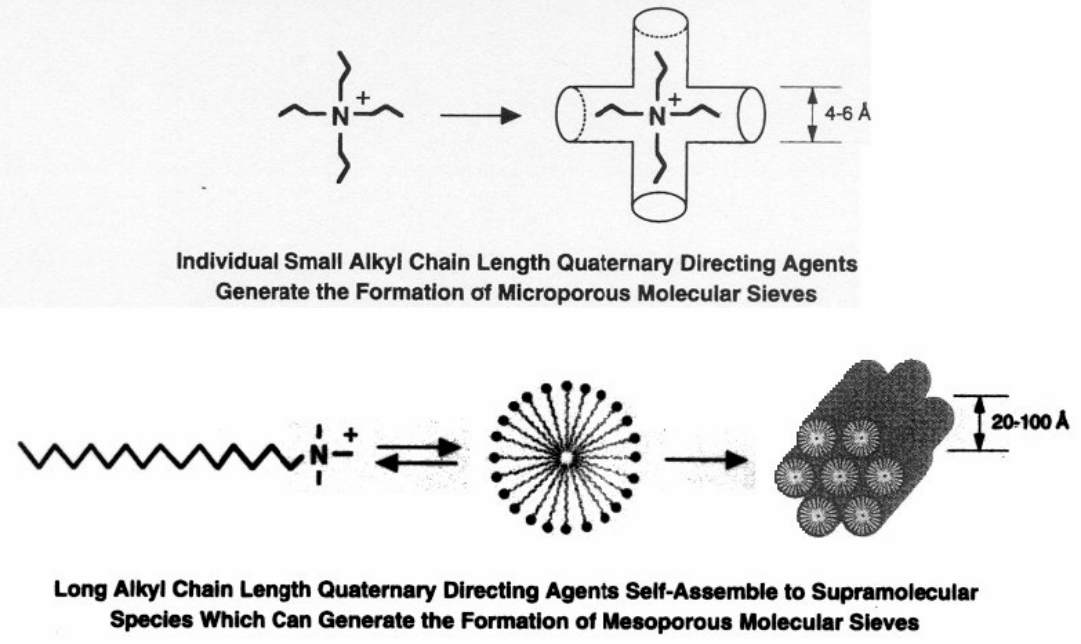

Figure 1.2. Formation of microporous and mesoporous molecular sieves by using short and long alkyl chained quaternary ammonium salts [19].

The Mobil researchers proposed a liquid crystal templating (LCT) mechanism for the M41S family, particularly MCM-41, because of the similarity between the liquid crystalline surfactant assemblies and M41S family. They proposed two mechanistic pathways for the 2D hexagonal structured MCM-41 [12, 20]. (Scheme 1.1):

1) The hexagonal lyotropic liquid crystalline (LC) phase is formed first and then the inorganic precursor species deposit on the micellar rods of the LC phase.

2) The inorganics mediated, in a way, the ordering of the surfactants into the hexagonal arrangement. The surfactants were not ordered but the silica species organize the structure formation.

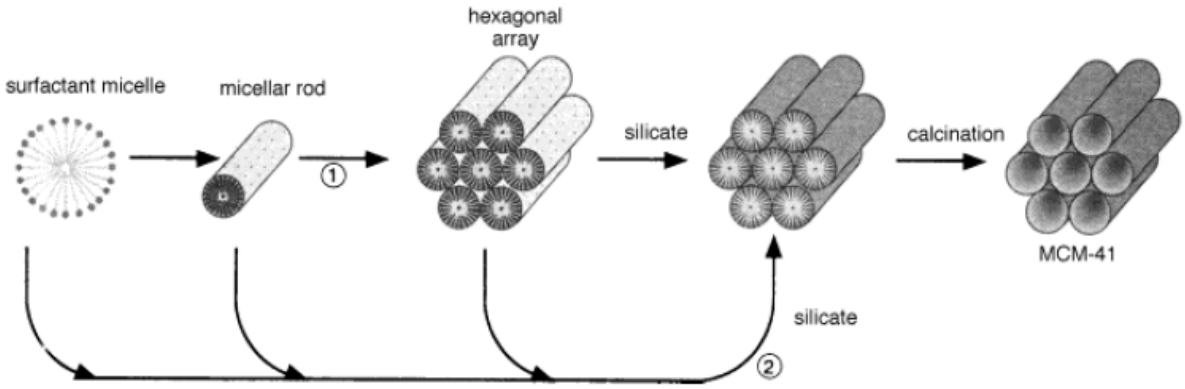

Scheme 1.1. Two possible pathways for LCT [20].

In both cases the positively charged ammonium head groups of the surfactants interact with the inorganic components that are negatively charged at the high pH values used and pack into a solid framework. The silica species surrounds the hexagonally arranged surfactant micellar rods. It is now a common consensus that pathway 1 is unlikely, because the surfactant concentrations used are much below the critical micelle concentration (CMC) necessary for hexagonal LC formation [21]. The second mechanistic pathway of LCT was assumed as a cooperative self-assembly of the ionic ammonium surfactant and the silicate precursor species below the CMC.

Later a generalized liquid crystalline templating mechanism [22] was proposed based on electrostatic interaction of the inorganic precursor (I) and the surfactant head group (S). In this model, the synthesis of MCM type mesoporous materials was based on the aggregation of cationic surfactant (S^+) and anionic inorganic species (I^-). However various types of pathways such as (S^-I^+), ($S^+X^-I^+$) X= Cl^-, Br^- or ($S^-M^+I^-$) M= Na^+, K^+ were used to synthesize mesoporous materials [22], see Figure 1.3.

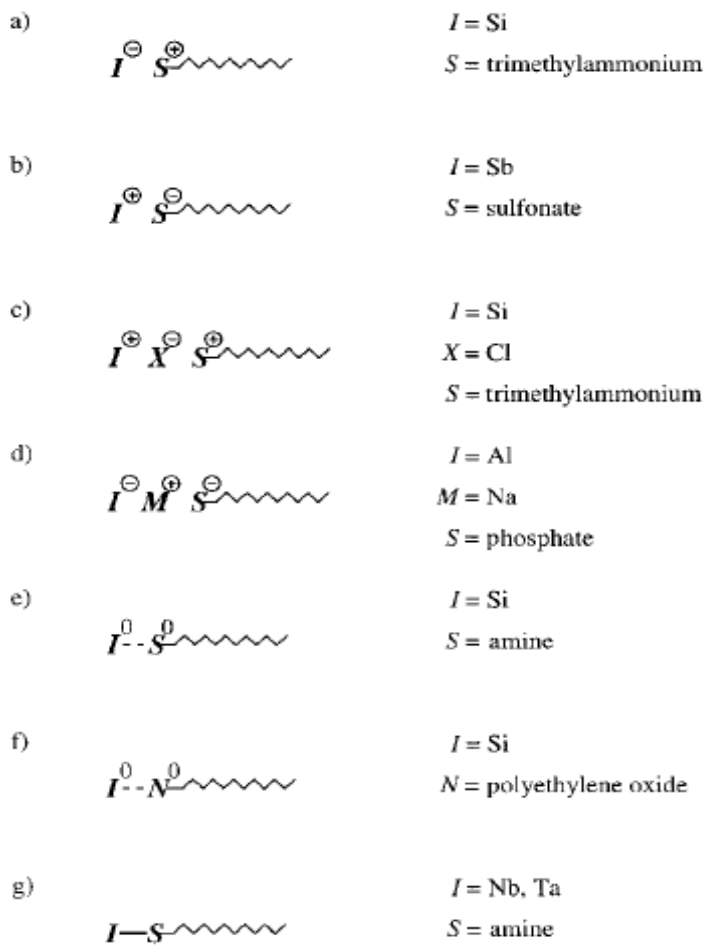

Figure 1.3. Schematic representation of the various types of inorganic-surfactant head group interactions: electrostatic: a) S^+I^-, b) S^-I^+, c) $S^+X^-I^+$, and d) $S^-M^+I^-$; hydrogen bonding: e) S°I° and f) N°I°; and covalent bonding: g) S-I. [18]

In acidic media, pH~2 the silicate species become cationic (I^+) but still cationic surfactant (S^+) can be used to synthesize mesoporous materials by $S^+X^-I^+$ system [22, 23].

Here counter ion X^- behaves as a shielding agent between the S^+ and I^+. The materials synthesized by this approach are known as "acid prepared mesostructures" (APM) or SBA [18,22].

To predict the phase of a given LC system as a first approximation of the mesophase of the silica, two parameters were considered to be important for the two synthesis routes of the synthesis of silicate mesoporous molecular sieves. For the basic route (S^+I^-) used to synthesize the M41S family, made up of three well defined mesostructures: MCM-41, MCM-48, and MCM-50, the key synthesis parameter that determined the mesophase was surfactant/silicon molar ratio. The surfactant /silicon molar ratio as a prediction parameter was first suggested by Vartuli et al [24], see Table 1.2. At ratios below 1 the hexagonal phase MCM-41 is observed and between 1 and 1.5 cubic phase, MCM-48 is observed and at higher ratios lamellar phase, MCM-50 is observed.

Name	Space group&Mesophase	Parameter
MCM-41[1, 24]	hexagonal, p6m	[surfactant]/[Si]<1
MCM-48[1, 24]	cubic, $Ia3^-d$	[surfactant]/[Si] =1-1.5
MCM-50[1, 25]	lamellar, p2	[surfactant]/[Si] =1.2-2
SBA-1[26, 27]	cubic, $Pm3^-n$	$g=1/3$[a]
SBA-2[28]	3D hexagonal, $P6_3/mmc$	$g<1/3$[a]
SBA-3[26]	2D hexagonal, p6m	$g=1/2$[a]
	Lamellar	g=1

[a] $g= V/a_0 l$.

Table 1.2. Mesophases of silicate molecular sieves and the synthesis parameters [18].

In the acidic route ($S^+X^-I^+$), used to synthesize the cubic SBA-1, 3D hexagonal SBA-2 and 2D hexagonal SBA-3, the key synthetic parameter to predict the mesophase was the packing parameter. The packing parameter is related to the overall volume, V of

the surfactant, effective head group area, a_o, and surfactant chain length, l. The packing parameter g was defined by Huo et al [28] as $g = V/ a_o.l$. When the packing parameter g is 1/3 the cubic SBA-1 is observed and over this value the structure tends to be 3D hexagonal SBA-2. At higher g levels, when g is equal to 1/2, the 2D hexagonal structured SBA-3 is observed and when g is equal to 1 the observed mesophase becomes lamellar, Table 1.2. For the acidic preparation route, there is a tendency from cubic structure to hexagonal and lastly to lamellar structure as the g parameter increases.

Due to the different precipitation conditions and charge balance requirements, the acid-derived materials (SBAs) have thicker pore walls and a framework charge different from the base-derived mesoporous materials. For instance, the overall framework charge of SBA-3 (acidic condition)was slightly positive whereas the framework of MCM-41(basic condition) was negative. One important thing that was observed for the SBA materials was that the space group of SBA-2 is $P6_3/mmc$. Its structure is hexagonal close-packed (hcp) array of spheres (known as 3D hexagonal); whereas this structure is rarely found in the traditional LC systems.

Stucky and his group [29] introduced a family of highly ordered mesoporous silica structures by using commercially available nonionic alkyl poly(ethylene oxide) oligomeric surfactants ($C_nH_{2n+1}(OCH_2CH_2)_mOH$) and Pluronics [triblock poly(ethylene oxide)-poly(propylene oxide)-poly(ethylene oxide) (PEO-PPO-PEO) copolymers] in acidic media.They achieved to synthesize mesostructured materials in 20-300 Å range. Stucky`s group found that the nonionic oligomeric surfactants frequently form cubic or 3D hexagonal mesoporous silica structures, whereas the nonionic triblock copolymers tend to form hexagonal (*p6mm*) mesoporous silica structures. They also found out that the surfactants with short EO segments tend to form lamellar mesostructured silica at room temperature.The EO/PO ratio of the copolymers is an important parameter and lowering this ratio of the triblock copolymer advances the formation of lamellar mesostructured silica, while increasing this ratio promotes cubic mesostructured silica formation [29]. The calcined ordered mesoporous silicas produced by this path are thermally stable in

boiling water for 48 h. Note also that the MCMs lack this property. This higher stability is most probably due to the thicker walls of these materials (31-64 Å), compared to the MCM-41 (10-15 Å).

In this process, that takes place in acidic media the non-ionic surfactant molecules interact with the proton (H^+) and this promotes the hydrogen bonding interaction between the inorganic precursors and the surfactants by the shielding of the X^- anions. Briefly, the assembly of the structure takes place by a $(S^0\ H^+)(X^-I^+)$ pathway. SBA-15, one of the best of this SBA family, is prepared by either Pluronic P123 ($EO_{20}PPO_{30}EO_{20}$) or $C_{16}EO_{10}$ and has a 2D hexagonal structure (p6mm). SBA-15 has very promising properties compared to MCM-41, it has pores sizes up to 300 Å (120 Å for MCM-41) and has thicker walls than MCM-41, that are up to 64 Å and pore volumes up to 2.2 cm^3/g, and BET surface areas up to 910 m^2/g [18]. Table 1.3 gives shows the types of mesoporous materials and gives information about their properties (mesophase and d -spacing) and from which surfactant they are produced.

Table 1.3. General properties of SBA and MCM type mesoporous silicas [18].

Name of the Material	Surfactant(s)	Mesophase	d [*] (Å)
MCM-41	$[CH_3(CH_2)_nN(CH3)_3^+]Br^-$	2D hexagonal	15-120
MCM-48	$[CH_3(CH_2)_nN(CH3)_3^+]Br^-$	cubic	80.33-92
MCM-50	$[CH_3(CH_2)_nN(CH3)_3^+]Br^-$	lamellar	36.2
SBA-1	$[CH_3(CH_2)_nN(CH3)_3^+]Br^-$	cubic	
SBA-2	$[CH_3(CH_2)_nN(CH3)_3^+]Br^-$	3D hexagonal	40.8-57.3
SBA-3	$[CH_3(CH_2)_nN(CH3)_3^+]Br^-$	2D hexagonal	
SBA-11	$C_{16}EO_{10}$	*Pm*3h*m* cubic	56.6
SBA-12	$C_{18}EO_{10}$	3D hexagonal (*P*6$_3$/*mmc*)	49-77
SBA-14	$C_{12}EO_4$	3D cubic	45.3
SBA-15	P123,$C_{16}EO_{10}$	2D hexagonal(p6mm)	103-108,64.1
SBA-16	F127 $EO_{106}PO_{70}EO_{106}$	cubic (*Im*3h*m*)	124

[*] d is the d(100) value of the material.

1.2. True Liquid Crystalline Templating (TLCT)

The lyotropic liquid crystalline phase of a polyethylene oxide surfactant was first used by Attard et al. for the synthesis of monolithic mesoporous silicates [30] which is basicly a one piece bulk material without cracks. Tetramethylorthosilicate (TMOS) was directly added into the previously existing LC mesophase to produce a hexagonal mesostructured silica; Attard et al. also showed that the cubic and lamellar phases could be synthesized by using various tail chain length. This method was considered as a TLCT path, which also showed the possibility of the pathway 1, proposed LCT mechanism for MCM-41 (Scheme 1.1). In this method the existence of the LC mesophase is more important than the interaction of the silica precursors and the surfactant to cooperate and form the mesophase.

Göltner and co-workers [31] showed that nonionic amphiphilic diblock copolymers with a polyethylene oxide head group and a polystyrene tail group could also be used as templates to create crack-free mesoporous silica monoliths. Amphiphilic diblock copolymers (ABCs) are known to form micelles when mixed with water or other suitable solvents [32]. Additionally they form lyotropic liquid crystalline phases at higher polymer concentrations. Göltner and Antonietti et al [31] also demonstrated that ABC templates show a number of advantages. Firstly, polymer chemistry is very rich and the polymeric amphiphile can be synthesized or modified to the desired product. Thus, a rich family of surfactants can be available for mesoporous material preparation. Secondly, a larger size of the templating is achieved, which determines the pore diameter (as an important property) and the wall thickness (for the stability) of the mesoporous materials.

Another alternative approach for the synthesis of mesoporous molecular sieves was proposed by Pinnavaia et al [33]. They have used primary amine nonionic surfactants for the synthesis. The primary amine nonionic surfactants at low concentration [33] yielded similar materials to M41S. Note that the oligo(ethylene oxide) surfactants [34] forms less regular mesostructures than M41S (this was proven by the presence of a single X-ray diffraction peak at low angles) but they still exhibite high specific surface area and narrow pore size distributions. In the category of nonionic surfactants both primary amines and oligo(ethylene oxide), C_nEO_m surfactants were used to mediate the formation of mesoporous materials[33,34]. However natural alkyl amines are costly and toxic therefore they are not suitable for large-scale production of mesoporous materials, whereas the C_nEO_m type surfactants are biodegradable and offer synthetic flexibility. Additionally with the C_nEO_m type surfactants, it is possible to prepare mesoporous transition metal oxides that are not accessible by electrostatic templating method. The metal alkoxides that readily hydrolyze to the corresponding metal oxide can also be templated by C_nEO_m type nonionic surfactants [34].

1.3. Metal Containing Liquid Crystalline Mesophases

Solids, liquids and gasses are the three most known forms of matter. In the solid state, the forces between the molecules are strong and the molecules have firm arrangement, therefore each molecule occupies a certain place which means that they have a positional order. The matter can be either amorphous or crystalline in solid state. In crystalline case, molecules are also oriented in a specific direction; it means that they have orientational order additional to the positional order. In this situation highly ordered arrangement causes additive attractive forces. In liquid state, the intermolecular forces are less than the solid state and molecules have neither positional order nor orientational order. The molecules in the gas phase have even less intermolecular forces so they also do not have positional and orientational order.

The liquid crystalline (LC) state is the state of the matter which has the properties of both liquid and solid states. In LC phase, the molecules or aggregates have some orientational order but no positional order in all directions [35]. The orientational order of the molecules is represented in Figure 1.4 [35]. In the LC phases, the molecules have tendency to stay in some direction rather than others. This phase can be distinguished from isotropic liquid phase by its opaque appearance and solid phase by its flow properties. There are two main liquid crystalline phases in terms of order. One is Nematic, which has orientational order and no positional order. Other is Smectic, which has orientational order and positional order only in one dimension, is formed in layered structures.

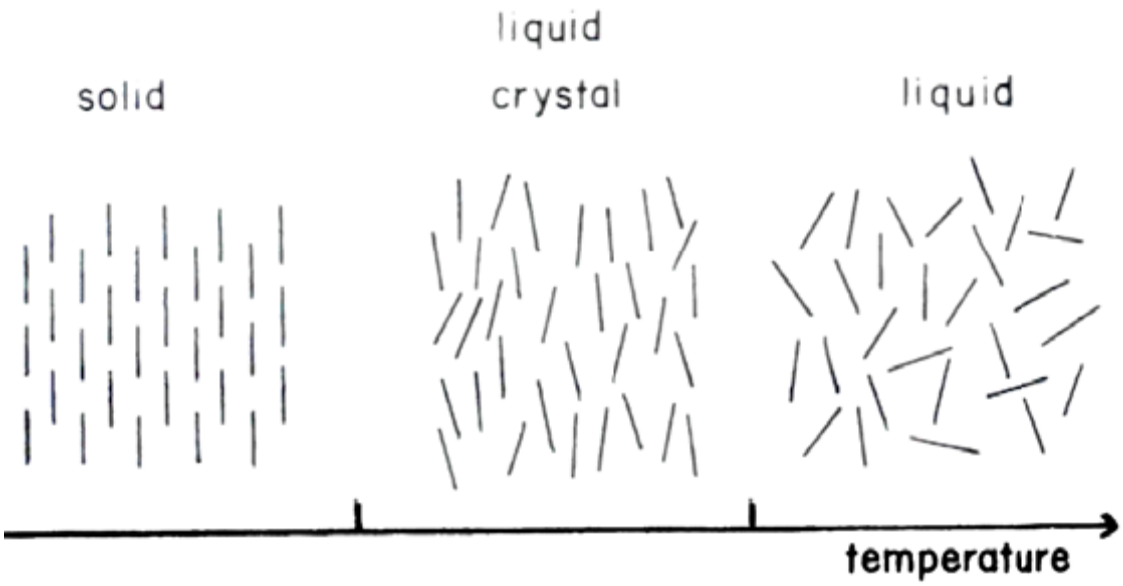

Figure 1.4. Representative phase transition, from solid to liquid crystal and then to liquid phase.

The LC phases are also divided into two categories according to their formation, thermotropic and lyotropic LCs. The thermotropic LCs include calamitic (rod like), discodic (disc like) and polymeric LCs. They are obtained by heating of solid crystals of certain materials. Particularly, as the temperature increases, the thermotropic mesophases change phases from crystal to smectic then to nematic and finally to the liquid phase [35-36].

Lyotropic liquid crystals (LLC) are multi component systems formed in mixtures of amphiphilic molecules and a polar solvent. The LLC formation depends on the concentration of the former amphiphiles in an appropriate solvent [35-38]. Amphiphilic molecules are consisted of a hydrophilic polar head attached to a hydrophobic hydrocarbon tail containing one or two alkyl chains. They have dual character and have both hydrophilic (affinity for water) and hydrophobic (affinity for oil) parts.

There are various kinds of surfactants, which can be classified as anionic, cationic, amphoteric and non-ionic based on their head groups. Figure 1.5 shows some examples

of surfactants. In this work two types of non-ionic surfactants are used, one is oligo(ethylene oxide) type with hydrophobic long alkyl chains and hydrophilic polyoxyethylene (-CH_2CH_2O-, PEO) head group and the other is the triblock poly(ethylene oxide)-poly(propylene oxide)-poly(ethylene oxide) (PEO-PPO-PEO) copolymers.

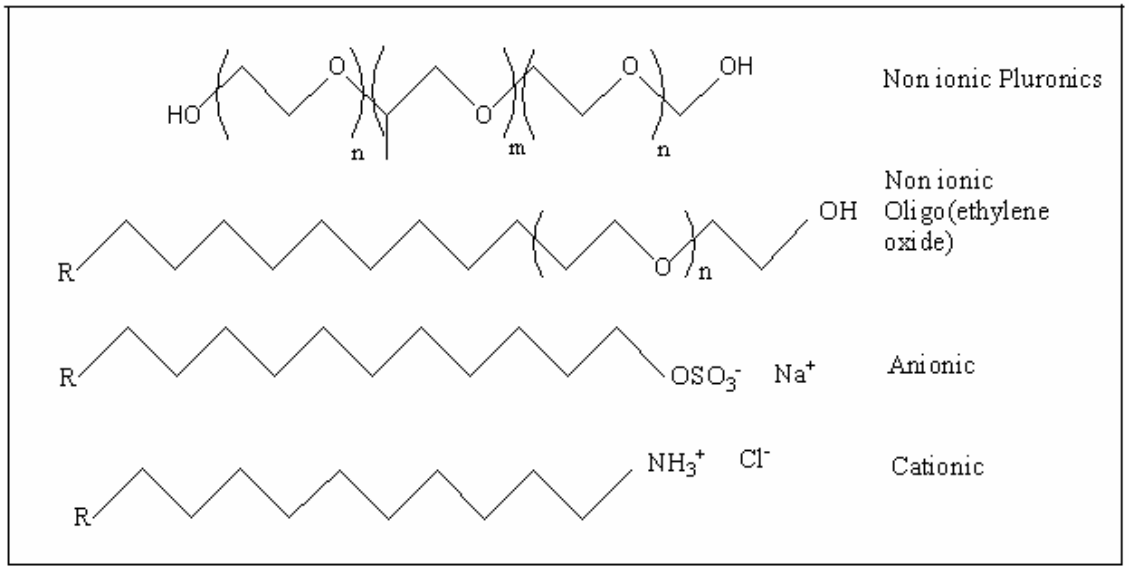

Figure 1.5. Various types of surfactants.

When surfactants are added into water their hydrophobic parts tend to stay away from water. This tendency to avoid water causes the surfactant molecules at very low concentrations to stay on the air/water interface with hydrophobic part orients towards air to decrease the interaction with water. As the concentration of the surfactant is increased the dissolved surfactant molecules assemble and form micelles. The required concentration for the micelle formation is called the Critical Micelle Concentration (CMC) [39]. Further increase in surfactant concentration far beyond the CMC leads to the ordered mesostructure formation. In the micelle structure the hydrophobic hydrocarbon chains orient themselves inside the aggregate and the polar head groups adjust themselves toward the aqueous phase.

The formation of micelles from the surfactant molecules and finally the formation of the various mesostructures are shown in Figure 1.6.

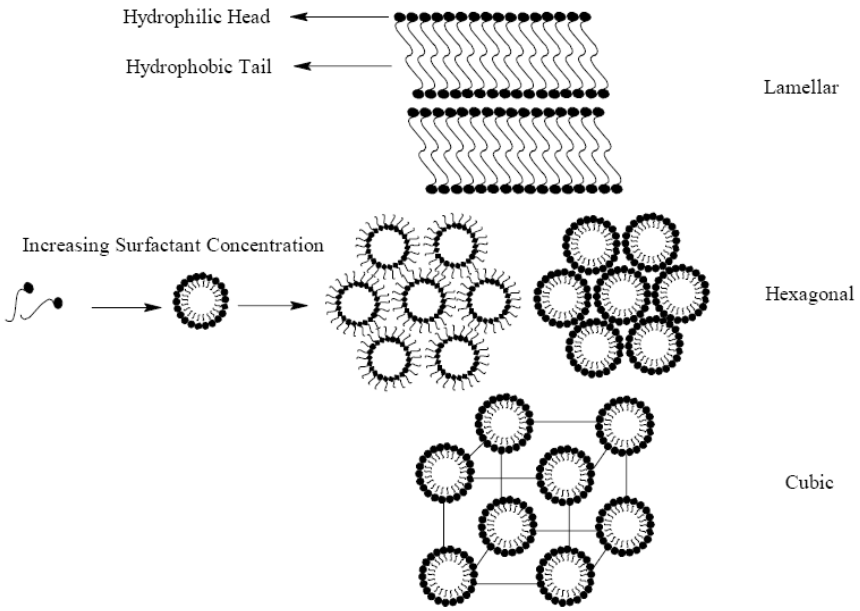

Figure 1.6. Frequently observed lyotropic liquid crystalline phases, formed when a solvent and amphiphilic macromolecules are mixed [39].

The micelle structures are self-assembly of the surfactant molecules which originates from the weak intermolecular forces such as van der Waals, dipole-dipole interactions and hydrogen bonds (not due to strong covalent or ionic bonds) so the structure of the micelle may change in size or shape in response to changes in concentration, salt content, temperature, pH. Therefore, it is possible to obtain mesophases with different structures by changing the surfactant concentration and/or temperature. Figure 1.7 [40] shows the phase diagram of the $C_{16}H_{33}(CH_3)_3NBr$ ($C_{16}TMABr$) which shows structural changes with surfactant concentration and temperature. Note that these kinds of phase diagrams can also be obtained by changing the pH and salt concentration.

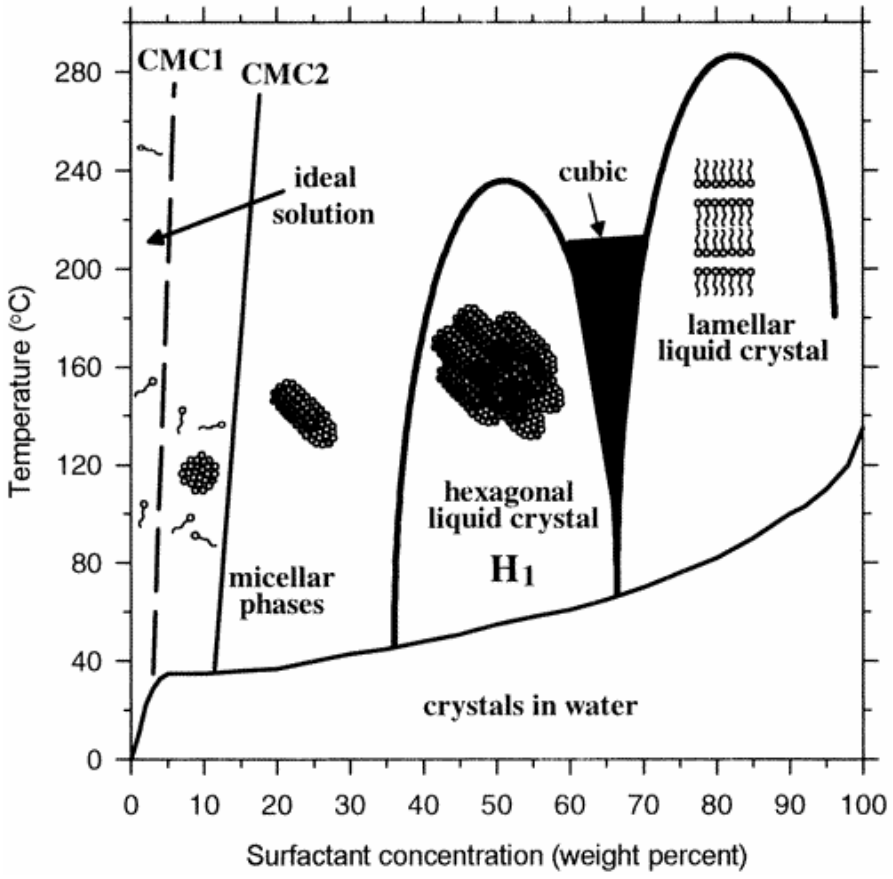

Figure 1.7. Schematic phase diagram for C_{16}TMABr in water [39].

Dag et al. introduced a new lyotropic liquid crystalline (LLC) system of oligo(ethylene oxide) surfactants with transition metal salts (TMS), $[M(H_2O)_n]X_m$ (without water as a solvent) [40]. The LLC phase was formed by mixing appropriate amounts of the TMS and the oligo(ethylene oxide) surfactants. In this binary system the transition metal aqua complexes induces the oligo(ethylene oxide) surfactants to self-assemble into a LC phase. In this LC mesophase formation the hydrogen bonds formed between the metal aqua complex hydrogens and the ethoxy oxygens has an important role. This LC phase is stable for months up to 3.0 salt/surfactant mole ratios.

Dag et al. also found out that the structure of the $[M(H_2O)_x]Y_2$:C_nEO_m binary mesophases usually display 2D hexagonal structure in nitrate systems and cubic in perchlorate systems. However the chloride salt binary systems do not have the mesophase. Indeed the chloride TMS are almost insoluble in the oligo(ethylene oxide) surfactant media[41].

1.4 Hofmeister Series and Salt Effects on the Self assembly

It is well known that oligo(ethylene oxide) molecules form LC mesophases depending on the concentration of water in the media. The LC phase occurs because the oil-like tail group of the amphiphile tends to minimize the interaction with water and forms micelles whereas the hydrophilic part likes to stay outside the micelle in the water regions. Usually these systems included metal salts as the third or fourth component [42-48] of the mesophase. Recently in our group the liquid crystalline (LC) phase behavior of different transition metal aqua complexes, $MY_x.nH_2O$ (M= Co^{+2} , Ni^{+2}, Cd^{+2}, Zn^{+2}, Fe^{+2})(Y= NO_3^-, Cl^-, SO_4^{-2} , CH_3COO^-), with oligo(ethylene oxide) type non-ionic surfactants (salt:C_nEO_m) were investigated [49]. The system shows LC phase with or without addition of water into the system [49].

Synthesis of mesoporous solid materials using LC systems is known and it has been well established that the polymerization of the silica takes place in the hydrophilic domains of the LC mesophase [30]. In this assembly process, the LC phase acts as a structure-directing agent (template). In this thesis we also used LC templating method to produce mesoporous silica with high internal surface area and cavities that are essential for catalysis and high adsorptive capacity. Usually an electrolyte is added to improve the properties of the materials [50]. Addition of electrolytes is also known to affect the structure of the LC phase [51-56]. Therefore electrolytes will also play an important role in the structure of silica materials.

The effects of electrolytes on the solubility of the surfactant are separated into two categories. One of which is the effect of anions on solubility of the surfactant molecules. This effect is known for almost more than hundred years as the Hofmeister effect. Hofmeister divided the anions into two categories according to their effects on the solubility of proteins (the same tendency is observed for the solubility of the surfactants) [57]. Anions such as NO_3^- and ClO_4^- that increase the solubility of the surfactants are known as “salting-in” and the others such as SO_4^{2-} an Cl^- that decrease the solubility of

the surfactants are known as “salting-out” anions [58]. Hofmeister stated that the salting out effect of the anions decreases as the following:

$$SO_4^{2-} > HPO_4^{2-} > CrO_4^{-} > CO_3^{2-} > \mathbf{Cl^-} > Br^- > NO_3^- > I^- > ClO_4^- > SCN^-$$

Ions on the left of Cl^-, which represents a borderline, reduce the solubility of proteins and surfactants. They are generally called salting-out ions, water structure-makers or cosmotropic ions. The opposite holds for ions on the right of Cl^-, known as salting-in, or water-structure-breakers, or chaotropic anions. These anions increases the solubility of surfactants in water.

The well known properties of the salting-out anions are that they have low polarizability and high charge. They hold their hydration water strongly in the solution and they do not interact with other ions directly but with the coordinated water molecules. These properties for the salting-in anions are vise versa: high polarizability, low charge and easy lose of the hydration water.

As mentioned above the effects of the electrolytes are emphasized with their different properties. One is the hydrophilicity change of the surfactant and the other is the structure formation of water. The salting-out electrolytes will decrease the hydrophilicity of the surfactants whereas salting-in anions will increase the hydrophilicity of the surtactant in the media. Similar properties of anions are discussed by biologist from another point of view. They categorize the electrolytes as, some makes water a better solvent (structure breakers) and some makes it a worse solvent (structure makers) for EO chains [59]. The association of water molecules which is enhanced by structure makers and the distruption of the association of water by structure breakers is shown below:

$$nH_2O \rightleftharpoons (H_2O)_n$$

The structure breaking anions I^- and SCN, have low electronegativity high polarizability and weak electrostatic fields, so they disrupt the structure of water and salt-

in the surfactant, whereas the SO_4^{2-} and PO_4^{3-} anions are less polarizable and they are more electronegative therefore they are structure makers and salt-out the surfactant [52].

In addition to this anion effect on solubility there is also cation effect (or coordination effect) which comes due to the coordination of anions to the transition metal cation. Obviously, this effect is not observed with alkali or earth alkali metal cations. However, anions, which coordinates to the metal cation are also important because not all anions have the same ability to coordinate.Upon coordination, the net charge (or ionic strength) in the solution decreases that increases the solubility of the salts in the nonionic surfactants(or LC media). This is observed for the salt:C_nEO_m systems of transition metal nitrate and perchlorate salts.

Although ClO_4^- anion is more salting-in according to the Hofmeister series NO_3^- salts of the same metal cation is more soluble in the salt:surfactant systems. This observation is not a result of Hofmeister effect but due to some other effect which decreases the ion density (ionic strength) of the media. This effect is due to the coordination reaction given below [41] :

$$[M(H_2O)_4]^{2+} + 2NO_3^- \rightleftharpoons [M(H_2O)_3(ONO_2)]^+ + NO_3^- + H_2O$$

The fact is that ClO_4^- anion cannot coordinate to the metal cation; therefore the ion density in the perchlorate system is higher; higher the ion density, lower the solubility of the perchlorate salts.

Another interesting example is the coordination of Cl^- ion to the Co^{+2}cation in the $[Co(H_2O)_6]Cl_2$:C_nEO_m system .Usually metal chloride salts are insoluble in the binary salt: surfactant systems except cobalt (II) chloride ($[Co(H_2O)_6]Cl_2$). The solubility of the cobalt (II) chloride salt is enhanced by the following equilibrium reaction [41]:

$$n\,[Co(H_2O)_6]^{2+} + (2n)Cl^- \rightleftharpoons \qquad \textbf{(Rxn. 1.)}$$

$$((n-m)/2)[Co(H_2O)_6]^{2+} + (3n-m)H_2O + ((n-m)/2)[CoCl_4]^{2-} + m[Co(H_2O)_4Cl_2]$$

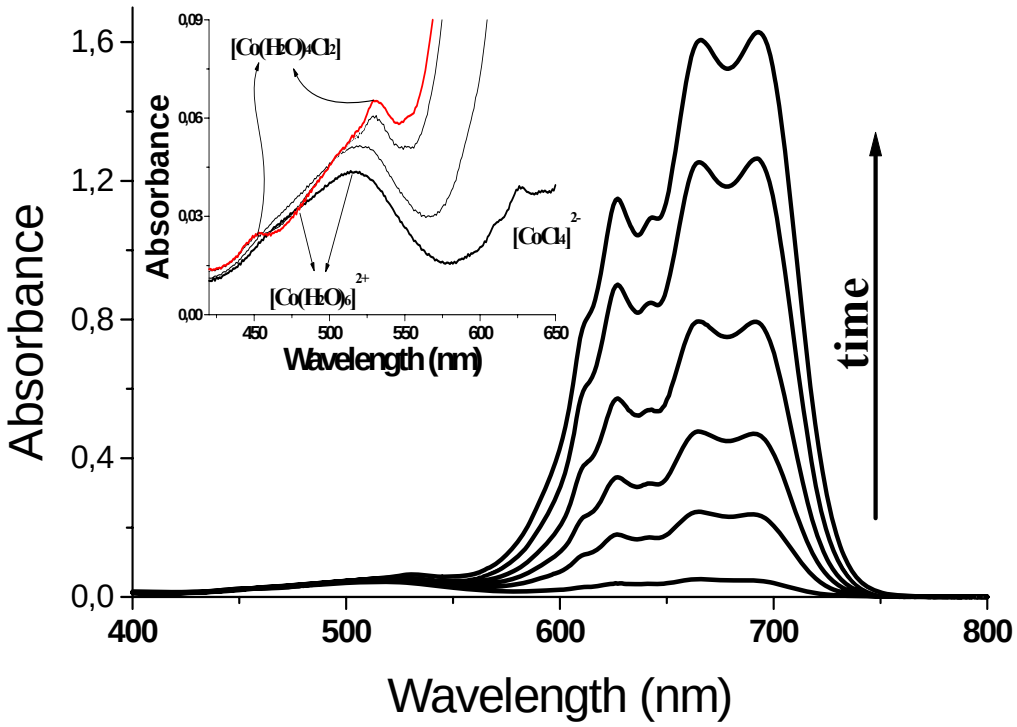

Figure 1.8. UV-vis absorption spectra of $[Co(H_2O)_6]Cl_2$:H_2O:C_nEO_m during the water evaporation. The inset shows the expanded, 400-600 nm spectral range with the neutral $[Co(H_2O)_4Cl_2]$ complex and $[Co(H_2O)_6]^{2+}$complex ion species[41].

The liquid (with excess water) and LC samples with enough water content are purple in color and upon the evaporation of water color changes to a sharp blue. Dag et al monitored the evaporation of water by UV-vis/near-IR spectrophotometry in the visible region [41]. The bands at around 690 nm, which originates from the $[CoCl_4]^{2-}$ ion, increase in intensity with water evaporation [60], see Figure 1.8.

$[Co(H_2O)_4Cl_2]$ complex is also observed during the water evaporation process. The peaks at 454 and 530 nm are characteristic for the $[Co(H_2O)_4Cl_2]$ complex [41,60]. These observations prove that there is an equilibrium between $[Co(H_2O)_4Cl_2]$ neutral and $[Co(H_2O)_6]^{2+}$,$[CoCl_4]^{2-}$ ion complexes as stated in the above equilibrium reaction.

Note that at the right hand side of the equilibrium reaction (Rxn. 1) there is water and this says that water is the key determining component of the equilibrium which is parallel with the observations.

Recently Dag et al.[61] introduced the effects of TMSs type and the concentration on the LC mesophase by working on LLC mesophase of TMS:oligo(ethylene oxide) nonionic surfactants ($C_nH_{2n+1}(CH_2CH_2O)_mOH$, denoted as C*n*EO*m*), systems. They found that the nitrate salts are more soluble in the surfactant media than the perchlorate salts. This is due to the coordination of nitrate ions to the transition metal cation. The coordination of nitrate ion to the transition metal cation decreases the ion density of the media and increases the solubility of the salt in the surfactant.The structure of the $[M(H_2O)_x]Y_2$:C_nEO_m (Y is Cl-, NO_3^-, and ClO_4^-) mesophase is usually 2D hexagonal in nitrate systems(some nitrate salts also display cubic structure at high salt concentrations), cubic in perchlorate systems. The structure of the LC changes from hexagonal to cubic phase as the ion density of the TMS:C_nEO_m system increases. At the same mole ratios the nitrate salts display hexagonal where as the perchlorate salts display cubic. This observation is due to lower ion density of the nitrate sample due to the coordination [61]. Dag et al carried out an experiment to observe the ion density effect on the LC mesophase. In their experiment they held the metal ion /$C_{12}EO_{10}$ molar ratio constant (at 2.0 molar ratio) in a $[Cd(H_2O)_4](NO_3)_2$/$[Cd(H_2O)_4](ClO_4)_2$:$C_{12}EO_{10}$ mixed-salt systems. The change of the structure from 2D hexagonal (perchlorate free sample) to 3D hexagonal (1.5:0.5 of NO_3^-/ClO_4^- molar ratio) and to cubic (0.2:1.8 of NO_3^-/ClO_4 molar ratio) is proven by XRD and POM techniques, see Figure 1.9 for the XRD patterns and Figure 1.10 for the POM images below [41].

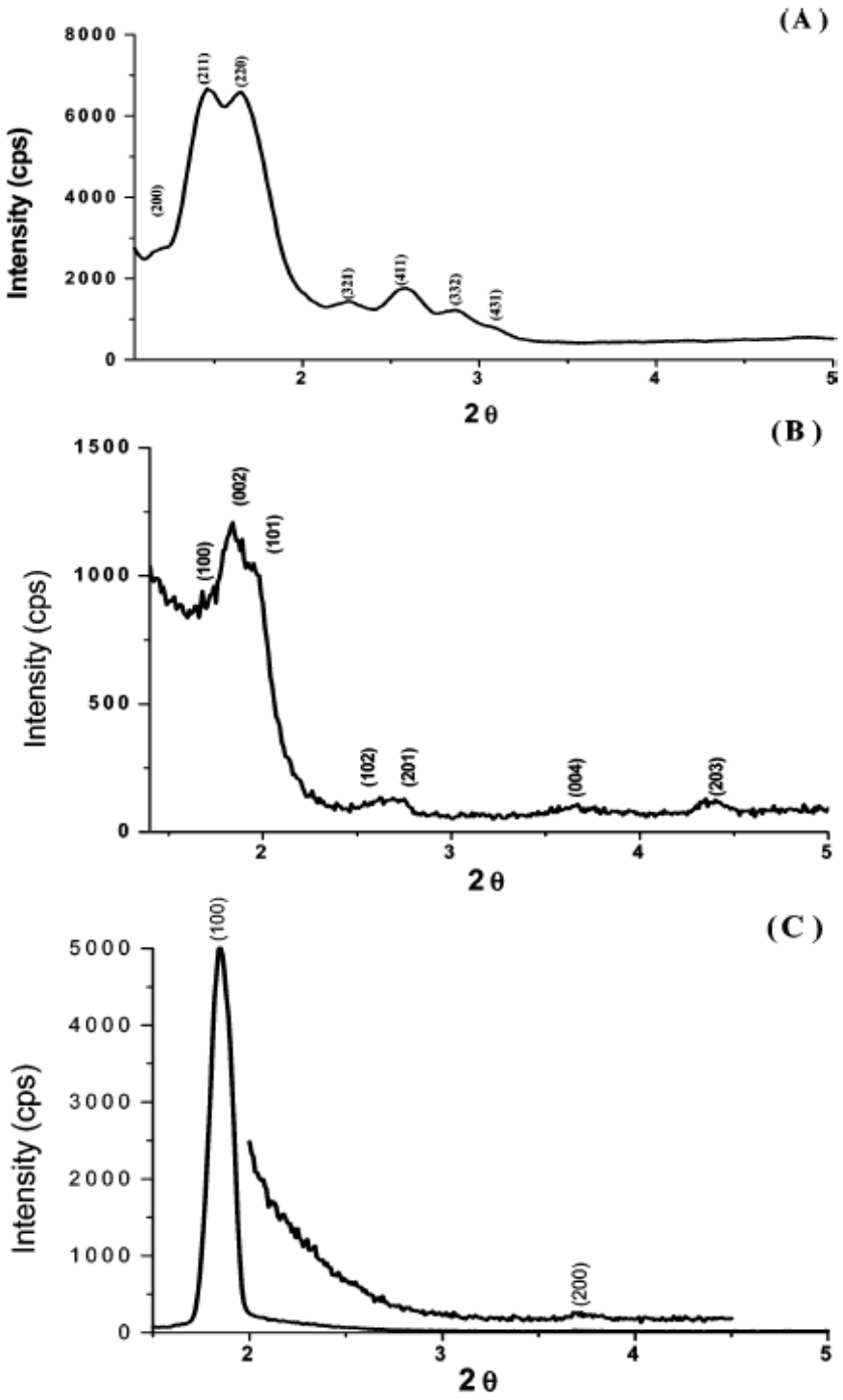

Figure 1.9. XRD patterns of $[Cd(H_2O)_4](NO_3)_2/[Cd(H_2O)_4](ClO_4)_2$:$C_{12}EO_{10}$ mixed-salt systems. The nitrate-to-perchlorate mole ratios are (A) 0.0:2.0, (B) 1.5:0.5, and (C) 1.8:0.2 (the metal ion-to-surfactant moleratio is 2.0 in all samples) [41].

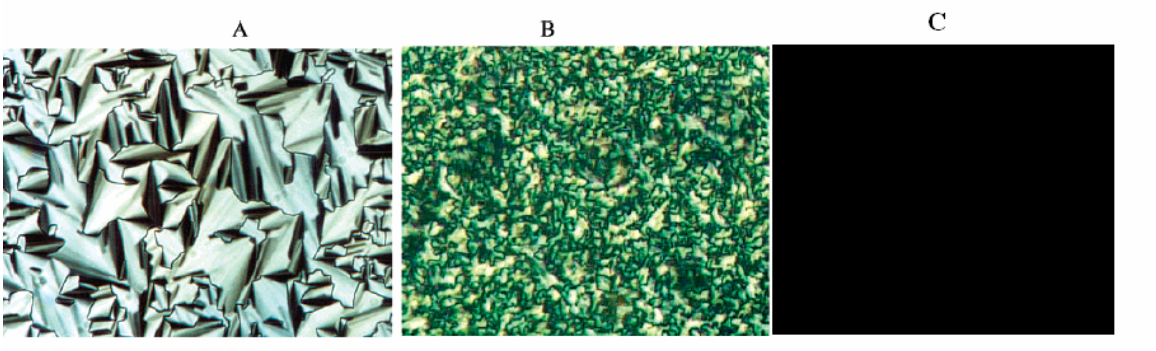

Figure 1.10. The POM images of the $[Cd(H_2O)_4](NO_3)_2/[Cd(H_2O)_4](ClO_4)_2$:$C_{12}EO_{10}$ mixed-salt systems. The nitrate-to-perchlorate mole ratios are (A) 1.8:0.2, (B) 1.5:0.5, and (C) 0.0:2.0 (the metal ion-to-surfactant mole ratio is 2.0 in all samples)[41].

1.5. Salts (Electrolytes) in Synthesis of Inorganic Mesoporous Materials and Their Effects on the Mesoporous Products

Electrolytes are almost always present in the synthesis of mesoporous materials. Salts are known to have significant effects on the formation mechanism of mesoporous materials. Electrolytes generally increase the stability of the materials by developing the interface properties [50]. Note that if LCT is used for the mesoporous material synthesis the effects of the salt on the LC will also affect the structure of the mesoporous materials.

It is known that MCM-41 has high thermal and hydrothermal stability against air and oxygen containing water vapor. However, it has a low hydrothermal stability in boiling water and aqueous solutions [62-64].Chen et al.[62] reported that pure-silica MCM-41 could be heated up to 1123 K and do not lose its stability. Additionally Kim et al.[63] showed that the powder X-ray diffraction (XRD) pattern and BET surface area of the MCM-41 were not significantly affected by heating up to 1170 K in air and in O_2 containing water vapor with pressures up to 2.3 kPa (0.023 atm). More recently, Kim and Ryoo [64] reported that the mesoporous structure was even stable against 100% steam

flow at 770 K. In contrast to such stability of MCM-41 in air, O_2, and steam at high temperatures, it was found that MCM-41 collapses during heating in boiling water and in aqueous solutions [64]. The structural loss involved silicate hydrolysis in water and aqueous solutions.

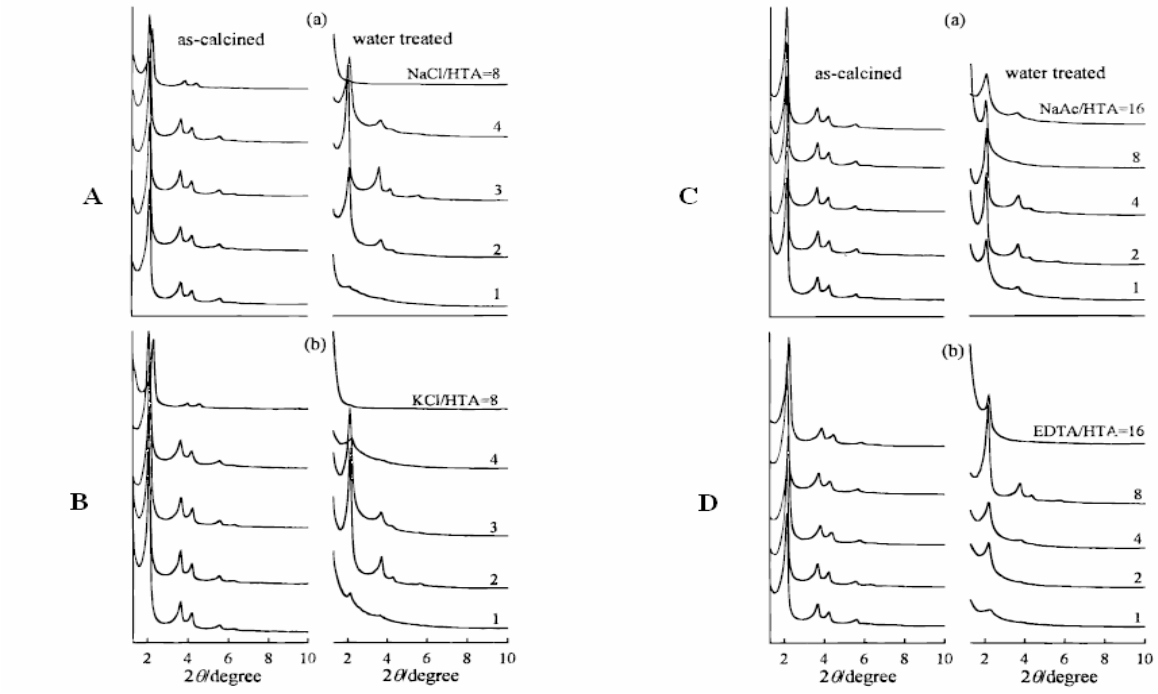

Figure 1.11. XRD patterns of MCM-41 displayed relative to the amounts of inorganic salts added to the synthesis mixtures: (A) NaCl, (B) KCl, (C) Sodium acetate, (D) Na_4EDTA. Numbers given to XRD patterns are salt-to-HTACl molar ratio. The "water treated" data were collected after heating the calcined samples in boiling water for 12 h [64].

Ryoo and Jun [65] introduced that low hydrothermal stability in hot water and aqueous solutions which was a critical problem for many applications of the mesoporous molecular sieve MCM-41 could be overcame and improved remarkably by using various salts like sodium chloride, potassium chloride, sodium acetate, and ethylenediaminetetraacetic acid tetrasodium salt (Na_4EDTA). High-quality MCM-41

samples investigated under XRD gave very insignificant losses in boiling water. Improvement by addition of salt in the synthesis media can easily be seen in Figure 1.11. The XRD patterns of MCM-41 with addition of different salts with different amounts are shown in Figure 1.11: Graphs include additional salts as follows (A) NaCl, (B) KCl, (C) Sodium acetate, and (D) Na_4EDTA. The numbers on the XRD patterns are the salt/HTACl molar ratios. It is seen for all the experiments that the addition of salt stabilizes the structure against boiling water. However after an upper limit the salt loses its benefit.

In addition, Stucky and Zhao[66] reported that the addition of inorganic salts, especially highly charged salts such as K_2SO_4, can increase the interaction of silicate species with hydrophilic head groups of nonionic block copolymers and the strong interaction of head groups with the silicate species can result in long-range ordered domain of silica-surfactant mesostructures finally the long-range order favors the formation of mesoporous single crystals. Briefly, Stucky and Zhao found that extra salt addition stimulates the formation of single crystal materials instead of amorphous materials.

In their experiments Stucky and Zhao [66] used non ionic triblock copolymer surfactants (F108) and K_2SO_4 in acidic media and they achieved to synthesize cubic (*Im*3*m*) mesoporous single crystals**.** However with the same reactants without adding salt, they only obtained amorphous gel. A decrease of concentration of K_2SO_4 from 0.5 to 0.25 mol/L resulted in no precipitates from solution. They found that Na_2SO_4 also gives single crystals when it is used instead of K_2SO_4. This means that the anion has more effect on the structure and highly charged anions favor the formation of single crystals. However, using the anion Cl^- instead of SO_4^{2-} gave rise to mixed morphologies.

In this thesis we have studied the effect of salt, type and amount on the synthesis of mesostructrued silica, produced by LCT. The resulting materials were characterized by

XRD, POM, FT-IR and micro-Raman spectroscopy. As the salt concentration or more generally as the ion density increases the structure of the mesostructured silica also tends to shift from hexagonal to cubic mesophases. These observations will be extensively discussed throughout the results and discussion parts.

2. EXPERIMENTAL

2.1 Materials

All chemicals and solvents were reagent grade and used as received without any further treatment.

Several surfactants were used throughout this work; homogeneous polyoxyethylene 10 lauryl ether $C_{12}H_{25}(OCH_2CH_2)_{10}OH$, (designated as $C_{12}EO_{10}$) and Brij 76 ($C_{18}EO_{10}$) are commercially available from Aldrich, Germany. The triblock copolymers having a poly(ethylene oxide)-poly(propylene oxide)-poly(ethylene oxide) (EO-PO-EO) so called Pluronics, L64 ($PEO_{13}PPO_{30}PEO_{13}$, M_{av} = 2900), P65 ($PEO_{20}PPO_{30}PEO_{20}$, M_{av} = 3500), and P123 ($PEO_{20}PPO_{70}PEO_{20}$, M_{av} =5800) were generously donated by BASF Corp. and used without further treatment.

Cobalt(II) nitrate hexahydrate($[Co(H_2O)_6](NO_3)_2$), 98 % pure), cobalt(II) chloride hexahydrate ($[Co(H_2O)_6]Cl_2$, 98 % pure),Cobalt(II) perchlorate hexahydrate ($[Co(H_2O)_6](ClO_4)_2$), zinc(II)nitrate hexahydrate ($[Zn(H_2O)_6](NO_3)_2$) and zinc(II)perchlorate hexahydrate ($[Zn(H_2O)_6](ClO_4)_2$) were obtained from Aldrich, Germany. HNO_3 and $HClO_4$ were obtained from Aldrich, Germany. Tetramethylorthosilicate (TMOS, %98 pure) was obtained from Aldrich and Fluka.

2.2 Synthesis

2.2.1 Synthesis of Liquid Crystal Phase with Inorganic Salts

The surfactant:water:metal salt samples are prepared by directly mixing 1.0 g of surfactant with 1.0 g of water and than adding the transition metal salt (TMS) complexes to the mixture or the TMS is first dissolved in water and then the surfactant is added to the mixture. For homogenizing purposes, the mixture is first rinsed and subsequently is

heated up to melting point, finally cooled to the room temperature (RT). These heating-cooling cycles are repeated until homogenization. An easier way of homogenizing is placing the samples into a shaking water bath for several hours at temperatures around the melting points.

1.0 gram of surfactant is mixed with metal salts, in mole ratios TMS/surfactant varying from 0.0 to 15.0. The samples are either examined in their LC phases or treated further for the silica production. Some TMS:Surfactant samples are prepared without water addition but these samples are harder to homogenize so most of the samples are prepared with water.

LC mesophase of the pluronics are prepared using a similar procedure. The ternary samples, H_2O:TMS:Pluronic are prepared by first dissolving the appropriate amount of $[Zn(H_2O)_6]NO_3$ salt in 1.0-3.0 g of water and then adding 1.0 g of Pluronic to this clear solution. Pluronics with higher molecular weights are even harder to homogenize than the C_nEO_m type surfactants. The resulting mixtures are usually homogenized by heating the mixtures to their melting point in sealed vials. Note that some samples are already liquid at this stage. Therefore homogenizing the ternary samples is a relatively easy process. The Pluronic LC mesophases are prepared between 0.0 and 15.0 salt/Pluronic mole ratios. Additionally LC samples with various salt/ethoxy(EO) mole ratios were also prepared.

2.2.2 Synthesis of Mesoporous Silica by Liquid Crystal Templating (LCT)

Mixing 1.0g of surfactant, 1.0 g of water and the transition metal salt (TMS), 0.1g of HNO_3 and tetramethylorthosilicate (TMOS) respectively gives a clear solution. The solution is rinsed for a few minutes for homogenizing and then casted as a film (thin) or monolith (thick) samples. The nitric acid (HNO_3), perchloric acid ($HClO_4$) and hydrochloric acid (HCl) have been used as acid sources for the silica polymerizations in the metal nitrate, metal perchlorate and metal chloride systems, respectively.

In the case of Pluronic surfactants, the preparation route is similar;

3.0 g water, x g TMS, 1.0 g Pluronic and 0.1g HY (acid, Y=NO_3^-, ClO_4^- or Cl^-) are added respectively and then the mixture is homogenized by either heating and cooling cycles or mixing with a magnetic stirrer. Lastly 1.7g of TMOS is added as the silica source.

After the mixing steps, the homogenized mixtures are either spread over the glass slides to produce monoliths (monolith comes from the Greek words mono, means one, and lith, means piece) or they are diluted with extra 9.0 grams of water and dip coated on the glass surfaces. The dip coating is done by a home made dip coater which takes in and out the glass slide into the solution with a constant speed. Both, films and monoliths are kept at RT for drying and polymerization. The monoliths are 1.0-2.0 mm thick and the dip-coated samples are several microns thick. The monoliths are used for POM, XRD and micro-Raman measurements. The dip-coated film samples are used to examine using FT-IR and XRD techniques.

2.2.3. Calcination of the LC Templated Mesoporous Silica

The homogenized samples of TMS:surfactant:Silica system is spread on a glass or plastic holder and dried for 2 days. The dried sample is then crushed to obtain a fine powder. The powder is calcined in the following way; first placed in an oven and the temperature is increased from 25˚C to 200˚C in 2 hours and kept at 200˚C for 1 hour. The sample is cooled and the XRD pattern is recorded. In the second step it is heated up to 300˚C in 3 hours and kept at 300˚C for 1 hour again the sample is cooled and XRD pattern is recorded. Finally it is heated up to 500˚C in 5 hours and kept at 500˚C for 5 hours. The calcinations may also be done in one step as heating up to 500˚C in 5 hours and keeping at 500˚C for 5 hours but gradually heating gives the best results.

2.3 Instrumentation

2.3.1 Polarized optical microscopy

Polarized optical microscopy (POM) images has been used to characterize the mesophases formed from salt:surfactant and salt:surfactant:silica systems. The POM images were recorded in transmittance mode on a Meije techno ML 9400 series Polarizing Microscope with transmitted light illumination, using convergent white light between parallel and cross polarizers.

2.3.2. X-Ray Diffraction

The X-Ray diffraction (XRD) patterns were collected on a Rigaku Miniflex diffractometer using a high power Cu-K_α source operating at 30 kV/15 mA. Both the dip coated samples and monoliths were prepared on microscope slides. The XRD patterns of a sample were collected at least twice in the 1-5 2θ range with a scan rate of 0.5θ /min. The high angle diffraction patterns of some samples were also recorded between 1-20 2θ values.

2.3.3. FT-IR Spectroscopy

The transmission FT-IR spectra were recorded with a Bomem Hartman MB-102 model FT-IR spectrometer. A standard DTGS detector was used with a resolution of 4 cm^{-1} and 32 scan for all samples. The samples were prepared as a thin film over a Si(100) wafer or in some cases the samples was sandwiched between two wafers. The FT-IR spectra of the samples were recorded in 200- 4000 cm^{-1} range.

2.3.4 Micro-Raman Spectroscopy

The Micro-Raman spectra were recorded on a LabRam confocal Raman microscope with a 300 mm focal length. The spectrometer is equipped with a HeNe laser operated at 20 mW, polarized 500:1 with a wavelength of 632.817 nm, and a 1024 x 256 element CCD camera. The signal collected was transmitted through a fibre optic cable into a grating with a 600 g/mm spectrometer. The Raman spectra were collected by manually placing the probe tip near the desired point of the sample on a glass slide.

3. RESULTS AND DISCUSSION

CHAPTER 1

3.1.1. Effects of Transition Metal Salts on Synthesis of Mesostructured Silica

In this work the LC mesophases of $C_{12}EO_{10}$ and Pluronics surfactants with some transition metal salts(nitrates, chlorides and perchlorates) were used as template for mesostructured silica synthesis. The synthesized samples were characterized by means of microscopy (POM), diffraction (XRD) and spectroscopy (FT-IR and micro-Raman) techniques. For the synthesis of mesostructured silica, HY (Y=NO_3^-, Cl^- and ClO_4^-) and TMOS are added as the acid and silica sources into the LC mesophase, respectively. The silica polymerization takes place in the hydrophilic regions of the LC mesophase. We have intensively studied the solid phase formed by $[Co(H_2O)_6](NO_3)_2$, $[Co(H_2O)_6]Cl_2$, $[Co(H_2O)_6](ClO_4)_2$ transition metal salts, oligo(ethylene oxide) type and Pluronic ($PEO_xPPO_yPEO_x$) nonionic surfactants, acid and TMOS.

3.1.2. Polarized Optical Microscopy (POM) of Mesostructured Silica

The polarized optical microscopy (POM) is a very powerful tool for structural determination of LC mesophases. The optical texture observed between cross polarizers is helpful in identifying the structure of the LC mesophase. The most frequently observed and the best-known structures are hexagonal and cubic structures in mesoporous silica materials. The cubic structure is isotropic; therefore the POM image of a cubic mesophase is dark. However the hexagonal structure is anisotropic and displays a focal conic fan texture between cross polarizers.

Generally, the POM images of similar systems do not show much variance. In this thesis, the salt concentration and salt type were used as parameters. A number of different type of POM images were observed depending on the anion type and ion density of the systems. In the $[Co(H_2O)_6](NO_3)_2$:$C_{12}EO_{10}$:HNO_3:TMOS systems, the fan texture is observed for the salt free samples and in the samples up to 1.2 salt/surfactant mole ratio. However the POM images are totally dark in the samples with 1.6 salt/surfactant mole ratio and above as shown in Figure3.1.1. It means that the structure is hexagonal up to 1.2 mole ratio and it is converted to cubic structure above 1.2 mole ratio (or disordered amorphous phase). The mesostructured silica samples are stable up to 2.0 mole ratio. Above 2.0 mole ratios, the salt ions slowly crystallize and separate from the mesophase over 2 days. Over 4.0 mole ratios, it takes only one hour for salt ions to crystallize out. Since the LC mesophase has been used as reaction and templating media, the LC mesophases of salt:surfactant systems are also studied. The salt systems, such as $[Co(H_2O)_6](NO_3)_2$:$C_{12}EO_{10}$ with or without water forms an LC mesophase[40] that displays fan texture up to 3.0 salt/surfactant mole ratio. The $[Ni(H_2O)_6](NO_3)_2$:$C_{12}EO_{10}$ and $[Co(H_2O)_6](NO_3)_2$:$C_{12}EO_{10}$ samples with a mole ratio above 3.0 undergo recrystallization [40,61]. Note also that the mesostructured silica obtained from $[Co(H_2O)_6](NO_3)_2$:$C_{12}EO_{10}$:HNO_3:TMOS mixture shows structural change from hexagonal to cubic at around 1.2 salt/surfactant ratio. However the $[Co(H_2O)_6](NO_3)_2$:$C_{12}EO_{10}$ LC system behave similarly at around 3.0 mole ratio. For both LC mesophase and mesostructured silica systems as the salt ion concentration is increased, the structure tends to change from hexagonal to cubic. However the change for the silica systems occur at lower salt/surfactant ratios, therefore we can say that silica acts as a hydrophilic material and mimics the salt ions. Based on our data it can be generalized that there is an equilibrium between the hydrophilic and hydrophobic regions and increasing hydrophilic content with respect to hydrophobic content, shifts the equilibrium forward to the cubic mesophase from the hexagonal mesophase. The reverse is also possible if we decrease the hydrophilic content (or increase the hydrophobic content) there will be a shift from cubic to hexagonal phase.

As the hydrophilic content increases---->

Hexagonal ----------Cubic

<-------As the hydrophobic content increases

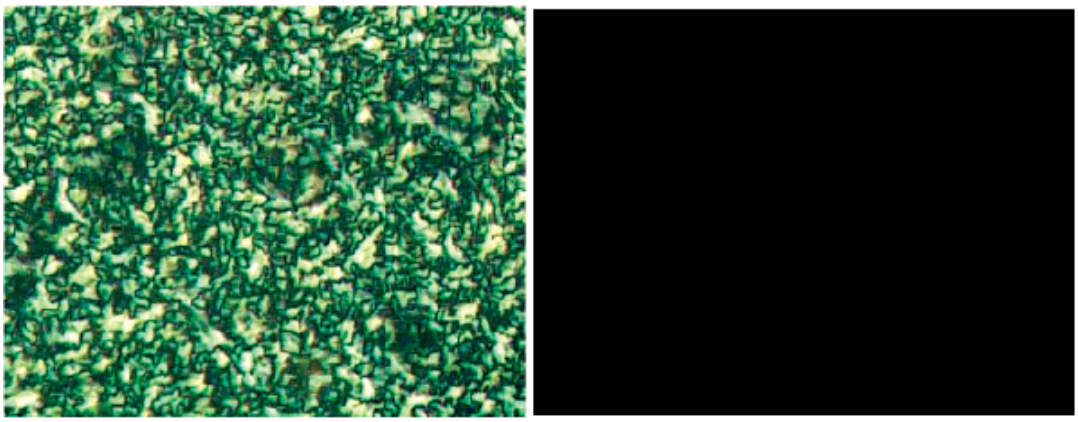

A B

Figure 3.1.1. POM image for the A) hexagonal and B) cubic mesophases of $[Co(H_2O)_6](NO_3)_2$:$C_{12}EO_{10}$:HNO_3:TMOS salt system.

The POM images of $[Co(H_2O)_6](ClO_4)_2$:$C_{12}EO_{10}$:$HClO_4$:TMOS surfactant silica systems were also recorded where the image for salt free sample is birefringent. The images over 0.2 $[Co(H_2O)_6](ClO_4)_2/C_{12}EO_{10}$ mole ratio were dark between the cross polarizers. Note that in the salt free system there is still ClO_4^- anion that comes from 0.1g of $HClO_4$ but the image is still birefringent and addition of small amounts of $[Co(H_2O)_6](ClO_4)_2$ salt makes the image darken. Above 1.0 mole ratio the perchlorate salt ions crystallize out from mesostructured silica after about 2 hours of aging. From the POM image it could be concluded that (see also the XRD results part) the perchlorate salts make the system undergo phase change to cubic over 0.2 salt/surfactant mole ratio. Remember that for the $[Co(H_2O)_6](NO_3)_2$:$C_{12}EO_{10}$:HNO_3:TMOS system this ratio is 1.2. This shows that ClO_4^- anion behaves more hydrophilic than the NO_3^-. As a result of this hydrophilic effect, the phase change for the perchlorate salt occurs at a lower salt/surfactant mole ratio. However, according to the Hofmeister series the ClO_4^- anion is more salting-in than the NO_3^- anion, therefore ClO_4^- anion would be expected to be more

hydrophobic than the NO_3^- anion. Here the reason for such a disagreement with the Hofmeister series is again the coordination of NO_3^- anion to the metal cation. Coordination lowers the ion density in the media and as a result the transition metal nitrate salt becomes more soluble (and behaves less hydrophilic) in the media. Note that the perchlorate salt crystallizes out at lower mole ratios (1.0 mole ratio) than the nitrate salts (2.0 mole ratio) so the solubility of the perchlorate salts are also lower than the nitrate salts.

As the salt concentration or the ionic strength of the system increases, the structure tends to change from the hexagonal to the cubic mesophases. The silica species, which form during hydrolysis and polymerization of TMOS, resemble the effect of salt in the system, adding the silica species increases the hydrophilic content of the mixture. The silica systems turn from hexagonal into cubic phase at lower salt ratios than the silica free salt:$C_{12}EO_{10}$ LC systems. The 3D hexagonal mesophase was observed in the $[Mn(H_2O)_4](NO_3)_2$:$C_{12}EO_{10}$ and $[Co(H_2O)_6](NO_3)_2$:$C_{16}EO_{10}$ systems between 1.2 and 3.0 salt-to-surfactant mole ratios [49]. Below 1.2 mole ratio the $[Mn(H_2O)_4](NO_3)_2$:$C_{12}EO_{10}$ and $[Co(H_2O)_6](NO_3)_2$:$C_{16}EO_{10}$ systems have 2D hexagonal mesophase. However in the silica systems we observe the hexagonal mesophase up to 1.2 mole ratio and this is smaller than the ratio of the salt:C_nEO_m LC (3.0 mole ratio) systems. We know that the silica species are not ionic but still they are polar and they have dipoles, therefore they act as hydrophilic species and resemble the salt ions and increase the hydrophilic content of the media.

Another question is how the surfactant carbon chain length affects the structure of LC and as a result the silica systems. In the literature, it is mainly thought that the forces that hold the micelles are the organic part of the surfactant molecules that stay together. It is also known that adding extra hydrophobic material to the mixture increases the stability of the micelle [67]. So we tried to address this question by increasing the hydrophobic tail of the surfactant molecules. This may reverse the effect of the salt ions (or the ionic strength). A surfactant with a longer carbon chain $C_{18}EO_{10}$ ($C_{18}H_{37}(CH_2CH_2O)_{10}OH$) has been used to address this question. Samples of $[Co(H_2O)_6](NO_3)_2$ salt with two different surfactants ($C_{18}EO_{10}$ and $C_{12}EO_{10}$) at 2.0

salt/surfactant mole ratio were prepared and they were investigated under cross polarizers. The samples of $[Co(H_2O)_6](NO_3)_2$:$C_{12}EO_{10}$:HNO_3:TMOS system displayed a dark image. This is expected because the $[Co(H_2O)_6](NO_3)_2$:$C_{12}EO_{10}$:HNO_3:TMOS system above 1.2 salt/surfactant mole ratio forms cubic mesophase. However the samples of $[Co(H_2O)_6](NO_3)_2$:$C_{18}EO_{10}$:HNO_3:TMOS system displayed fan textures that indicates formation of hexagonal structure. This proves our equilibrium suggests (shown below) that as we increase the hydrophobic content of the media the structure turns from cubic mesophase to hexagonal mesophase.

As the hydrophilic content increases------>

Hexagonal ----------Cubic

<-------As the hydrophobic content increases

3.1.3. XRD ANALYSIS

The X-ray diffraction is also a very powerful technique in analyzing the structure of mesophases. It provides information about the crystallinity, structure type and degree of order in the samples. The method is based on the Bragg`s diffraction law given below:

$$n\lambda=2d\sin\theta$$

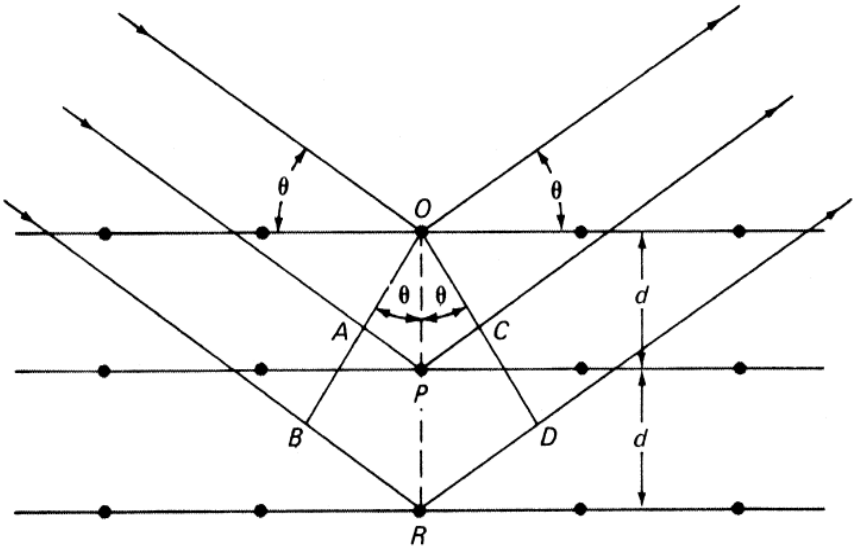

Diffraction of X-rays by a crystal.

The intensity and the resolution of the diffraction lines from the mesoporous silica materials are based on the density gradient between the silica walls and pores or organics [28]. The nature of diffraction lines namely position, intensity, line width and resolution are all related to the structure and crystallinity of the materials. The materials studied in this work, usually have diffraction lines at low angles, namely between 1-5 2θ values. In mesostructured materials, micellar aggregates form ordered mesostructures; therefore the diffraction of these samples will be at small angles mostly within the 1-10 2θ range. Most of our experiments are performed within the 1-5 2θ range.

The most frequently observed structures of mesoporous materials are hexagonal, cubic and lamellar structures. Examples of XRD patterns for hexagonal, cubic and lamellar mesophases are given in Figure 3.1.2.

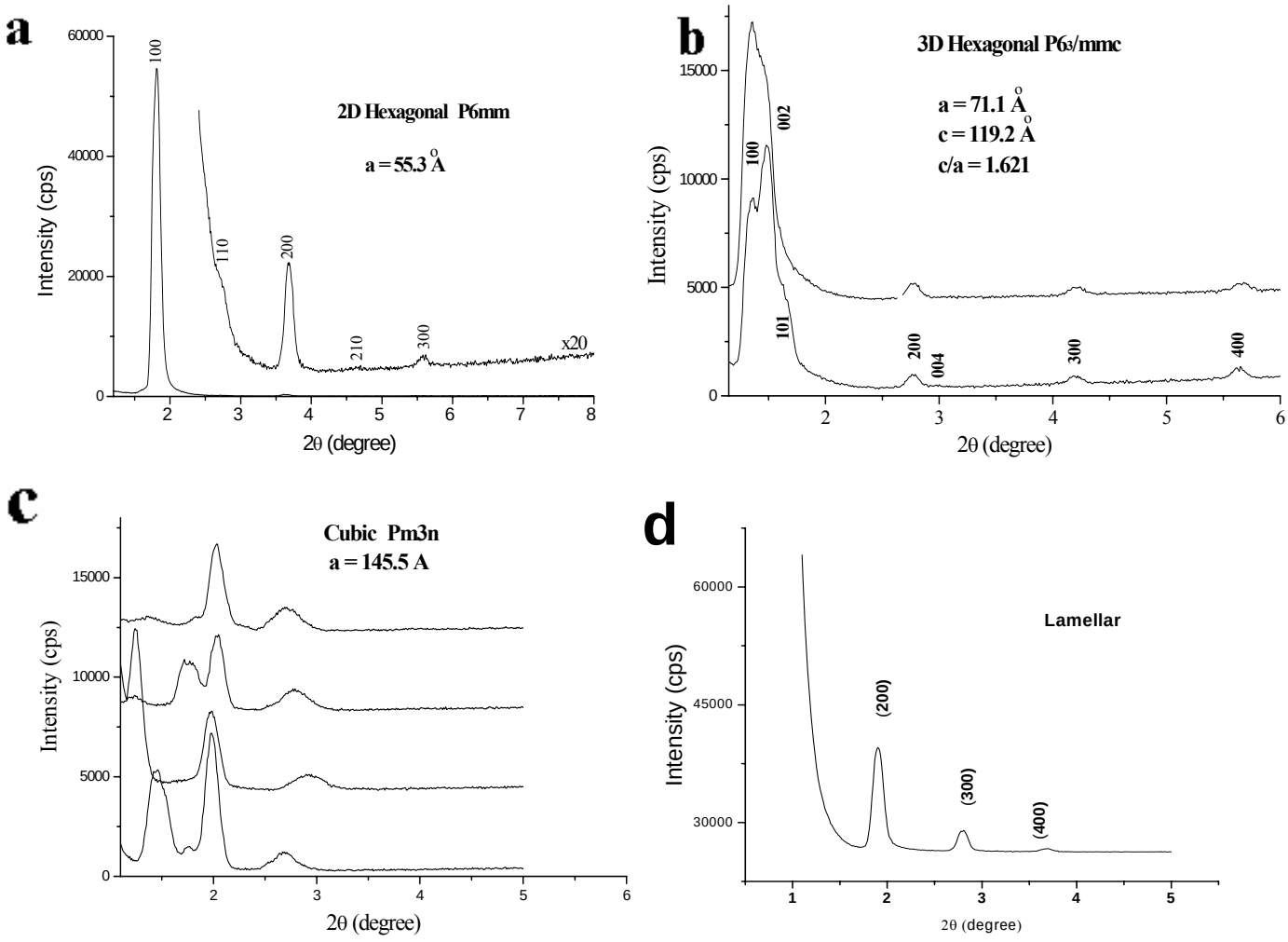

Figure 3.1.2. Typical XRD patterns of mesostructured materials a) 2D hexagonal, b) 3D hexagonal, c) cubic [61], d) lamellar.

Note that the 2D hexagonal mesophase displays only hk0 lines and lamellar mesophase displays only h00 lines. This is because in the 2D hexagonal structure the 3rd dimension is not ordered and in lamellar structure only one dimension is ordered. In lamellar phases the d-spacing is related to the (h00) values as follows:

d= a/h and the plot of d-spacing versus 1/h will give us a linear plot with a slope that is equal to **a** parameter. In cubic phase the relation is $1/d^2=(h^2+k^2+l^2)/a^2$ and the plot of d-spacing versus $1/(h^2+k^2+l^2)^{1/2}$ gives a linear plot with a slope **a.** In 3D hexagonal phase the relation is $1/d^2 = 4/3(h^2+hk+k^2)/a^2 +l^2/c^2$ and when 2D hexagonal is considered the *l*

parameter is not defined and the relation then becomes as $1/d^2 = 4/3(h^2+hk+k^2)/a^2$. For the 3D hexagonal phases the d-spacing versus $(8/(10.667(h^2+hk+k^2)+3l^2))^{1/2}$ gives the linear plot with slope equal to **a.**

In this work we have usually observed a single line at low angles. Especially the dip-coated samples display an intense single line at around 2˚. Thus it is difficult to make an appropriate assignment on the structure type. At least three diffraction lines are required to determine the structure type. However, if the synthesis conditions are not properly established, there may be more than one phase such as hexagonal, lamella or cubic mesophases may coexist in the samples [68]. Comparison of POM and XRD data were used to make appropriate assignments of the structures.

3.1.3.1 Mesostructured Silica Monoliths using $[Co(H_2O)_6](NO_3)_2$:$C_{12}EO_{10}$ LC Systems

The silica monoliths of $[Co(H_2O)_6](NO_3)_2$ salt with $C_{12}EO_{10}$ surfactant, HNO_3 and TMOS in varying salt concentrations were prepared and the structures were examined by using XRD. Figure 3.1.3 shows a set of data obtained from different salt/surfactant mole ratios. The salt-free sample and samples up to1.2 mole ratio in their XRD patterns display two major lines one, at around 2˚ and the other at around 4˚. The XRD pattern of the silica sample with 0.4 salt/surfactant mole ratio displays a more complex pattern that is consistent with the 3D hexagonal structure with a c/a parameter of 1.632 with a=52.5 Å and c=85.7 Å . The salt ratio of the sample affects the structure of the resulting materials. A salt-free sample and samples with 0.4 and 1.2 mole ratios display fan texture under POM and the XRD patterns fit well with the hexagonal parameters. Above the mole ratio of 1.2 the POM images display no image (dark) it means that above 1.2 mole ratio the material is isotropic (sign of cubic phase). The XRD patterns well suit the cubic structure. As the salt concentration increases in the media the structure changes from hexagonal to cubic phase and the change occurs in between the 1.2 and 1.5 mole ratios. Above 3.0 mole ratio the cubic phase is still preserved but the stability of the materials decreases and the extra salt crystallizes out. Increasing the salt amount decreases the time for crystallization.

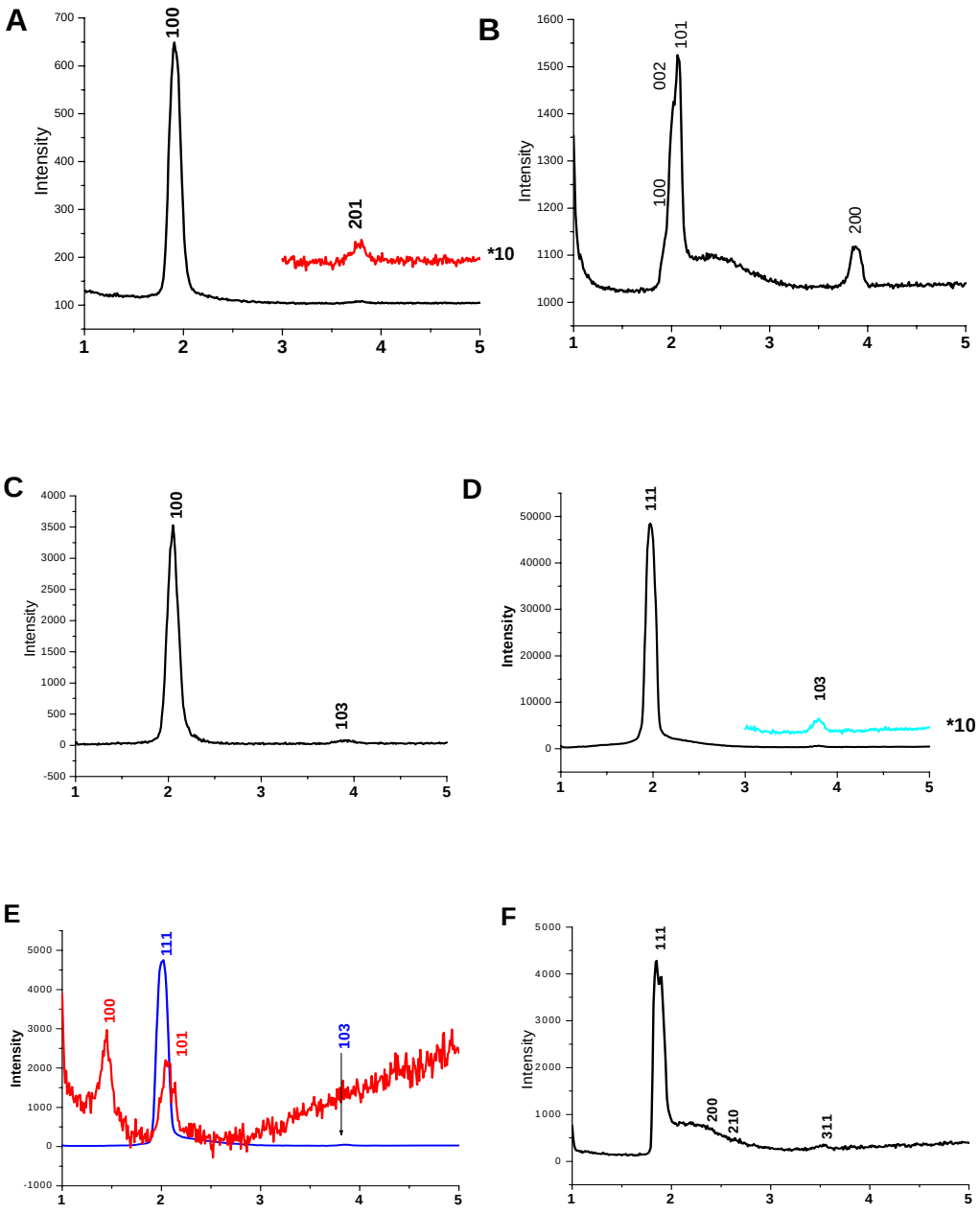

Figure 3.1.3. The $[Co(H_2O)_6](NO_3)_2$:$C_{12}EO_{10}$:HNO_3:TMOS samples with varying salt concentrations. A) Salt-free sample (silica without any salt addition), salt/surfactant mole ratio B) 0.4 assigned as hexagonal , C) 1.2 assigned as hexagonal , D)1.6 assigned as cubic, E)2.0 assigned as cubic, F) 3.0 assigned as cubic, X axis is the 2θ angle.

The reason for the change in the structure is the increase in ion density (ionic strength). The surface of a micelle is hydrophilic (aqua) and the inner core of the micelle is hydrophobic (organic). The Transition Metal Salt (TMS) ions cumulate more on the hydrophilic side of the micelles. As the amount of ions increases the ion density on the surfaces of the micelles increases. As a response the micelles try to increase their surface area to stabilize the structure. This is the main reason for the structure change in the salt:CnEOm:TMOS mesophases upon increasing the salt concentration. Sakya et al proposed a model for a similar phase change as shown in Figure 3.1.4 [69].

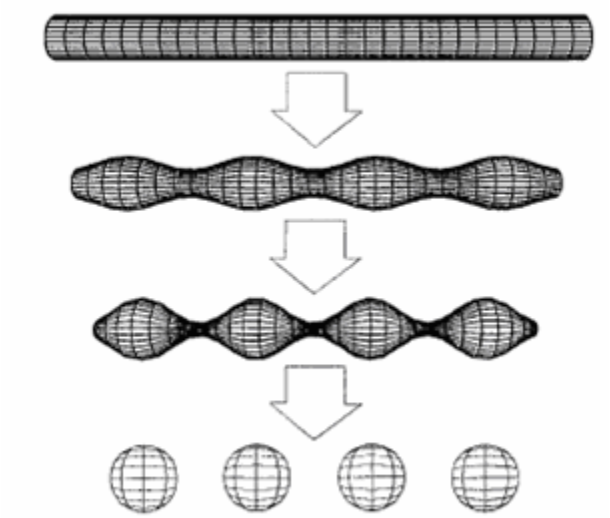

Figure 3.1.4. Suggested mechanism for the HI-Im3m transition. Undulations form in the hexagonal phase rods, with the rods being "pinched" at regular intervals, and this continues until the narrowest points along the rods are pinched off, and discrete micelles form.

The surface area increase can also be proven mathematically. If we assume that the radius of the cylinder and the spheres are the same and if we take also the volumes of the two are equal, then the formation of n spheres from a cylinder will increase the surface area of the structure. Here **r** is the radius of the cylinder and the spheres; **h** is the length of the cylinder.

$$\pi.r^2.h = n\ (4/3)\ \pi r^3$$

$$h=4n.r/3 \qquad \textbf{(Eq. 1)}$$

Surface area of n spheres vs. surface area of a cylinder (Both with the same radius)

$$n.\ 4\ \pi r^2 > 2\pi r(r+h) \quad \text{use } \textbf{Eq. 1}$$

$$2nr > r + 4nr/3$$

$$2nr/3 > r$$

$$2n/3 > 1$$

$$2n/3 > 1 \text{ for all n`s } n> 1$$

Beck et al [20] showed that in addition to isolation of the hexagonal MCM-41 class, other materials with different geometries could be synthesized. Some of these were prepared by varying the surfactant to silicon mole ratio. At a $C_{16}H_{33}(CH_3)_3N^+$/Si ratio of less than 1, the predominant product appears to be the hexagonal phase, MCM-41. As the $C_{16}H_{33}(CH_3)_3N^+$/Si ratio increases beyond 1, a cubic phase is produced [20]. In their work, a cationic surfactant was used. As the surfactant concentration is increased the ion density of the media increases (due to the surfactant charge) and upon surfactant concentration increase a phase transition from hexagonal to cubic is observed, similar to our case. Additionally, in another work, Zhao et al used C_nEO_m type non-ionic oligo surfactants for mesoporous silica synthesis and they observed that as they used a different surfactant with a larger number of ethoxy groups (larger m) there was a tendency of phase change from lamellar to hexagonal and then to cubic phase [29]. In Table 3.1.1 the surfactant types and the phases are given and the reason of this tendency of phase change is the same as ours.

Table 3.1.1. Physicochemical Properties of Mesoporous Silica (SBA) Prepared Using Nonionic Alkyl Poly(ethylene oxide) Surfactants [29].

surfactant	reaction temp	mesophase	d^* (Å)
$C_{16}EO_2$	RT	lamellar	64.3
$C_{12}EO_4$	RT	cubic	45.3 (44.7)
$C_{12}EO_4$	RT	lamellar	45.7
$C_{12}EO_4$	60 °C	L_3	42.4
$C_{16}EO_{10}$	RT	cubic	56.6 (47.6)
$C_{16}EO_{10}$	100 °C	hexagonal	64.1 (62.8)
$C_{16}EO_{20}$	RT	cubic	63.7 (49.6)
$C_{18}EO_{10}$	RT	$P6_3/mmc$	63.5 (51.0)
$C_{18}EO_{10}$	100 °C	hexagonal	77.4 (77.0)
$C_{18}EO_{10}$	RT	$P6_3/mmc$	49.1 (47.7)
$C_{12}EO_{23}$	RT	cubic	54.8 (43.3)

$^*d$(100) spacing or d value of characteristic reflection of the as-synthesized products; the number inside brackets is the d value after calcinations at 500 °C for 6 h

As the number of ethoxy groups increases the dipole charge increases and the charge density of the media causes the phase change. Another way of changing the surfactant is to increase the carbon chain length, the number n of C_nEO_m type of surfactants. As mentioned in the POM results increasing the carbon chain length makes a reverse phase transition from cubic to hexagonal.

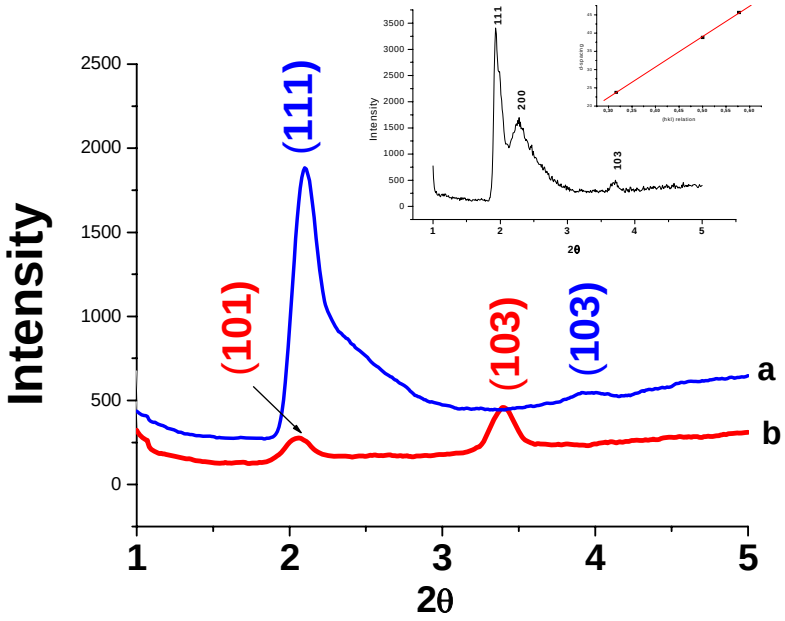

Figure 3.1.5. XRD patterns of samples with 2.0 moles $[Co(H_2O)_6](NO_3)_2$ salt /surfactant ratio with a) $C_{12}EO_{10}$ surfactant (dark under POM) b) $C_{18}EO_{10}$ surfactant (fan texture under POM). Inset is XRD of $[Co(H_2O)_6](NO_3)_2$ 2.0 salt /surfactant ratio with $C_{12}EO_{10}$ surfactant sample and the plot of the d-spacing versus (hkl) relation.

Figure 3.1.5 shows the XRD patterns of the two samples with the same (2.0) salt/surfactant ratio. The pattern of the sample with the $C_{12}EO_{10}$ surfactant is cubic with a parameter **a** equal to 85.6 Å. The pattern of the sample with the $C_{18}EO_{10}$ surfactant is 3D hexagonal with a parameter of **a** equal to 56.3 Å and **c**=91.9 with **c/a**=1.632. This kind of phase transition from hexagonal to cubic is also observed by Zhao et al [29]. The silica produced with $C_{16}EO_{10}$ is cubic at room temperature (RT) whereas the one with $C_{18}EO_{10}$ shows a hexagonal phase, Table 3.1.1 [29]. The reason for such kind of observations is explained by the equilibrium between the mesophases. If the hydrophilic content is increased the phase shifts from hexagonal to cubic and if the organic (hydrophobic) content is increased the reverse happens.

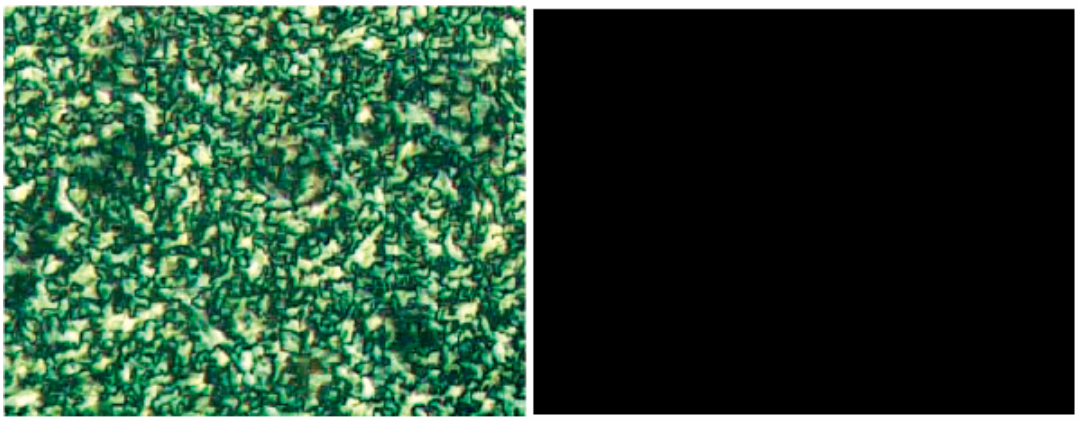

Figure 3.1.6. The POM images of $[Co(H_2O)_6](NO_3)_2$:C_nEO_m: HNO_3:TMOS system with salt/surfactant mole ratio of 2.0, **A)** with $C_{18}EO_{10}$ surfactant and **B)** with $C_{12}EO_{10}$ surfactant.

The POM images of these samples are shown in Figure 3.1.6. The POM images show parallel to the XRD data. As the carbon chain length is increased the structure turn from cubic to hexagonal. The POM images display this change by an image change from dark to fan-like texture (characteristic to 3D hexagonal mesophase).

3.1.3.2 The Mesostructured Silica Films of Co^{+2}-meso-SiO_2

The $[Co(H_2O)_6](NO_3)_2$:$C_{12}EO_{10}$:silica film samples were prepared by dip-coating and investigated by XRD technique. To the LC mixture of the salt and surfactant extra 9.0g of water was added and followed by the catalyst HNO_3 and silica source TMOS. The microscope slides were then dip coated from these solutions. The mesostructured silica was produced as a very thin film on the slides. The XRD patterns of the film samples display a single line. The thin films can only be detected by XRD but not under POM. This makes our assignment harder.

Figure 3.1.7 gives the patterns of dip coated samples with various salt/surfactant mole ratios. Single XRD line for each sample is not enough to assign a structure type and

a space group for these samples but we can say that the mesophase exists and the lines are all under 2 and above 1.5 2θ value.

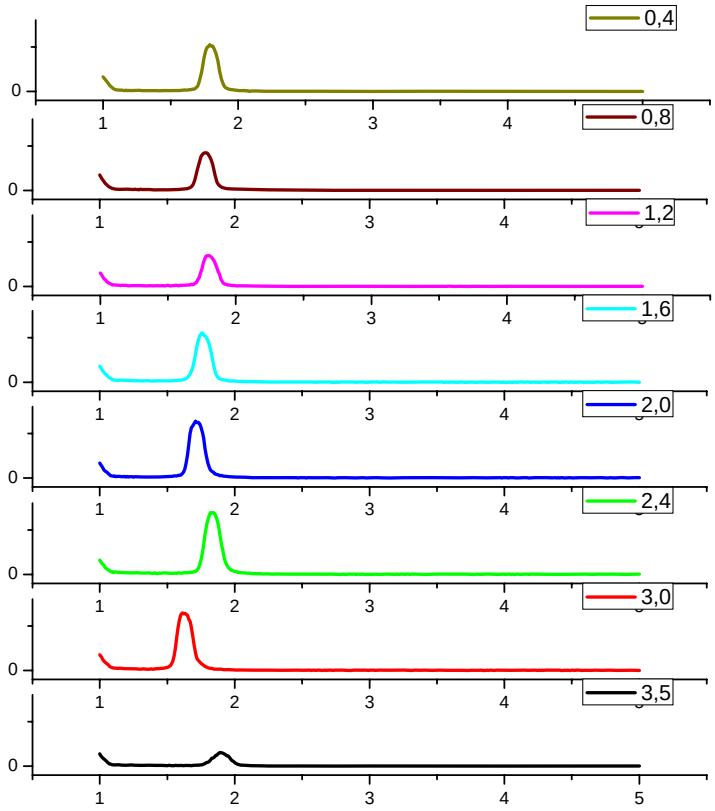

Figure 3.1.7. XRD patterns of dip-coated $[Co(H_2O)_6](NO_3)_2$:$C_{12}EO_{10}$:Silica samples with various salt/surfactant mole ratios.

3.1.3.3 Monoliths of $[Co(H_2O)_6](ClO_4)_2$:$C_{12}EO_{10}$:$HClO_4$:TMOS systems

We also investigated the effect of the $[Co(H_2O)_6](ClO_4)_2$ salt on the silica products. The samples with salt/surfactant ratio 0.2, 0.4, 0.6, 0.8, and 1.0, 2.0 and 3.0 were investigated. The $[Co(H_2O)_6](ClO_4)_2$:$C_{12}EO_{10}$:$HClO_4$:TMOS systems are found to be stable up to 1.0 salt/surfactant ratio. Above 1.0 mole ratio the salt crystallizes out and the mesophase does not exist over 2.0 mole ratio. The POM images and the XRD patterns were recorded for the samples. The POM images displayed no image (dark) over 0.2

mole ratio. Although the intensity of the diffraction lines decreased by the time, the mesophase still existed after two days, Figure 3.1.8

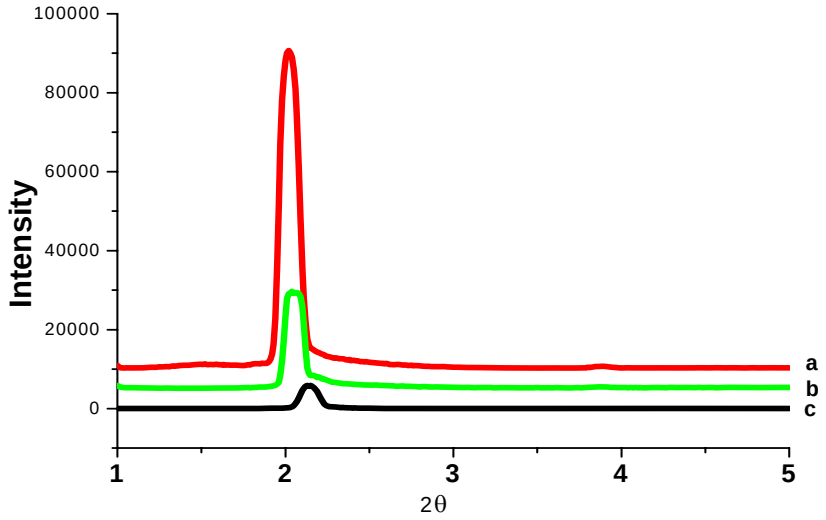

Figure 3.1.8. The XRD spectra of the $[Co(H_2O)_6](ClO_4)_2$**:**$C_{12}EO_{10}$:$HClO_4$:TMOS system with 0.2 mole ratio by time, a) in15 minutes, b) after 1 day, c) after 2 day

The XRD patterns gets broader over 0.4 mole ratio. This indicates that above 0.4 mole ratio the structural order decreases and the XRD patterns looks like the XRD pattern of a powder (see Figure 3.1.9).

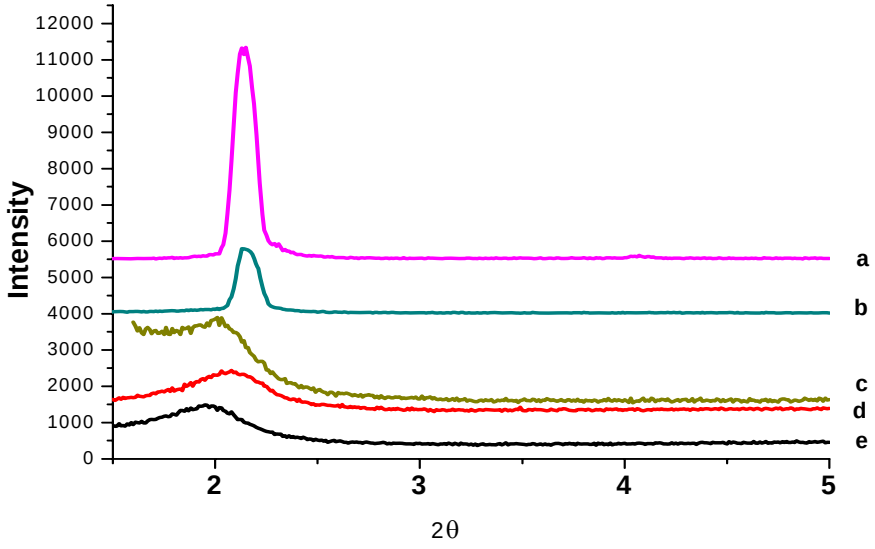

Figure 3.1.9. The XRD patterns of 1 day aged samples of $[Co(H_2O)_6](ClO_4)_2$:$C_{12}EO_{10}$:$HClO_4$:TMOS system with mole ratios a) 0.2, b) 0.4, c)0.6, d)0.8, e)1.0

For the preparation of the perchlorate silica samples, $HClO_4$ acid was used as a catalyst therefore the system already had the perchlorate ion before adding salt. The effect of the ClO_4^- ion from the acid and the salt sources were studied by changing the amount of the acid in the salt free mixtures. The mixture contained 1.00g water:1.00g surfactant:1.70g TEOS and various amounts of $HClO_4$ between 0-0.1grams. Formation of LC mesophase by surfactant and water is a process which competes with silica polymerization. So the silica formation should be completed after the mesophase is formed and before the water evaporates. The amount of acid becomes important because it determines the rate of the silica polymerization. If the silica polymerization is slow in salt free samples, as water evaporates the mesophase collapses so silica polymerization cannot be templated by LCT and eventually silica becomes disordered. If the silica polymerization is fast then it will polymerize before the LC mesophase is formed so silica will again be disordered.

In the case of 0.03 and 0.06g of acid the polymerization process is not fast enough so the texture under POM is first birefringent and after some time (~20min) the texture turns dark. The XRD line which is very sharp at the beginning is also broadened over 20 minutes. This is due to the slow polymerization of the silica. The initial structure at the beginning is due to LC mesophase so it is hexagonal. Therefore we observe a fan texture and a sharp XRD line but the amount of acid used is not enough to polymerize the silica at the time before water evaporates. That is why the structure of the LC cannot be preserved. As water evaporates, the LC mesophase dissipates and silica becomes disordered, therefore the XRD pattern becomes broader in time and POM image becomes dark, see Figure 3.1.10.

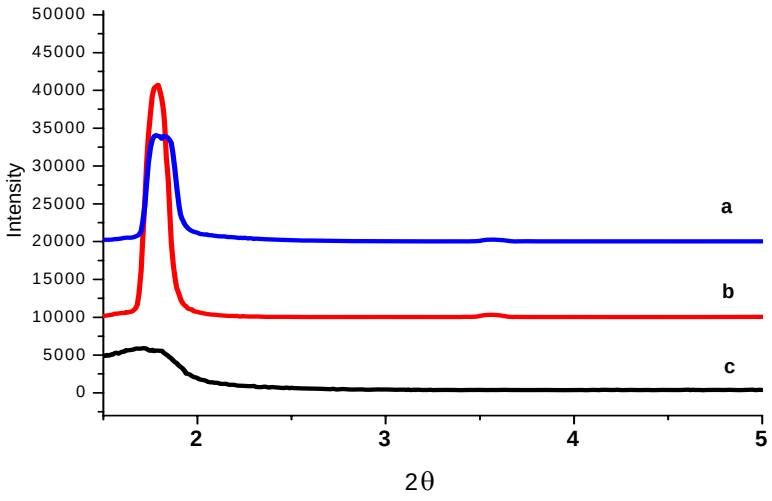

Figure 3.1.10. The XRD patterns of salt free-samples of $C_{12}EO_{10}$:$HClO_4$:TMOS system with 0.060 g $HClO_4$ by time a) immediately after preparation, b)10 minutes, c) 20 minutes.

However as 0.10 gram of acid is added the sharp diffraction line and the bright fan texture are stable. It means that 0.10 gram acid is an optimum amount for the silica polymerization and the LC formation so the structure is preserved by the solid silica after water evaporation. In Figure 3.1.11, the XRD patterns for the 0.10 gram acid added samples are given.

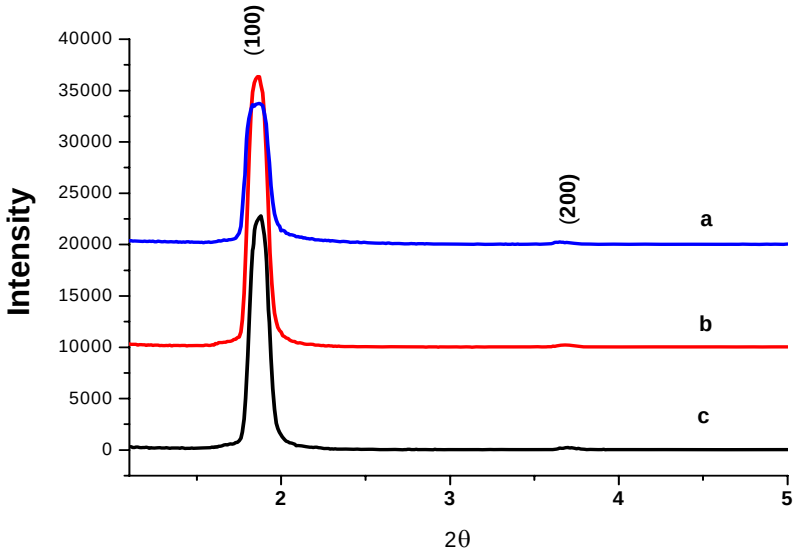

Figure 3.1.11. XRD patterns of salt free-samples of $C_{12}EO_{10}$:$HClO_4$:TMOS system with 0.1 g $HClO_4$ by time a) immediately, b) 20 minutes, c) 1 day after preparation.

The XRD pattern of the sample prepared using 0.10 g $HClO_4$ displays diffraction lines due to (100) and (200) planes of the hexagonal structure. Similarly the 0.03g and 0.06g $HClO_4$ added samples also display lines of hexagonal structure immediately after preparation of the samples but after a while the phase vanishes. Figure 3.1.12 shows the XRD patterns for 0.03 g $HClO_4$ added $C_{12}EO_{10}$:$HClO_4$:TMOS samples and their changes by aging.

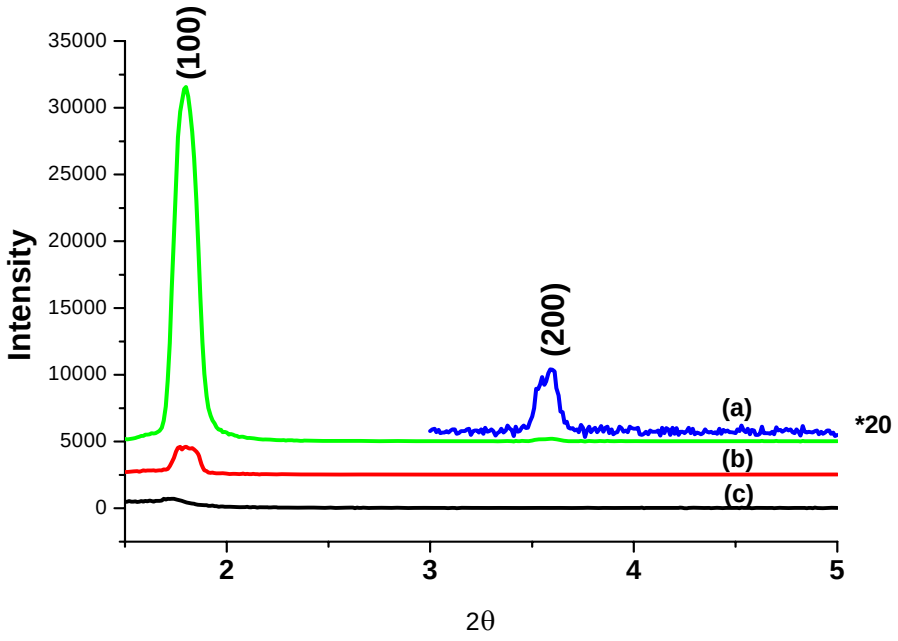

Figure 3.1.12. XRD patterns of salt free-samples of $C_{12}EO_{10}$:$HClO_4$:TMOS system with 0.03 g $HClO_4$ by time a) immediately, b) 10 minutes, c) 2 hours after preparation. The hexagonal (100) and (200) diffraction lines are shown for (a).

3.1.4 FT-IR and Micro-RAMAN SPECTRAL ANALYSIS

Although the NO_3^- ion is less salting-in than the ClO_4^- ion according to the Hofmeister series, nitrate salts are more soluble than perchlorate salts. If the salts used were alkali metal salts instead of TMSs, there would be no deviation from the Hofmeister series. The coordination of the NO_3^- ion to the transition metal cation is the key point for such a deviation from the Hofmeister series. Coordination of NO_3^- ion to the transition metal cation can be easily detected by using FT-IR and micro-Raman spectroscopy. Figure 3.1.13 shows FT-IR spectra of $NaNO_3$ salt and the

$[Co(H_2O)_6](NO_3)_2$:$C_{12}EO_{10}$:Silica system with 1.2 salt/surfactant ratio recorded immediately, 3 hours after preparation and 1 day after preparation. In the spectrum of $NaNO_3$ the broad peak

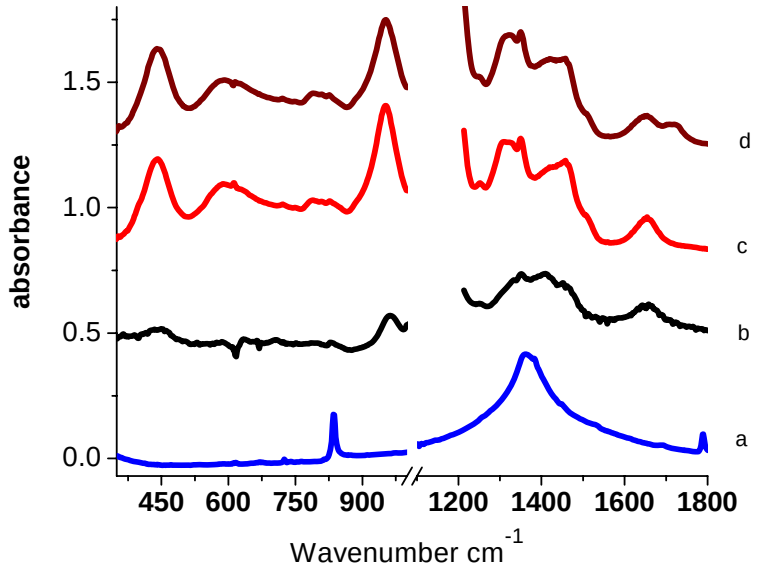

Figure 3.1.13. The FT-IR spectra of $[Co(H_2O)_6](NO_3)_2$:$C_{12}EO_{10}$:Silica system with 1.2 salt/surfactant ratio and solid $NaNO_3$. a) $NaNO_3$, b) $[Co(H_2O)_6](NO_3)_2$:$C_{12}EO_{10}$:Silica system immediately after preparation, c) 3 hours after preparation d) 1 day after preparation.

at 1365 cm^{-1} belongs to the free nitrate but when the nitrate ion is coordinated to the metal cation coordination lowers the symmetry of the free nitrate ion from the D_{3h} to C_{2v} point group; therefore, the degeneracy of the IR active E` modes of the free nitrate ion (asymmetric and bending modes) is lifted and split into two non-degenerate IR-active B_2 and A_1 modes [49,70]. Therefore, two peaks are observed around the free-nitrate ion-frequency regions in the IR spectrum. In the $[Co(H_2O)_6](NO_3)_2$:$C_{12}EO_{10}$:Silica FT-IR spectra, the single nitrate peak is splitted into two peaks at 1317 and 1455 cm^{-1}. The splitting energy provides information regarding the type of coordination and is relatively smaller in the unidentate coordination than in the bidentate coordination in similar complexes [70].

The coordination of NO_3^- ion to the transition metal cation can also be detected by the micro-Raman spectroscopy. Figure 3.1.14 shows the micro-Raman spectrum of single $[Co(H_2O)_6](NO_3)_2$ to be a reference and the spectra of $[Co(H_2O)_6](NO_3)_2$:$C_{12}EO_{10}$:Silica systems with various salt/surfactant mole ratios

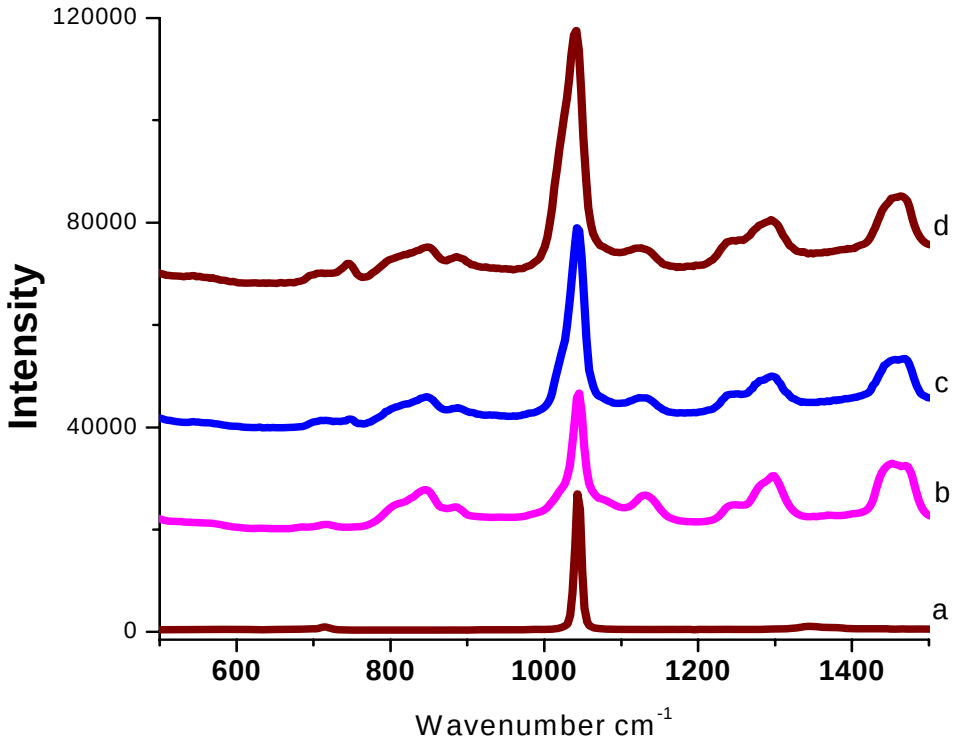

Figure 3.1.14. Micro-Raman Spectra of a) $[Co(H_2O)_6](NO_3)_2$ and $[Co(H_2O)_6](NO_3)_2$:$C_{12}EO_{10}$:Silica system with salt/surfactant ratios b)0.6, c)1.4, d) 1.6.

The free nitrate symmetric stretching peak in the micro-Raman spectra is observed at 1042 cm^{-1} however as the concentration of the salt increases a shoulder at 1020 cm^{-1} appears [40]. The shoulder at 1020 cm^{-1} is better detected at high concentrations of salt (especially at 1.6 and 2.0 mole ratios). The reason for the shoulder peak is the coordination of NO_3^- ion to the metal cation. As NO_3^- ion is coordinated to the metal cation, the nitrate$^-$ peak shifts to a lower energy.

CHAPTER 2

3.2.1. LC Mesophases of Pluronics

The LC mesophases of L64 ($PEO_{13}PPO_{30}PEO_{13}$), P65 ($PEO_{20}PPO_{30}PEO_{20}$) and P123 ($PEO_{20}PPO_{70}PEO_{20}$) with water and water/oil are known in the literature [71-77]. However, this is the first time pluronics are shown to have LC mesophases without any additional water. In this work we found out that Pluronics show LC behavior in the presence of transition metal aqua complexes. The LC mesophase is observed in both H_2O:$[Zn(H_2O)_6](NO_3)_2$:Pluronic and $[Zn(H_2O)_6](NO_3)_2$:Pluronic systems. In the formation of the mesophase the coordinated water molecules play an important role. They interact with the head groups [(PEO) units] of the surfactant molecules and act as structure-directing agents. This formation of TMS:Pluronic LC mesophases is similar to the LC mesophases of the TMS:C_nEO_m systems, in which oligo(ethylene oxide) type surfactants were used instead of Pluronics [40,41,49,61]. Mainly $[Zn(H_2O)_6](NO_3)_2$ was used as a salt source for the LC mesophases of L64, P65, and P123. The behavior of the structures was extensively investigated in various TMS/Pluronics mole ratios. Although only the existence of LC mesophases for the $[Zn(H_2O)_6](NO_3)_2$:Pluronic and $[Zn(H_2O)_6](ClO_4)_2$:Pluronic systems are shown here, it could be extended to most of the first and some of the second row transition metal nitrates, perchlorates and some chlorides [40,41,49,61].

The LC mesophase of the $[Zn(H_2O)_6](NO_3)_2$:L64 system is observed between 2.0 and 5.0 $[Zn(H_2O)_6](NO_3)_2$ to L64 mole ratio (on average these mole ratios correspond to 13 and 5 CH_2CH_2O units of L64 per Zn(II) ion, or 16.5 and 33.1 w/w % $[Zn(H_2O)_6](NO_3)_2$/L64, respectively). In LC $[Zn(H_2O)_6](NO_3)_2$:Pluronic systems the mesophase is stable up to a mole ratio of 6 in the P65 and a mole ratio of 15 in the P123 surfactants. At higher salt concentrations, the systems slowly draw away the salt crystals within a few weeks. However, freshly prepared samples are homogeneous and the low and intermediate salt containing samples are stable for months (no salt crystals are

observed over 10 months by means of microscopy, spectroscopy and XRD). Particularly systems with salt/pluronic mole ratio of 2-3 in L64, 2-4 in P65 and 2-7 in P123 are stable for months. It is also observed in the LC mesophases of the TMS:Pluronic systems that as the molecular weight of the pluronic increases the amount of salt it can contain also increases. Note that the average molecular weights of the Pluronics are as follows: P123=5800g/mole, P65 =3400g/mole and L64= 2900g/mole, increasing in the following order L64< P65< P123.

3.2.2.XRD and POM Results of LC mesophases of H_2O:$[Zn(H_2O)_6](NO_3)_2$:Pluronic(L64, P65, P123) Systems

Although the mesophases of H_2O:$[Zn(H_2O)_6](NO_3)_2$:L64 (Figure 3.2.1) and H_2O:$[Co(H_2O)_6]$ $(NO_3)_2$:L64 diffract at low angles, the diffraction line(s) eventually disappears with complete water evaporation or by aging. If the $[Zn(H_2O)_6](NO_3)_2$ or $[Co(H_2O)_6](NO_3)_2$ salts are dissolved directly in L64 (with no extra water) the homogenized mixtures do not diffract at low angles. However, when a shear force is applied, the samples obtained after complete evaporation of the free water and water free prepared samples both diffract at low angles. It means that the LC mesophase exists both in the presence and the absence of the free water in the $[Zn(H_2O)_6](NO_3)_2$:L64 systems. However, the mesophase is disordered (worm-like) and can not be detected by XRD without the shear force which orients the mesophase. The mesophase of TMS:L64 is sensitive to the amount of salt and water. However, it is difficult to determine the structure of the mesophases due to the lack of higher order diffraction lines, Figure 3.2.1.

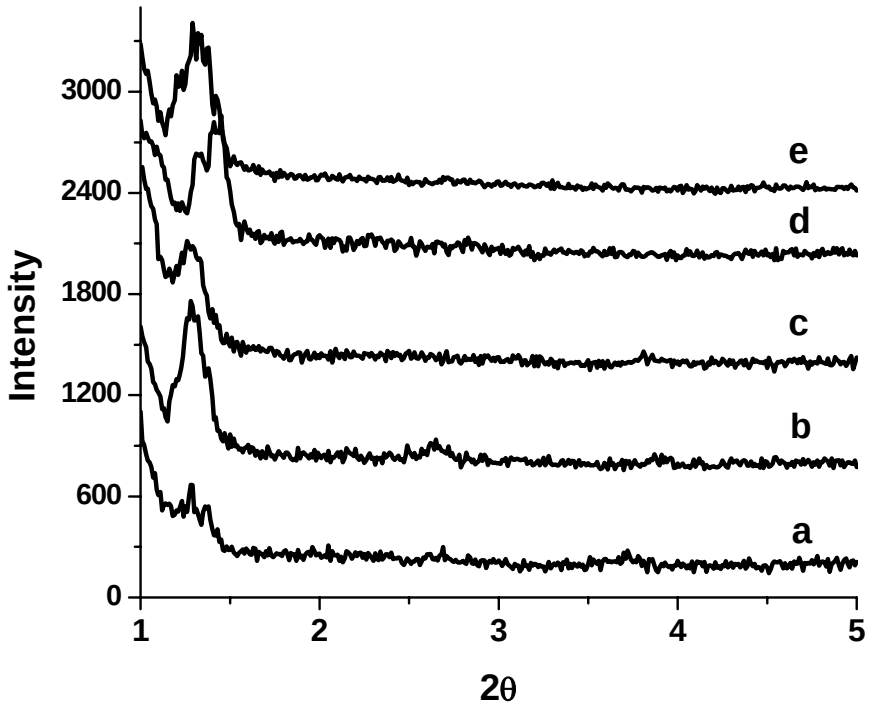

Figure 3.2.1. The XRD patterns of $[Zn(H_2O)_6](NO_3)_2$:L64 with salt-to-L64 mole ratios of a) 2.25, b) 2.75, c) 3.25, d) 3.75 and e) 4.0.

The key feature of $[Zn(H_2O)_6](NO_3)_2$:P65 and $[Zn(H_2O)_6](NO_3)_2$:P123 samples is that they are more ordered and do not require shear force to be observed with XRD. The $[Zn(H_2O)_6](NO_3)_2$:P65 samples diffract at low angles with higher order diffraction lines. The XRD and POM data for the mesophase of $[Zn(H_2O)_6](NO_3)_2$:P65 samples can be assigned as of a 3D hexagonal mesophase . Figure 3.2.2 shows the XRD patterns of LC $Zn(H_2O)_6](NO_3)_2$:P65 samples with 3, 4, 5, and 6 $[Zn(H_2O)_6](NO_3)_2$/P65 mole ratios in the 2θ range of 1.0 to 5.0 and the POM image of 6 $[Zn(H_2O)_6](NO_3)_2$/P65 mole ratio, Figure 3.2.3. The texture in the POM image along with the assignments of the XRD proves the existence of the 3D hexagonal mesophase, Figure 3.2.3.

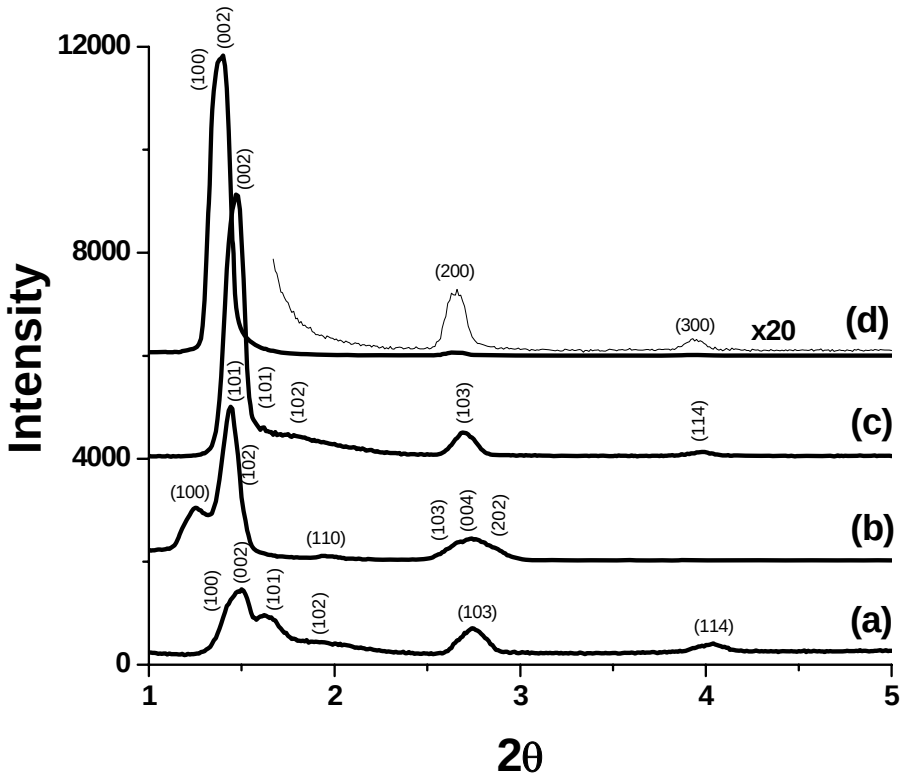

Figure 3.2.2. The XRD patterns of $[Zn(H_2O)_6](NO_3)_2$:P65 with salt surfactant mole ratios of (a) 3.0, (b) 4.0 (c) 5.0, (d) 6.0

Figure 3.2.3. POM image of the $[Zn(H_2O)_6](NO_3)_2$:P65 with salt/surfactant mole ratio 6.

The assigned diffraction lines and the d-spacings of the $[Zn(H_2O)_6](NO_3)_2$:P65 LC mesophase for different salt/pluronic mole ratios are shown in Table 3.2.1. For the $[Zn(H_2O)_6](NO_3)_2$:P65 system the unit cell parameter **a** varies between 70.3 and 79.7 Å. The XRD pattern of a sample with 3 mole ratio displays up to 6 diffraction lines in the 2θ range of 1.0^o-5.0^o, Figure 3.2.2 (a). These lines are indexed as the (100), (002), (101), (102), (103), and (114) reflections of the $P6_3/mmc$ space group of 3D hexagonal mesophase with unit cell parameters of **a** = 71.2 Å and **c** = 116.4 Å with **c/a** ratio of 1.635. The unit cell parameters for the other samples are as follows: for 4 mole ratio

a=79.7Å and c=131.2Å with c/a=1.646, for 5 mole ratio a=73.1, c= 119.4, c/a= 1.633 and for 6 mole ratio a=76.6Å, c=125.2Å, c/a=1.635.

3 mole	ratio	4 mole	ratio	5 mole	ratio	6 mole	ratio
d (Å)	**(hkl)**	**d (Å)**	**(hkl)**	**d (Å)**	**(hkl)**	**d (Å)**	**(hkl)**
61.2	(100)	69.0	(100)	63.3	(100)	66.3	(100)
58.2	(002)	60.9	(101)	59.7	(002)	62.6	(002)
54.5	(101)	47.0	(102)	55.9	(101)	33.2	(200)
43.0	(102)	40.4	(110)	43.5	(102)	22.1	(300)
32.2	(103)	36.7	(103)	32.8	(103)		
22.2	(114)	32.8	(004)	22.1	(114)		
		30.9	(202)				

Table 3.2.1. d-spacing and (hkl) values obtained from different mole ratios of the $[Zn(H_2O)_6](NO_3)_2$:P65 LC mesophase using the diffraction patterns in Figure 3.2.2.

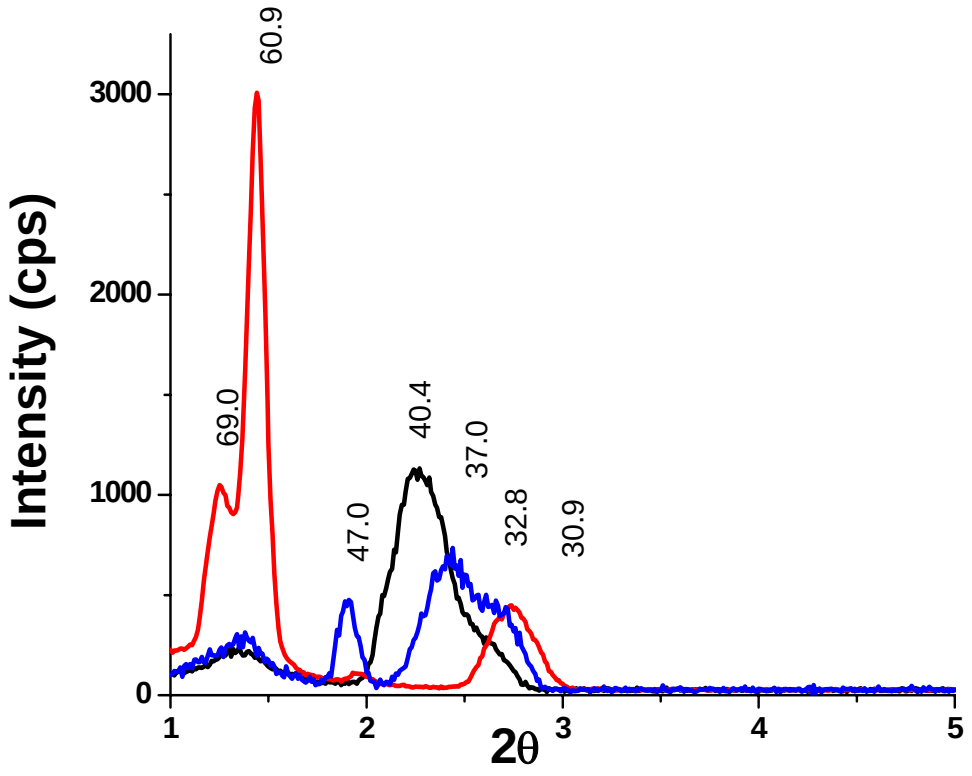

Figure 3.2.4. The XRD patterns of the LC $[Zn(H_2O)_6](NO_3)_2$:P65 system with a 4.0 mole ratio at 3 different orientation (sample is 1 day old).

The XRD pattern of the $[Zn(H_2O)_6](NO_3)_2$:P65 sample with 4 mole ratio is sensitive to the rotations in the beam-detector axis. The diffraction patterns for this sample were recorded by rotating the sample in the beam-detector axis and as a response to rotation different reflections became intense at different orientations of the sample. However, all the diffraction lines could be indexed as the reflections of the 3D hexagonal mesophase. Figure 3.2.4 shows the XRD pattern of the sample with 4.0 mole ratio. The XRD pattern displays up to 7 diffraction lines. Here the d-spacing and (hkl) plane relation formula for the hexagonal structures $[1/d^2 = 4/3(h^2+hk+k^2)/a^2 + l^2/c^2]$ was rearranged by taking c/a ratio of 1.633 as $d = a[8/(10.667(h^2+hk+k^2)+3l^2)]^{1/2}$, and was used to prove the existence of the 3D hexagonal structure.

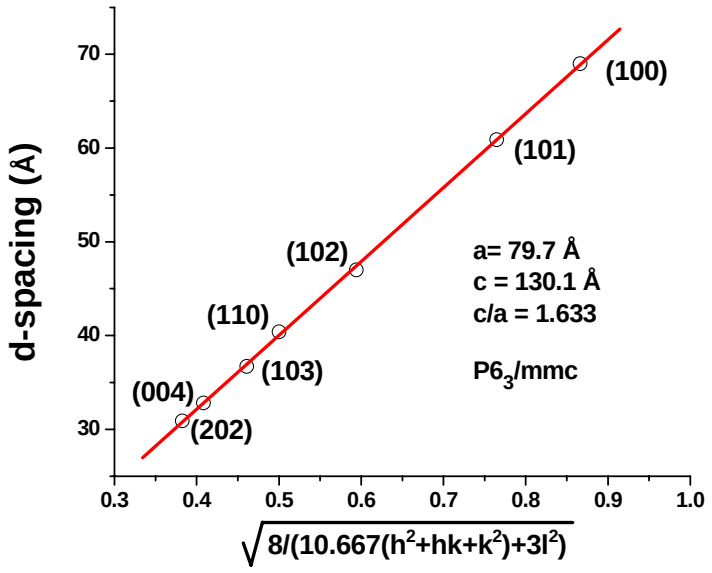

Figure 3.2.5. The the plot of d-spacing versus (hkl) relationship of the 3D hexagonal structure. The slope gives the parameter **a** which is 79.7Å.

The plot of the d-spacing versus $[8/(10.667(h^2+hk+k^2)+3l^2)]^{1/2}$ gives a linear fit with the slope equal to unit cell parameter **a**=79.7Å, Figure 3.2.5. In the sample with 6 $[Zn(H_2O)_6](NO_3)_2$/P65 mole ratio the hexagonal mesophase becomes highly oriented. The hexagonal mesophase of the sample with a $[Zn(H_2O)_6](NO_3)_2$/P65 mole ratio of 6 has 4 diffraction lines of (100), (002) and (200) and (300) planes with unit cell parameters **a** = 76.6 Å and **c** = 125.2 Å and **c/a** = 1.635, Figure 3.2.2 (d). The fan-like

POM image between the crossed polarizers is also consistent with the hexagonal mesophase, Figure 3.2.3.

There is a rich structural chemistry of $[Zn(H_2O)_6](NO_3)_2$:P123 LC mesophases. They are also sensitive to both $[Zn(H_2O)_6](NO_3)_2$ salt and water concentration of the media. Figure 3.2.6 shows the XRD patterns of the LC $[Zn(H_2O)_6](NO_3)_2$:P123 mesophases of various mole ratios after complete water evaporation. The LC mesophase of $[Zn(H_2O)_6](NO_3)_2$:P123 appears at a $[Zn(H_2O)_6](NO_3)_2$ to P123 mole ratio of around 2 and it is stable up to a mole ratio of 15, Figure 3.2.6. The XRD pattern of the $[Zn(H_2O)_6](NO_3)_2$:P123 system with 2 TMS-to-P123 mole ratio is hard to assign but the sample with 15 mole ratio diffracts at higher orders and it well suits cubic structure. In one orientation the lines can be assigned for (200) and (400) plane while in another orientation the lines suit well with the (100), (300), (500) planes.

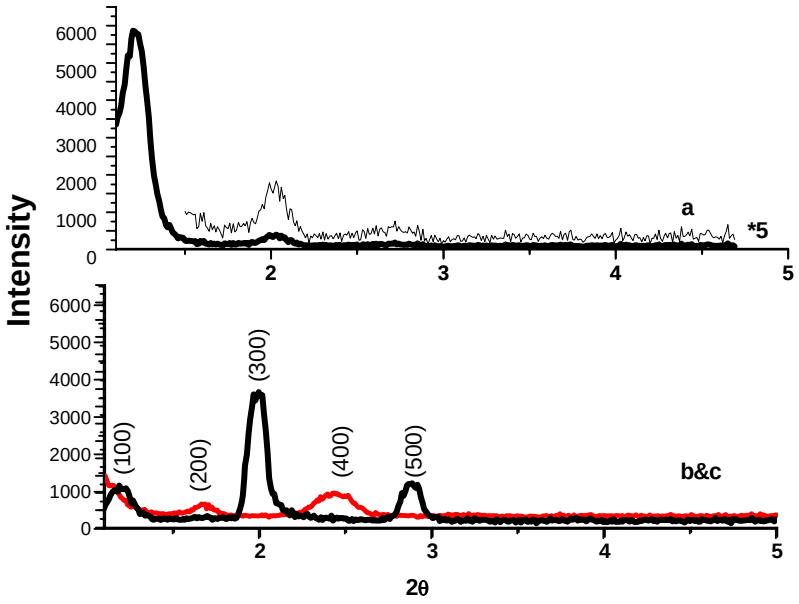

Figure 3.2.6.The XRD patterns of $[Zn(H_2O)_6](NO_3)_2$:P123 LC mesophases with a) 2, b) and c) 15 salt-to-P123 mole ratios.

In the LC $[Zn(H_2O)_6](NO_3)_2$:P123 mesophase, three different structure types, 2 cubic and a tetragonal mesophases have been identified, see Figure 3.2.7 to 3.2.9. Figure 3.2.7 displays the XRD patterns of $[Zn(H_2O)_6](NO_3)_2$:P123 with 4, 6, 7 and 9

$[Zn(H_2O)_6](NO_3)_2$/P123 mole ratios which can be indexed to a tetragonal (see also Figure 3.2.8), tetragonal, cubic and cubic mesophases, respectively. Here we observe that for the higher molar ratios the structure tends to be cubic, as the salt concentration increases. This is similar to the oligo(ethylene oxide) LC and silica systems [40]. Note also that the tetragonal mesophase has not been observed before in such systems.

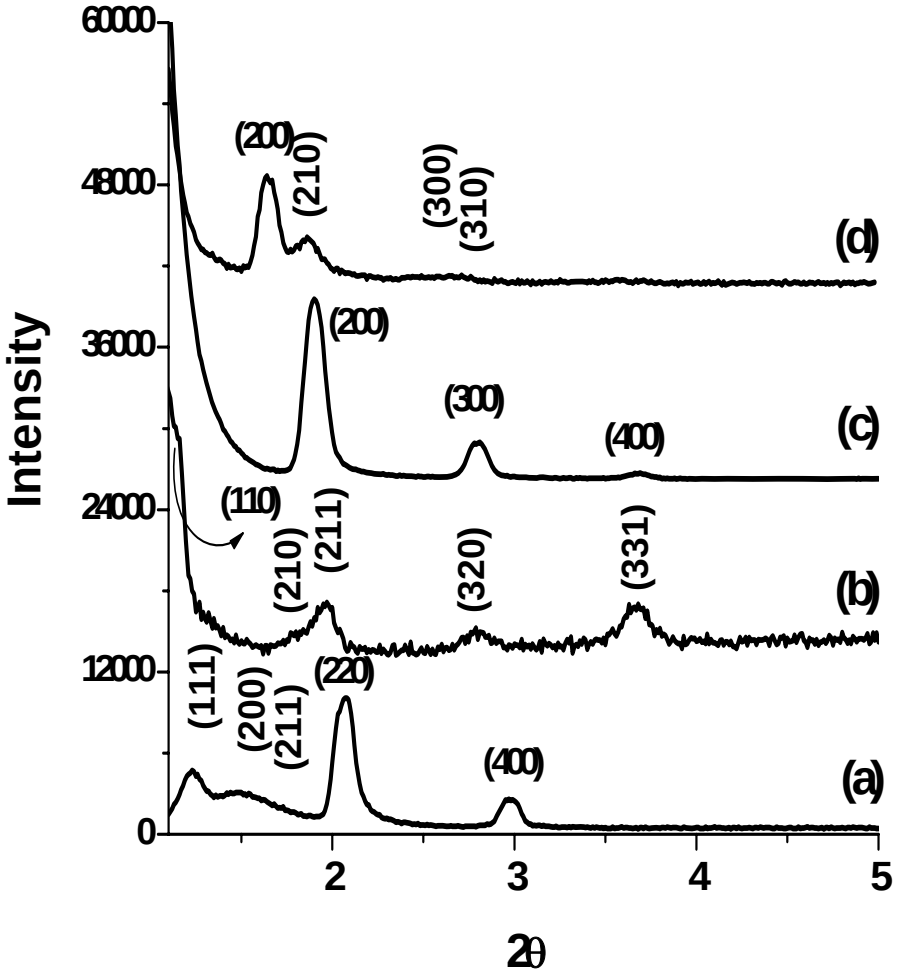

Figure 3.2.7. The XRD patterns of the $[Zn(H_2O)_6](NO_3)_2$:P123 systems after complete water evaporation with $[Zn(H_2O)_6](NO_3)_2$/P123 mole ratio of (a) 9.0 (b) 7.0, (c) 6.0 and (d) 4.0.

The H_2O:$[Zn(H_2O)_6](NO_3)_2$:P123 phase is disordered before the water evaporation. However as the water evaporates a well ordered tetragonal H_2O:$[Zn(H_2O)_6](NO_3)_2$:P123

mesophase is observed at a $[Zn(H_2O)_6](NO_3)_2$/P123 mole ratio of 4 . The tetragonal mesophase has also been observed at 5 and 6 salt-to-P123 mole ratios, Figure 3.2.8. In the water containing samples, the water concentration is unknown when the low angle diffraction lines appear and as the water evaporates(or by time) the XRD lines shift to higher angles which indicates that with the removal of water in the structure the mesophase shrinks. Almost all-excess water evaporates in 15-20 minutes (in thin film samples and longer in thicker samples), after all water evaporates the shrinkage stops and only changes in the XRD patterns are the intensities in the diffraction lines.

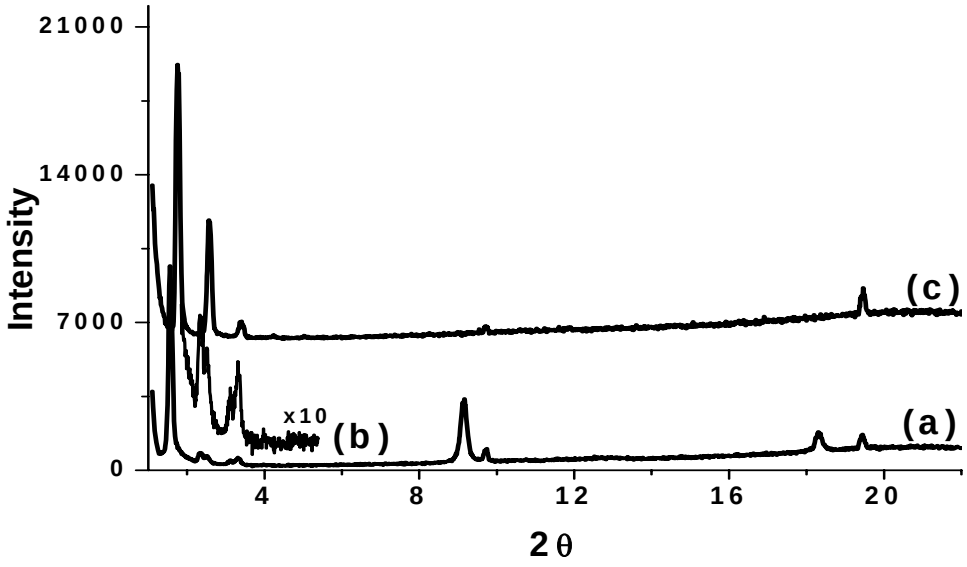

Figure 3.2.8 The XRD patterns of the LC $[Zn(H_2O)_6](NO_3)_2$:P123 systems (a) with a 4.0 salt to P123 mole ratio (b) is the same pattern as of (a) that is multiplied by 10 in the region of 2.0^o-5.5^o and (c) with a 6.0 salt to P123 mole ratio.

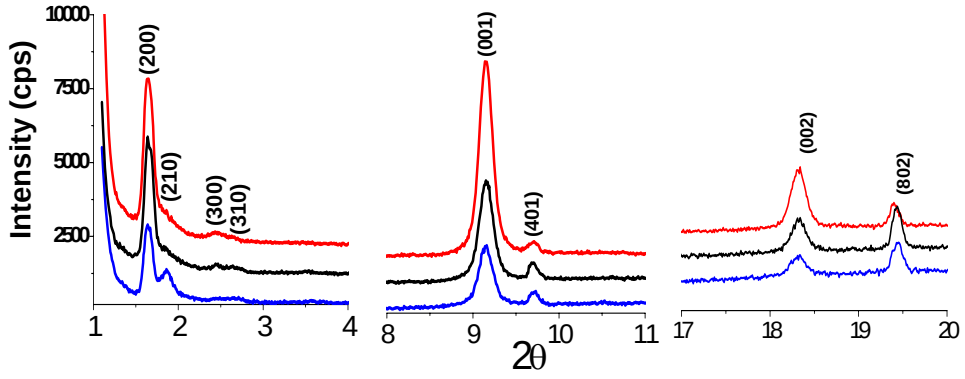

Figure 3.2.9. XRD pattern of 4.0 $[Zn(H_2O)_6](NO_3)_2$:P123 after one week of water evaporation, measured in different orientation (top) rotated to right (middle) as packed (bottom) rotated left with respect to beam-detector axis.

(a)		(b)	
d-spacing(Å)	(hkl)	d-spacing (Å)	(hkl)
57.0	(200)	50.4	(200)
37.6	(300)	34.2	(300)
35.0	(310)	26.1	(400)
28.5	(400)	20.8	(500)
27.1	(410)	17.6	(600)
26.5	(330)	9.10	(401)
9.70	(001)	4.55	(802)
9.16	(401)		
4.85	(002)		
4.58	(802)		

Table 3.2.2. The d-spacing and (hkl) values evaluated from the XRD two patterns of $[Zn(H_2O)_6](NO_3)_2$:P123 systems with a)4 and b) 6 mole ratio,(XRD patterns in Figure 3.2.8).

In the tetragonal mesophase, the d-spacing of the diffraction lines correlate well with $1/(h^2+k^2)^{1/2}$ and the plot of d-spacing versus $1/(h^2+k^2)^{1/2}$ gives a linear line with a slope equal to unit cell parameter, **a**. Note that the sample with a 4.0 mole ratio also diffracts at higher angles, between 9 and 20, 2θ. The XRD patterns of a one week old sample of 4.0 mole ratio were recorded in different orientations with respect to source-detector axis in the 1 to 20, 2θ range, Figure 3.2.9. Note also that the high angle

diffraction lines respond to the rotation of the sample, this indicates that these lines are also due to the planes of the LC mesophase. This sample diffracts up to 8 lines at 53.8, 47.2, 35.9, 33.7, 9.7, 9.1, 4.8 and 4.5 Å d-spacings, these lines correspond to the (200), (210), (300), (310), (001), (401), (002) and (802) planes, respectively, Figure 3.2.8. The unit cell parameters that are evaluated from the diffraction patterns are as follows, **a** = **b** = 106.7 Å and **c** = 9.7 Å. The **a** and **b** parameters were obtained from the plot of d-spacing versus $1/(h^2+k^2)^{1/2}$ using the (200), (210), (300) and (310) diffraction lines. Note that only (hk0) lines are used for the **a** and **b** parameters whereas the c parameter was found by using the $1/d^2= (h^2+k^2)/a^2 + (l^2/c^2)$. The unit cell parameters indicate that there is a molecular ordering along the c-axis in the tetragonal mesophase, Figures 3.2.8 and 3.2.9. This shows that the columnar tetragonal mesophase is also crystalline along the column axis.

When only the low angle lines are considered the sample with 6 mole ratio diffracts like a highly oriented lamellar mesophase (as observed from the first 5 lines). The low angle lines can be indexed as the (200), (300), (400), (500), and (600) reflections, like in lamellar mesophases. However, the diffraction lines at higher angles due to (401) and (802) reflections obviously indicate that the structure is tetragonal. It is also important to note that smearing the sample with a glass plate by applying a weak force can destroy the orientation of the sample with a 6 salt-to-P123 mole ratio. The smeared sample also displays a reflection due to the (001) plane (not shown).This means that in the sample there is also an orientation along the column axis. Another important point which suggests the existence of the tetragonal phase is that the smeared or scratched sample (using a sharp tip) shows birefringence between the crossed polarizer indicating that the mesophase is anisotropic (consistent with the assignment).

The $[Zn(H_2O)_6](NO_3)_2$:P123 system displays cubic mesophase in a salt-to-P123 mole ratio of around 7.0 and keeps the cubic structure at higher salt concentrations. The sample with a 7.0 mole ratio displays diffraction lines at 75, 47.4, 43.7, 31.5 and 24.1 Å d-spacings, corresponding to (110), (210), (211), (321), (331) lines, respectively. These lines belong to the Pm3n space group with a unit cell parameter, **a** = 103.8 Å. The unit cell parameters are evaluated from the slope of the plot of d-spacing versus

$1/(h^2+k^2+l^2)^{1/2}$, see Figure 3.2.7 (b). However, at higher salt concentrations the cubic phase crystallizes into different space groups. For instance at a 9 salt-to-P123 mole ratio, the diffraction pattern displays lines due to the (111), (200), (211) and (400) planes of Pn3m space group at 67.7, 58.5, 47.8 and 29.2 Å, respectively. The unit cell parameters for the sample with 9 salt-to-P123 mole ratio are relatively larger, **a** = 117.2 Å. The tendency of the system to increase its size (unit cell parameters) as the salt concentration increases is a result of the charge density increase.

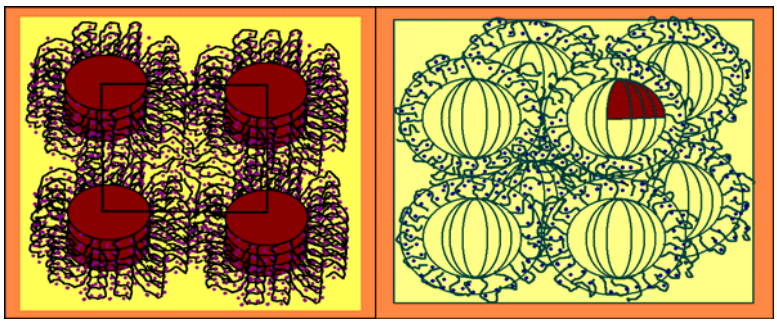

Figure 3.2.10. Schematic representation of the $[Zn(H_2O)_6](NO_3)_2$:P123 mesophases (left is the tetragonal and right is the cubic mesophases), small dots are representing the ions in the media, hairy parts represent PEO and the dark red parts represents the PPO units of P123).

A schematic representation of a tetragonal and cubic mesophases of $[Zn(H_2O)_6](NO_3)_2$:P123 are shown in Figure 3.2.10. At higher salt concentrations the phase becomes more disordered and it leaches out some of the salt crystals.

A 3D hexagonal mesophase is a commonly observed structure in mesostructured materials where the non-ionic surfactants are used as a templating agent [29,30,78]. However, the 3D hexagonal and a tetragonal mesophase with a well defined **c** parameter are rare in lyotropic liquid crystalline (LLC) systems. The 3D hexagonal and tetragonal mesophase can be observed in the $[Zn(H_2O)_6](NO_3)_2$:P65 and $[Zn(H_2O)_6](NO_3)_2$:P123 systems, respectively so it can be said that the salt:Pluronic systems are behaving more like in the mesostructured materials. Most likely, the function of metal aqua complexes in

the salt:Pluronic systems is similar to silica or other metal oxide species in the true liquid crystalline templating systems of metal oxides [30, 78,79]. Note also that the synthesis of mesostructured silica [78-80] or titania [81] in the LLC mesophase of a non-ionic surfactant produces an intermediate silicatropic or titaniatropic LC mesophase just before the phase becomes solid with the further polymerisation of silica or titania species, respectively. The salt:Pluronic systems could be categorised in the same group as silicatropic[78-80] or titaniatropic [81] LC mesophases.

3.2.3 FT-IR and micro-Raman Spectroscopy Results for the LC Mesophases of TMS:Pluronic Systems and Water Vaporization Process of the TMS:Pluronic Systems

The water evaporation process and thermal behavior of the LC H_2O:$[Zn(H_2O)_6](NO_3)_2$:Pluronic and $[Zn(H_2O)_6](NO_3)_2$:Pluronic systems have also been investigated using FTIR, micro-Raman spectroscopy and XRD methods, Figure 3.2.11, 3.2.12, 3.2.13 and 3.2.14, using the same samples for each measurements. It can be detected that the nitrate ion in the $[Zn(H_2O)_6](NO_3)_2$:Pluronic systems, coordinates to the metal cation through a ligand exchange mechanism [41]. By the evaporation of free water molecules in the LC media, the IR peaks due to the split asymmetric stretching modes of the coordinated nitrate ion at 1285 and 1490 cm^{-1} appear and dominate to the spectra, Figure 3.2.11. Note that the free nitrate ion has a doubly degenerate asymmetric stretching mode at around 1360 cm^{-1} and it splits into two non-degenerate modes upon coordination (symmetry of the free nitrate ion is lowered from D_{3h} to C_{2v} upon coordination)[49,70].

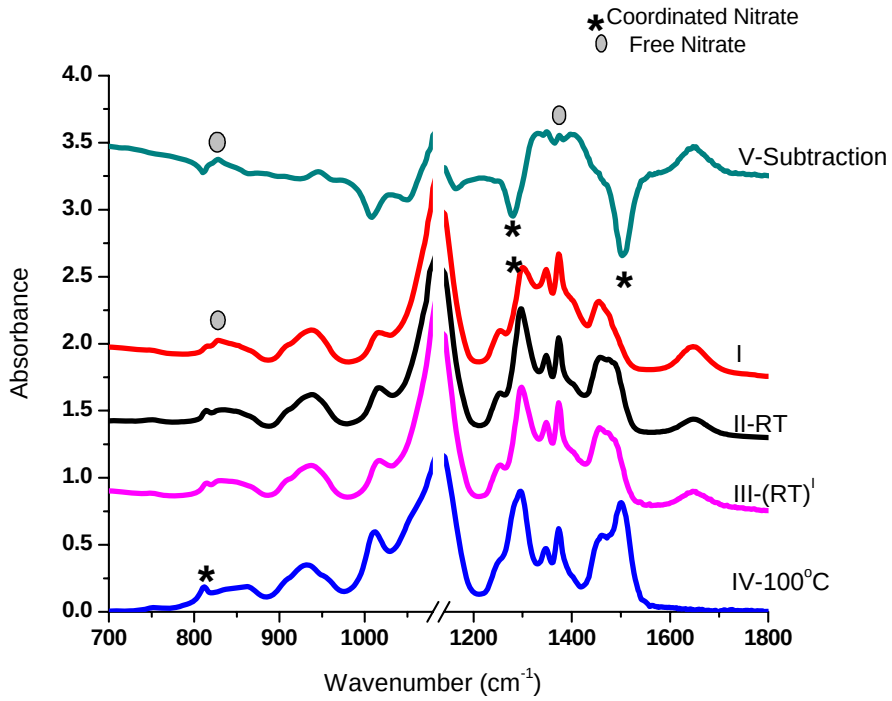

Figure 3.2.11. FTIR spectral changes with the evaporation of water from the $[Zn(H_2O)_6](NO_3)_2$:P123 system with 5.0 mole ratio (I) immediately after sample preparation,(II) after equilibrium at RT, (IV) heated at 100°C, (III) cooled to RT and (V) Subtraction of (IV) from (I).

The Zn-ONO_2 coordination could also be realized from the deformation modes at around 800-830 cm^{-1} and the inactive symmetric stretching mode (it becomes active upon coordination) observed at 1030 cm^{-1} of the coordinated nitrate ion [49, 70] (See also Figure 3.2.11).

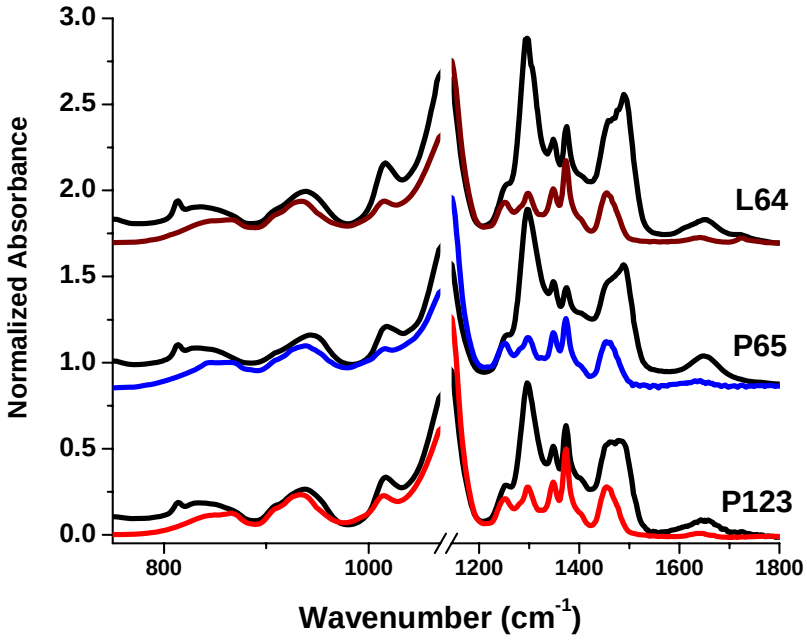

Figure 3.2.12. FTIR spectra of the $[Zn(H_2O)_6](NO_3)_2$:L64 and L64 (top), $[Zn(H_2O)_6](NO_3)_2$:P65 and P65 (middle) and $[Zn(H_2O)_6](NO_3)_2$:P123 and P123 (bottom) with the same salt/pluronic mole ratios (Zn(II)/PEO ratio was 6.15 in all samples).

For comparison purposes, Figure 3.2.12 shows the IR spectra of the pure L64, P65 and P123 with that of water free samples of $[Zn(H_2O)_6](NO_3)_2$:L64, $[Zn(H_2O)_6](NO_3)_2$:P65, and $[Zn(H_2O)_6](NO_3)_2$:P123. It is observed that major changes are taking place in the NO_3^- related peaks and some minor changes in the pluronics regions. This is a sign of the conformational changes for pluronics, as they are mixed with the TMS aqua complexes some interactions between the metal ions and the surfactant causes these conformational changes. The C-O stretching region of the pluronics shifts to lower energy in the salted systems indicating a hydrogen-bonding interaction between the ethoxy groups of the pluronics and coordinated water molecules of metal ion (M-O(H)H----$O(CH_2CH_2)_2$).

The coordination of NO_3^- to the metal cation can also be detected by Raman spectroscopy. The Raman active symmetric stretching mode at around 1056 cm^{-1} of the free nitrate ion shifts to 1030 cm^{-1} upon coordination, Figure 3.2.13. This peak is very sensitive to the water content of the media. If the water is completely removed from the mixture the peak at 1056 cm^{-1} almost disappears (Figure 3.2.11) which indicates that all

the nitrate ions in the media are coordinated to the metal ion. At equilibrium at room temperature, the nitrate ions are in coordinated ion ($M\text{-}O_2NO$ or $M\text{-}ONO_2$) and/or free ion (NO_3^-) states. To clarify the conformational changes on the pluronics and to understand the structural properties of the salt induced LC mesophases of this kind better further studies are required.

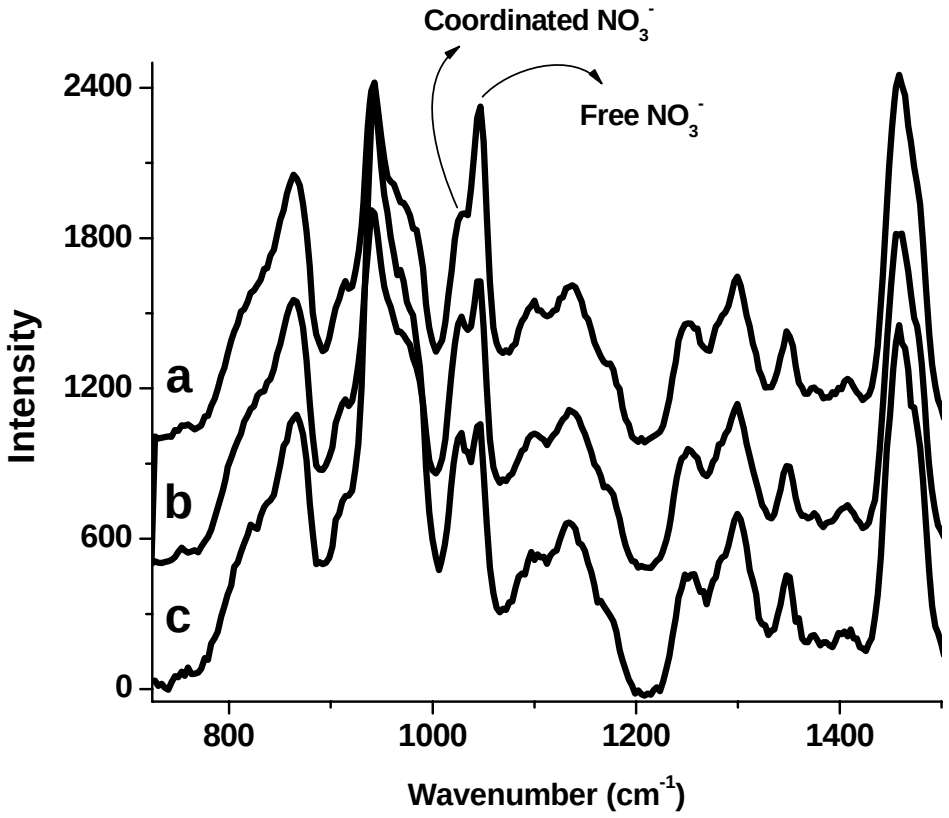

Figure 3.2.13. The micro-Raman spectra of $[Zn(H_2O)_6](NO_3)_2$:P123 with 6.15 salt to surfactant ratio before (a) and after (b) equilibrium at RT and heated (100°C) and cooled sample (c) in Figures 3.2.9 and 3.2.10.

We further investigated the $[Zn(H_2O)_6](NO_3)_2$:P65 and $[Zn(H_2O)_6](NO_3)_2$:P123 mesophases by first evaporating excess water at RT, then heating the samples between RT and 100°C using FTIR and micro-Raman spectroscopy and XRD techniques. During

the evaporation and heating processes the peaks, due to the coordinated nitrate ion at 1296 and 1496 cm^{-1} (splitting is 200cm^{-1} so it is bidentate coordination) in the IR spectra, gain intensity while the free nitrate ion signal at around 1370 cm^{-1} is losing its intensity, Figure 3.2.11. In the $[Zn(H_2O)_6](NO_3)_2$:Pluronics systems by heating, the equilibrium conditions between the free and coordinated nitrate ions change in favor of the coordinated nitrate ion in the media. However, cooling the sample restores the equilibrium. This can be observed from the spectrum which is comparable to the spectrum before heating (Figure 3.2.11 (II) and (III) look very similar to each other). Restoring of the equilibrium may take over a 1 hour to a 1 day period, it depends on the number of PPO units in the Pluronics, it is slow in P123(high number of PPO) and fast in P65(low number of PPO) systems. Heating definitely shifts the equilibrium reaction (eq.1.) in favor of coordination. The IR and Raman spectral changes suggest that complete water evaporation, due to the removal of coordinated water molecules, yields an intermediate complex in which two nitrate ions are coordinated to the metal ion. However, this complex is not stable and upon adsorption of ambient water, it decomposes into equilibrium species. After complete water evaporation the readsorption of water is almost immediate in the P65 and L64, but it takes several days in the case of P123.

$$\mathbf{[M(H_2O)_n]^{2+} + 2NO_3^- \rightleftharpoons [M(H_2O)_{n-2x}(O_2NO)_x] + (2x)H_2O + (2\text{-}x)NO_3^-} \quad \textbf{(eq. 1.)}$$

Evaporation and heating trends were also followed using the XRD method. The mixture of H_2O:$[Zn(H_2O)_6](NO_3)_2$:P123 with a 7.0 mole ratio is liquid before removal of certain amount of water (see first diffraction pattern, (a) in Figure 3.2.14).

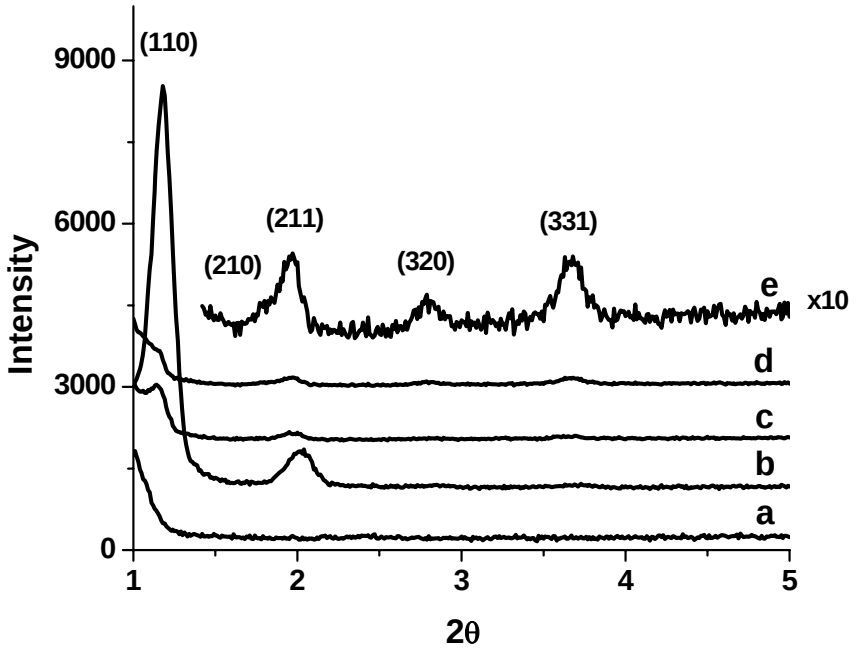

Figure 3.2.14. The XRD patterns of H_2O:$[Zn(H_2O)_6](NO_3)_2$:P123 with a 7.0 mole ratio, (a) before water evaporation (b) 1 hour after water evaporation at RT, (c) heated sample at around 100^oC (d) kept at RT for 1 hour after (e) x10 of (d).

The LC $Zn(H_2O)_6](NO_3)_2$:P123 mesophase gets oriented upon the removal of excess water. The XRD pattern displays two intense diffraction lines at 75 and 44 Å due to the (110) and (211) planes of the cubic phase. However, heating and cooling the samples chamges the orientation providing higher order diffraction lines. The heated and cooled samples display up to 5 diffraction lines at 75, 47.4, 43.7, 31.5 and 24.1 Å d-spacing, corresponding to the (110), (210), (211), (320) and (331) planes of cubic phase, respectively, Figure 3.2.14 . The structure of the mesophase is most likely same before and after the heating and cooling cycles.

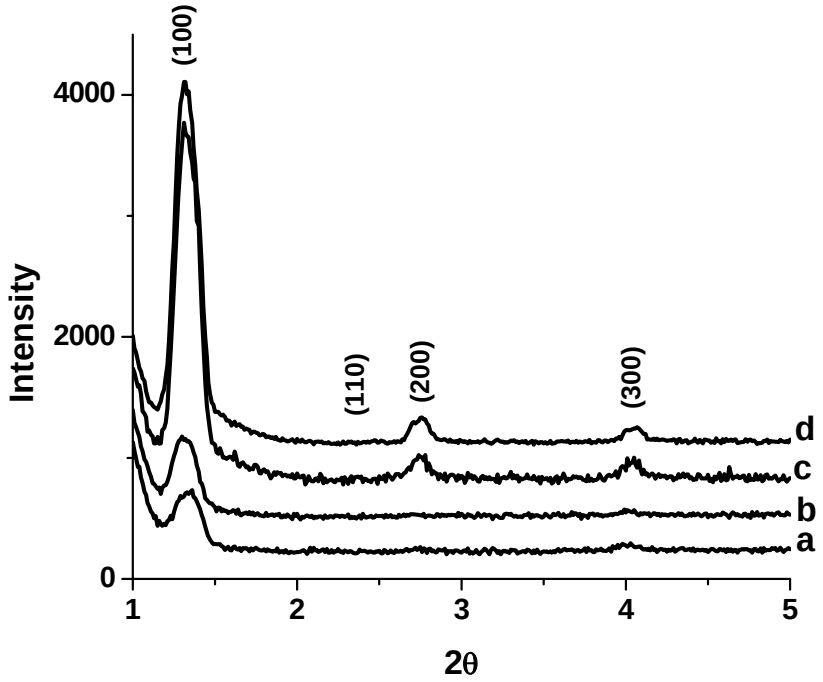

Figure 3.2.15. XRD pattern of 4.0 mole ratio H_2O:$[Zn(H_2O)_6](NO_3)_2$:P65 (a) immediately after phase appears upon water evaporation, (b) after 1 hour of water evaporation (c) heated (b) a few minutes for complete water evaporation on a hot plate and cooled to RT and (d) 1 hour cooling of (c).

The XRD pattern of the LC $[Zn(H_2O)_6](NO_3)_2$:P65 mesophase upon heating and cooling follows a different behavior. In the $[Zn(H_2O)_6](NO_3)_2$:P65 system, the heating and cooling upon evaporation of free water leads to a more oriented LC mesophase formation, Figure 3.2.15. Heating the $[Zn(H_2O)_6](NO_3)_2$:P65 mesophase with a mole ratio of 4.0 causes further orientation of the mesophase where the intensities of the diffraction lines increases by 5 folds. On the other hand, heating and cooling reduces the unit cell parameters upon contraction due to water evaporation, however it does not change the 3D hexagonal structure of the LC mesophase, Figure 3.2.15.

For the H_2O:$[Zn(H_2O)_6](NO_3)_2$:L64 mesophase the lines become ordered with the evaporation of some water but complete water evaporation makes the phase disordered. It is difficult to identify the structure of the LC $[Zn(H_2O)_6](NO_3)_2$:L64 mesophases. Further studies should be done to clarify the structural and thermal behavior of the TMS:L64 systems.

In all assembly processes discussed here, the coordinated water-ethoxy interaction plays a key role. The metal and nitrate ions are distributed in the hydrophilic domains of the LC media. The increase in the ion density (by increasing salt concentration or keeping the ions free in the media) of the media forces the mesophase to undergo phase changes to increase its hydrophilic free volume to accommodate the ions in the hydrophilic domains of the mesophase. The observed changes from 3D hexagonal to 2D hexagonal mesophase with decreasing water content in the P65, and the changes from tetragonal to cubic with increasing salt concentrations in the P123 are indirect measures for the above proposal. Note that we observe the similar effect of the ion density increase also in the TMS:surfactant:Silica systems.

The rigidity of the structure is related to the degree of the hydrophobic character and also the mass of the surfactant molecules. The P123 is the heaviest and most hydrophobic (PPO/PEO ratio is the largest) among the three pluronics with the richest structural diversity. This diversity is most likely driven by the balance between the hydrophilic and hydrophobic forces in the mesophases. The smallest number of EO groups that accommodate a metal ion is in the range of 2.5 to 3 in the P123 and 6.5 to 7 in the P65 and L64 systems. Note also that the number of EO units in both P65 and P123 and the PO units in the P65 and L64 are on average the same. Therefore, one could list the P123 as the least hydrophilic, then L64 and then P65. However, the solubility of $[Zn(H_2O)_6](NO_3)_2$ in P123 is the highest, therefore the salt ions, Zn(II) and nitrate in the media influence the hydrophilicity of the surfactant molecules. Since the nitrate ion is known as one of the hydrotropic anion in the Hofmeister's series, it enhances the hydrophilicity of the Pluronics in the systems with high salt concentrations.

3.2.4 $[Zn(H_2O)_6](NO_3)_2$:Pluronics:Silica and $[Zn(H_2O)_6](ClO_4)_2$:P123:Silica Systems

We used the rich structural chemistry of LC Pluronic mesophases as templates for the mesostructured silica synthesis. For the silica synthesis only P65 and P123 were used. Both pluronics were successful for the synthesis of mesostructured silica synthesis. The XRD patterns of the $[Zn(H_2O)_6](NO_3)_2$:P65:Silica systems clearly show the mesophase

up to 3 mole salt-to-P65 ratio. Over 5 mole ratio the phase vanishes and as the mole ratio decreases from 5 to 0 the intensity of the XRD lines increases which states that in salt:P65:silica systems salt addition decreases the order of the crystalline material and annihilates the mesophase over 5 mole ratio.

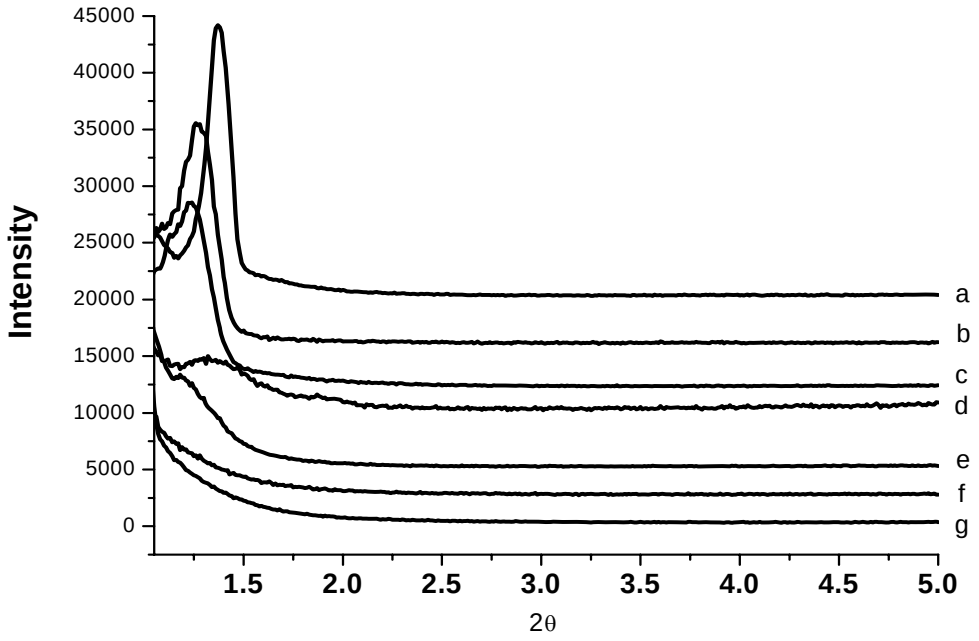

Figure 3.2.16. The XRD patterns of the $[Zn(H_2O)_6](NO_3)_2$:P65:Silica samples with a)0.0 1 hour after sample preparation and b)0.0 immediately after sample preparation, c)1.0, d) 3.0, e) 5.0, f) 7.0, g) 9.0 salt-to-P65 mole ratio.

The decrease in the intensity of the XRD line of the $[Zn(H_2O)_6](NO_3)_2$:P65:Silica samples as the salt concentration increase is mostly due to the ion density increase of the media and as a result the system loses its order.

The XRD pattern of the salt free sample and the sample with 1.0 mole ratio are similar with broad lines at 1.27 (69.4Å) with a shoulder at 1.22 (72.6Å) and at 1.23 (71.9Å) with a shoulder at 1.13 (77.9Å) respectively, Figure 3.2.16. Additionally the salt free samples also show a shift to higher 2θ angle as the excess water evaporates, Figure 3.2.16 (a) and (b). However, this information is not enough to assign the structure of the material. Note that the d-spacing values for the XRD lines are higher than the values

obtained from the oligo(ethylene oxide) type surfactant used silica mesophases which indicates that the unit cell parameters are increased with P65 usage.

The XRD patterns of the $[Zn(H_2O)_6](NO_3)_2$:P123:Silica samples display mesophases with higher numbers of XRD lines. Figure 3.2.17 shows the XRD pattern of the $[Zn(H_2O)_6](NO_3)_2$:P123:Silica system with 1.0 salt-to-P123 mole ratio. The XRD pattern gives lines assigned to (200), (300), (400) and (500) diffractions of lamellar structure.

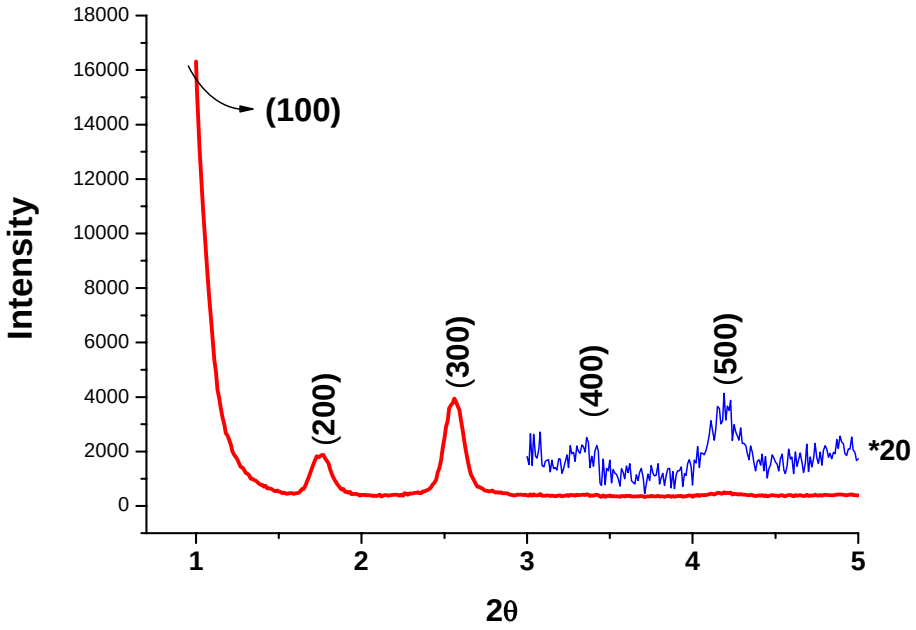

Figure 3.2.17. The XRD pattern of the $[Zn(H_2O)_6](NO_3)_2$:P123:Silica system with 1.0 salt-to-P123 mole ratio.

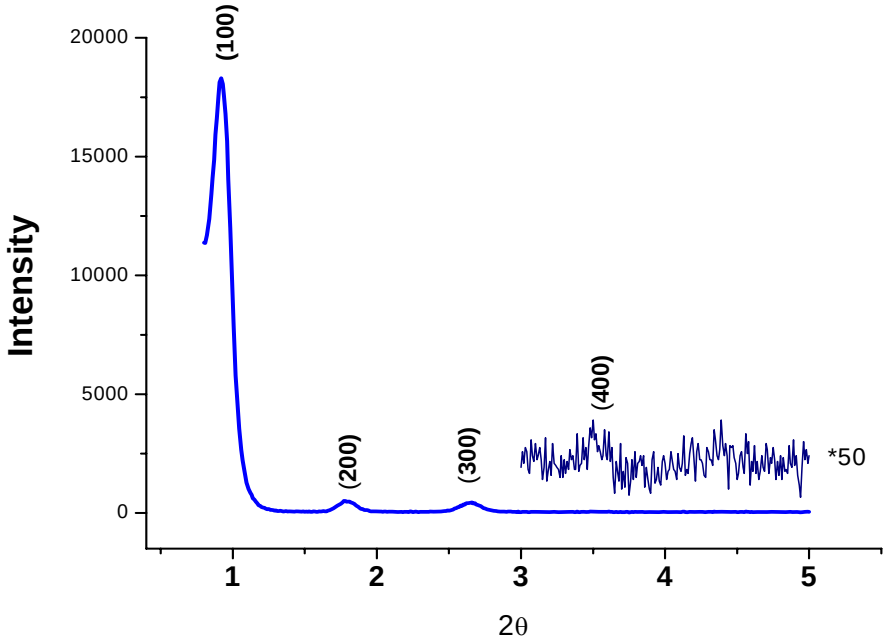

Figure 3.2.18. The XRD pattern of the $[Zn(H_2O)_6](NO_3)_2$:P123:Silica samples with 1.0 salt-to-P123 mole ratio. The pattern is taken after 5 days from the sample preparation.

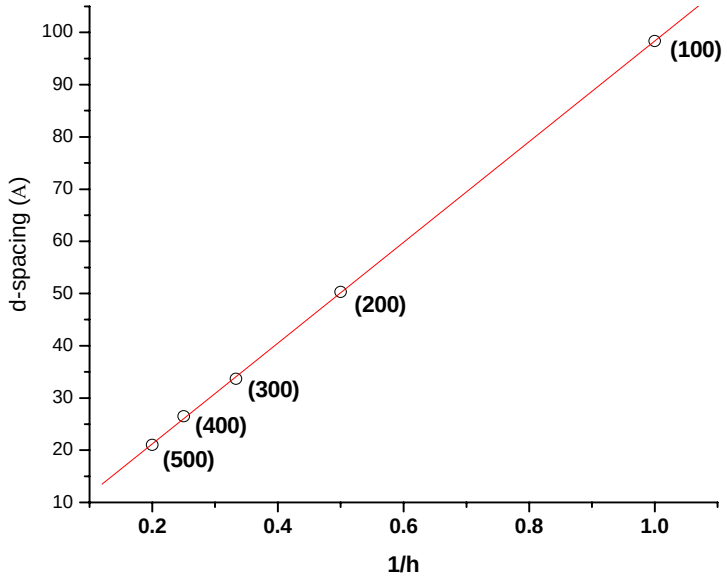

Figure 3.2.19. The plot of d-spacing of lines in Figure 3.2.17 versus 1/h. The slope of the plot gives the parameter **a** as 96.7 Å.

Figure 3.2.18 shows the XRD pattern of the $[Zn(H_2O)_6](NO_3)_2$:P123:Silica samples with 1.0 salt-to-P123 mole ratio. Note that the (100) plane of the lamella structure is observed at angles smaller than 1.0 and suits well with the assignment.

The d_{100} spacing was observed at 96.7 Å, Figure 3.2.19. This value is very large when compared with the d_{100} spacings of the oligo(ethylene oxide) templated silica systems (~50Å), so the molecular weight of the surfactant is increased the unit cell parameters also tend to increase.

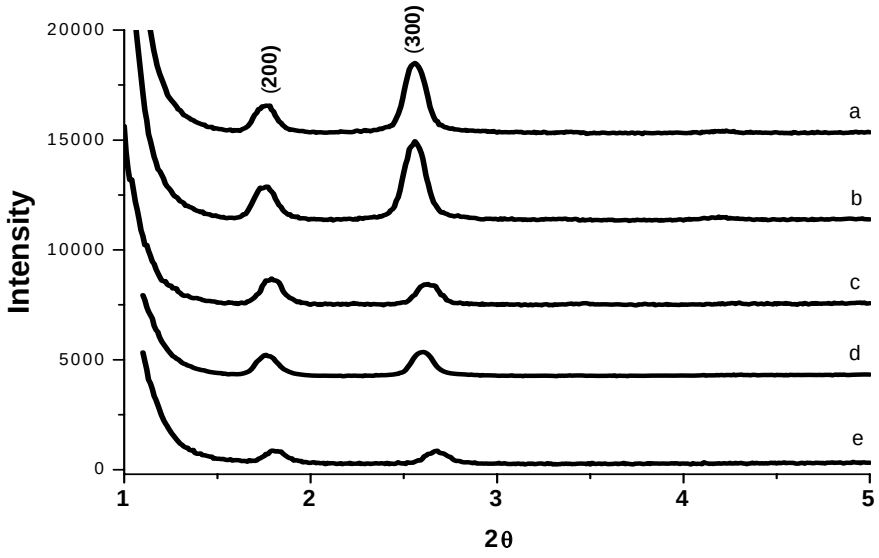

Figure 3.2.20. The XRD patterns of $[Zn(H_2O)_6](NO_3)_2$:P123:Silica samples with salt-to-P123 mole ratios a)0.0, b)1.0, c)5.0, d)7.0, e)9.0

The $[Zn(H_2O)_6](NO_3)_2$:P123:Silica system is stable up to a salt concentration of 9 salt-to-surfactant ratio. The XRD patterns of the samples up to 9 mole ratio display similar diffraction patterns, which mean that the system has lamellar structure up to 9 mole ratio, Figure 3.2.20. The XRD patterns in the 1-5 2θ angle range display the (200) and (300) planes, however they also display the (100) plane at around 0.9 (not shown). Note that a similar trend (decreasing of the intensity of the diffraction lines as a response to the salt concentration increase) observed in the TMS:P65:silica systems, is also observed from the $[Zn(H_2O)_6](NO_3)_2$:P123:Silica systems.

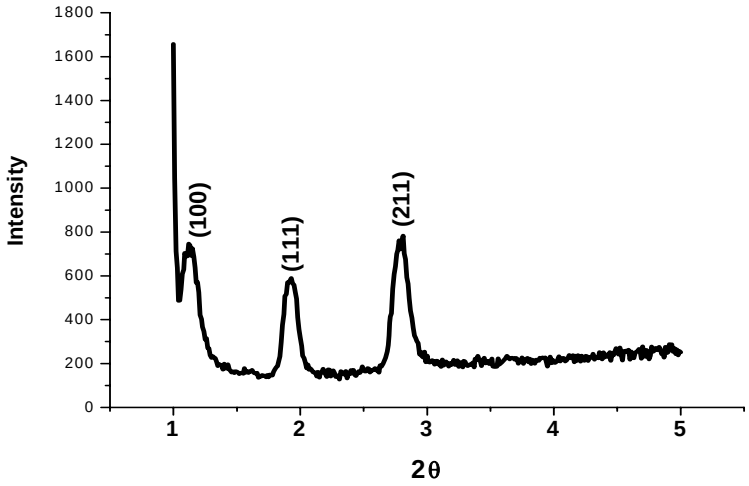

Figure 3.2.21. The XRD patern of $[Zn(H_2O)_6](ClO_4)_2$:P123:Silica system with 1 salt/P123 mole ratio.

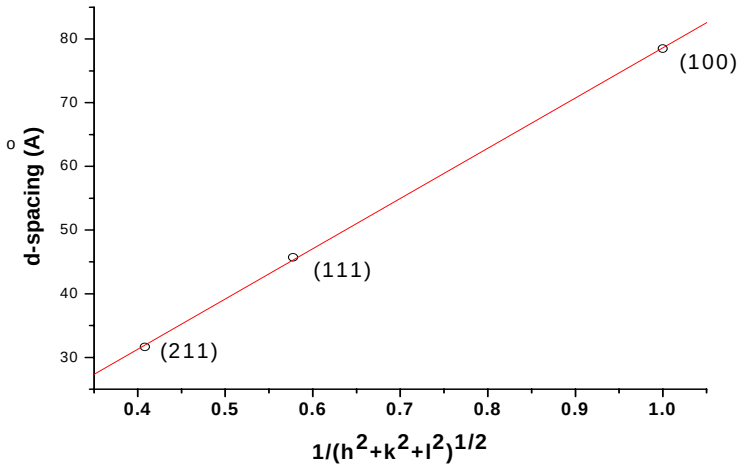

Figure 3.2.22. The plot of d-spacing versus the (hkl) relation for the cubic mesophase of $[Zn(H_2O)_6](ClO_4)_2$:P123:Silica system with 1 salt/P123 mole ratio.

If the perchlorate salt is used in the P123 systems, the structure of the mesophase changes from lamella structure. The structure of the $[Zn(H_2O)_6](ClO_4)_2$:P123:Silica system with 1 salt/P123 mole ratio is cubic. Figure 3.2.21 shows the XRD pattern of the sample with (100), (111), (211) lines at 78.6Å, 45.8Å and 31.5 Å, respectively. Figure 3.2.22 shows a linear plot of d-spacing versus the cubic (hkl) relation for the XRD pattern

in Figure 3.2.21. The plot gives the parameter **a** of the cubic mesophase as 78.9Å. Further studies should be done to understand the perchlorate salt effect better.

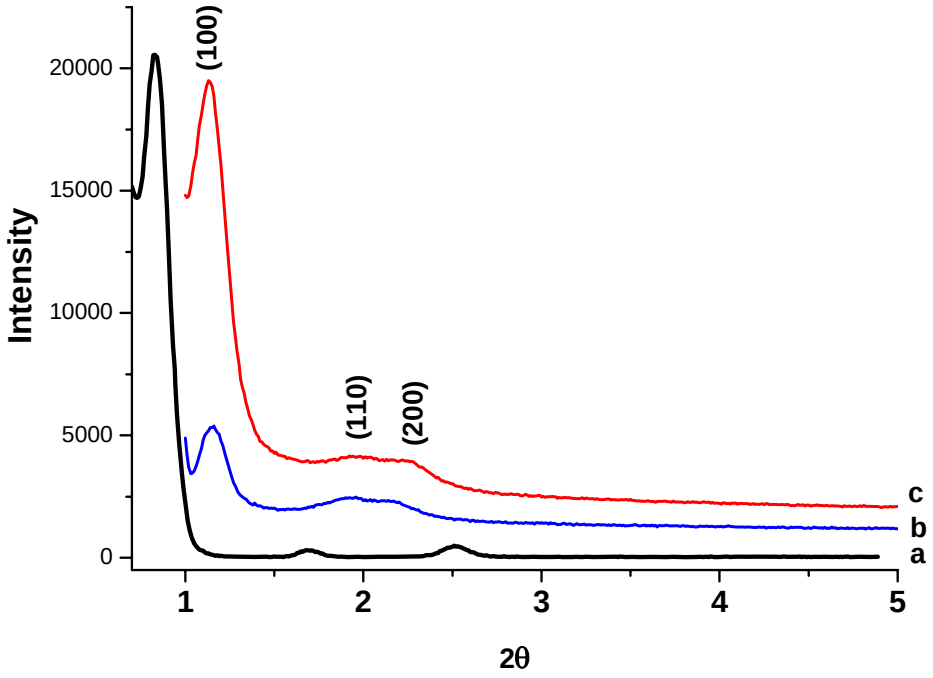

Figure 3.2.23. The XRD patterns of $[Zn(H_2O)_6](NO_3)_2$:P123:Silica with salt-to-P123 ratio 1 a) before calcination, b) calcined at 300˚C, c) calcined at 500˚C for 5 hours.

For the mesostructured silica synthesis the samples are usually calcined at high temperatures. In our work we also calcined the $[Zn(H_2O)_6](NO_3)_2$:P123:Silica sample up to 500˚C and we observed a phase change from lamellar to hexagonal upon calcination. Figure 3.2.21 displays the XRD pattern of $[Zn(H_2O)_6](NO_3)_2$:P123:Silica sample with 1 salt-to-P123 mole ratio before and after calcinations. The XRD pattern before calcination [Figure 3.2.23 (c)] has a lamellar structure with (100), (200), (300) planes at 100.6 Å, 50.3Å and 34.4Å, respectively. However after calcinations due to the phase change, 2D hexagonal mesophase is observed at 300˚C and 500˚C with (100), (110) and (200) planes, at 77.8, 46.1 and 39.4 Å, respectively, characteristic to 2D hexagonal structure in similar systems. Note that the intensity of the XRD line increases as the temperature of the calcinations increases, Figure 3.2.23. Note also that the calcination was done for 1 hour at 300˚C and after cooling it was heated 5 hours up to 500˚C and kept at 500˚C for 5 hours.

The intensity increase of the diffraction lines upon calcination at higher temperatures proves that the structure becomes more ordered upon further condensation of silanol groups, Si-OH.

4.CONCLUSION

The LC mesophase of some TMS:C_nEO_m systems have been used to produce mesostructured silica. The effects of $[Co(H_2O)_6](NO_3)_2$ and $[Co(H_2O)_6](ClO_4)_2$ salts to the LC mesophases and mesostructured silica were extensively studied in this thesis. The $[Co(H_2O)_6](NO_3)_2$:$C_{12}EO_{10}$:silica systems have hexagonal structure under 1.2 $[Co(H_2O)_6](NO_3)_2/C_{12}EO_{10}$ mole ratio whereas they have cubic mesophase above 1.2 mole ratio. The ions in the structure are mostly populated in the hydrophilic domains. In our case this mean that ions accumulate on the walls of the micelles and internal surface of the mesostructured silica. As the salt concentration increase, the coulomb interaction between the ions increases. These attractive and repulsive forces play an important role on the transformations of the structure of mesostructured silica materials. The $[Co(H_2O)_6](ClO_4)_2$: $C_{12}EO_{10}$:silica materials have cubic mesostructures at much lower salt concentrations (0.2 mole ratio) than the nitrate salt systems. This is due to the coordination of nitrate ion to the metal cation that reduces the ion density of the salt:surfactant:silica systems. The nitrate coordination is detected by both FT-IR and micro-Raman techniques.

However, if one increases the number of CH_2 group of the alkyl chain in the C_nEO_m type surfactants, a reverse effect is observed. For example, the $[Co(H_2O)_6](NO_3)_2$:$C_{18}EO_{10}$:silica systems have hexagonal mesophase up to a TMS/$C_{18}EO_{10}$ mole ratio of 2.0 which is much higher than the $C_{12}EO_{10}$ case (1.2). This observation suggests that there is an equilibrium between the hydrophilic and the hydrophobic content of the media. Increase in the hydrophilic content shifts the mesophase to the cubic structure whereas increase in the hydrophobic content shifts the equilibrium towards the hexagonal structure. The key point for the hexagonal to cubic mesophase change is the surface areas of the two structures. The surface area of the cubic structure is higher than the hexagonal structure which helps the coulomb interactions to decrease as the system shifts from hexagonal to cubic mesophase.

The LC mesophases of TMS:Pluronic (TMS= $[Zn(H_2O)_6](NO_3)_2$)) systems were also investigated in this work.The TMS(s) dissolves in the triblock Pluronic copolymers and produces LC mesophases. In this, the interaction of the coordinated water molecules and ethoxy groups of the PEO units ($M\text{-}OH_2\text{---}OCH_2CH_2\text{-}$), through hydrogen-bonding, and nitrate ion with the metal ion ($M\text{-}O_2NO$), through coordination, stabilize the LC mesophase into a different structure type. In the TMS:L64 system, the mesophase is quite disordered, however, the TMS:P65 and TMS:P123 systems are ordered and well structured. The H_2O:TMS:Pluronic systems are sensitive to the water content of the media and undergo structural changes by the evaporation of excess water in the media. The hexagonal mesophase in the $[Zn(H_2O)_6](NO_3)_2$:P65 systems and the tetragonal and cubic LC mesophases in the $[Zn(H_2O)_6](NO_3)_2$:P123 systems were identified. The $[Zn(H_2O)_6](NO_3)_2$:P123 mesophase is sensitive to the salt concentration, which can be increased up to a 15 mole ratio (it corresponds to ca. 42.6 w/w % and 2.67 EO/Zn(II)).

The LC mesophase obtained from salt:Pluronic system could be used as a reaction media to produce mesostructured materials. However, the mesostructured silica in the P123 system does not follow the structure of the LC mesophases. The structure obtained from the salt:P123:silica systems is usually lamella that transforms to 2D hexagonal mesoporous silica with calcinations under ambient conditions at 500^oC. Further studies are required to elucidate the origin of these transformations.

5.REFERENCES

[1] P. Behrens, “Mesoporous inorganic solids”, Adv. Mater., vol.5, pp.127-132, 1993.

[2] Y. Izumi, K. Urabe, M. Onaka, “Zeolite Clay and Heteropoly Acid in Organic Reactions”, Kodansha, 1992.

[3] M.T. Weller, “Inorganic Materials Chemistry”, Oxford Press, 1994.

[4] G.D. Stucky, J.E.M. Dougall, “Quantum Confinement and Host-Guest Chemistry: Probing a New Dimension”, Science, vol. 247, pp. 669-680, 1990.

[5] R. K. Iler, “The Chemistry of Silica”; J. Wiley & Sons, Inc.1979.

[6] K. Wefers, C. Misra, “Oxides and Hydroxides of Aluminum”; Alcoa Technical Paper No. 19, Revised, Alcoa Laboratories, 1987.

[7] T. J. Pinnavaia, Science, vol. 220, pp. 365-371, 1983.

[8] (a) D. E. W. Vaughan, R. J.Lussier, “In Proceedings of the 5th International Conference on Zeolites”, V. C. Rees, Ed., L. Hyden, pp. 94-100,1980.

(b) W. M. Meier, “In Studies in Surface Science & Catalysis”; vol. 28, p. 13, 1986.

[9] D. E. W. Vaughan, ACS Symp. Ser. 368, 308-325, 1988.

[10] M. E. Landis, B.A. Aufdembrink, P Chu, I. D. Johnson, G. W Kirker, K. M. Rubin, “Preparation of molecular sieves from dense layered metal oxides”, J. Am. Chem. Soc., vol. 113, pp.3189-3190,1991.

[11] R. M. Tindwa, D. K Ellis, G. Peng, A.Clearfield, J. Chem. Soc., Faraday Trans.1, vol. 81, pp. 545-548, 1985.

[12] C. Kresge, M. Leonowicz, W. Roth, C. Vartuli, J. Beck, " Ordered Mesoporous Molecular Sieves Synthesized by a Liquid Crystal Template Mechanism," Nature, vol. 359, pp. 710-712,1992

[13] P. B Moore, J Shen, Nature, vol.306, pp. 356-358, 1983.

[14] R. M. Dessau, J. L. Schlenker, J. B. Higgins, Zeolites, vol.10, pp.522-524, 1990.

[15] M. E. Davis, C. Saldarriaga, C. Montes, J. Garces, C. Crowder , "A molecular sieve with eighteen-membered rings", Nature, vol. 331, pp.698-699, 1988.

[16] M. Estermann, L.B. McCusker, C. Baerlochcr, A. Merrouche, H. Kessler, "A synthetic gallophosphate molecular sieve with a 20-tetrahedral-atom pore opening", Nature, vol.352, pp.320-323, 1991.

[17] A. Navrotsky, I. Petrovic, Y. Hu , C.Y. Chen, M.E. Davis, "Energetics of microporous materials" J. Non-Cryst. Solids, vol.192&193, pp. 474 – 477, 1995.

[18] J. Y. Ying, C.P. Mehnet, M.S. Wong, "Synthesis and Applications of Supramolecular-Templated Mesoporous Materials",Angew.Chem.Int.Ed.Engl., vol. 38, pp. 56-77, 1999.

[19] T. J. Barton, L.M. Bull, W.G. Klemperer, D.A. Loy, M. Misono, P.A. Monson, G. Pez, G.V. Cherer, J.C. Vartuli, O.M. Yaghi, "Tailored Porous Materials", Chem.Mater., vol. 11, pp. 2633-3656, 1999.

[20] J. S. Beck, J.C. Vartulli, W.J. Roth, M.E. Leonowicz, C.T. Kresge, K.D.Schmitt, D.H. Olson, F.W.Sheppard, S.B. McCullen, J.B. Higgins, J.L.Schlenker, "A New Family of Mesoporous Molecular Sieves Prepared with Liquid Crystal Templates", J.Am.Chem.Soc., vol. 114, pp. 10834-10843, 1992.

[21] J. C. Vartuli, C. T. Kresge, M. E. Leonowicz, A. S. Chu, S. B. McCullen, I. D. Johnson, E. W. Sheppard, "Synthesis of Mesoporous Materials: Liquid-Crystal Templating versus Intercalation of Layered Silicates" Chem. Mater., vol 6, pp. 2070 – 2077, 1994.

[22] Q. Huo, D. Margolese, U. Siesla, P. Feng, T.E. Gler, P. Sieger, R. Leon, P. Petroff, F. Schuth, G. Stucky, "Generalized Synthesis of Periodic Surfactant/Inorganic Composite Materials", Nature, vol. 368, pp. 317-321, 1994.

[23] Q. Huo, D. I. Margolese, U. Ciesla, D. G. Demuth, P. Feng, T. E. Gier, P. Sieger, A. Firouzi, B. F. Chmelka, F. Schüth, G. D. Stucky, "Organization of Organic Molecules with Inorganic Molecular Species into Nanocomposite Biphase Arrays" Chem. Mater. Vol. 6, pp.1176- 1191, 1994.

[24] J. C. Vartuli, K. D. Schmitt, C. T. Kresge,W. J. Roth, M. E. Leonowicz, S. B. McCullen, S. D. Hellring, J. S. Beck, J. L. Schlenker, D. H. Olsen, E. W. Sheppard, "Effect of Surfactant/Silica Molar Ratios on the Formation of Mesoporous Molecular Sieves: Inorganic Mimicry of Surfactant Liquid-Crystal Phases and Mechanistic Implications", Chem. Mater. Vol.6, pp.2317 -2326, 1994.

[25] J. C. Vartuli, C. T. Kresge,W. J. Roth, S. B. McCullen, J. S. Beck, K. D. Schmitt, M. E. Leonowicz, J. D. Lutner, E. W. Sheppard in Proceedings of the 209th ACS National Meeting, Division of Petroleum Chemistry 1995, pp. 21 -25.

[26] Q. Huo, D. I. Margolese, G. D. Stucky, "Surfactant Control of Phases in the Synthesis of Mesoporous Silica-Based Materials", Chem. Mater. Vol.8, pp.1147-1160, 1996.

[27] Q. Huo, D. Margolese, U. Siesla, P. Feng, T.E. Gler, P. Sieger, R. Leon, P. Petroff, F. Schuth, G. Stucky, "Generalized Synthesis of Periodic Surfactant/Inorganic Composite Materials", Nature, vol. 368, pp. 317-321, 1994.

[28] Q. Huo, R. Leon, P. M. Petroff, G. D. Stucky, "Mesostructure Design with Gemini Surfactants: Supercage Formation in a 3-D Hexagonal Array", Science, 268, 1324-1327,1995.

[29] D. Zhao, J. Feng, Q. Huo, B.F. Chmelka, G.D. Stucky, "Nonionic Triblock and Star Diblock Copolymer and Olygomeric Surfactant Synthesis of Highly Ordered Hydrothermally Stable, Mesoporous Silica Structures", J.Am.Chem.Soc., vol. 120, pp. 6024-6036, 1998.

[30] G. S. Attard, J.C. Glude, C.G. Göltner, "Liquid Crystalline Phases as Templates for the Synthesis of Mesoporous Silica", Nature, vol. 378, pp. 366-368, 1995.

[31] C. G. Göltner, S. Henke, M. C. Weissenberger, M. Antonietti, **"**Mesoporous Silica from Lyotropic Liquid Crystal Polymer Templates"**,** Angew. Chem. 1998, 110, 633 -636; Angew. Chem. Int. Ed., vol.37, pp.613- 616, 1998.

[32] M. Antonietti, S. Förster, J. Hartmann, S. Oestreich, "Novel Amphiphilic Block Copolymers by Polymer Reactions and Their Use for Solubilization of Metal Salts and Metal Colloids" Macromolecules, vol.29, pp.3800-3806, 1996.

[33] P. T. Tanev, M. Chibwe, T. J. Pinnavaia, "Titanium-containing mesoporous molecular sieves for catalytic oxidation of aromatic compounds", Nature, vol.368, pp.321-323, 1994.

[34] S. A. Bagshaw, E. Prouzet, T. J. Pinnavaia, "Templating of Mesoporous Molecular Sieves by Nonionic Polyethylene Oxide Surfactants". Science, vol.269, pp.1242-1245, 1995.

[35] J. Collings, Liquid Crystals, Princeton University Press, 1990.

[36] P. J. Collings, M. Hired, Introduction to Liquid Crystals, Taylor&Francis, 1997.

[37] D. Fennell Evans, Håkan Wennerström, The Colloidal Domain: Where Physics, Chemistry, and Biology Meet, Willey-VCH, 1999.

[38] D. Myers, Surfaces, Interfaces, and Colloids: Principles and Applications, VCH, 1991.

[39] N.K. Raman, M.T. Anderson, "Template-Based Approaches to the Preparation of Amorphous, Nanoporous Silicas", Chem.Mater., vol. 8, pp. 1682-1701, 1996.

[40] Ö. Çelik, Ö. Dağ, "A New Lyotropic Liquid Crystalline System: Oligo(ethylene oxide) Surfactants with $[M(H_2O)_n]X_m$ Transition Metal Complexes" Angew. Chem., Int. Ed., vol.40, pp.3800-3805, 2001.

[41] Ö. Dağ, S. Alayoğlu, I. Uysal, "Effects of Ions on the Liquid Crystalline Mesophase of Transition-Metal Salt:Surfactant (CnEOm)", J. Phys. Chem. B, vol.108, pp.8439-8446, 2004.

[42] P.V. Braun, P. Osenar, S.I. Stupp, "Semiconducting Superlattices Templated by molecular Assemblies", Nature, vol. 380, pp. 325-328, 1996.

[43] S. Eftekarzadech, S.I. Stupp, "Textured Materials Templated from Self-Assembling Media", Chem.Mater. vol. 9, pp. 2059-2065, 1997.

[44] V. Tohver, P.V. Braun, M.U. Pralle, S.I. Stupp, "Counterion Effects in Liquid Crystal Templating of Nanostructured CdS", Chem.Mater. vol. 7, pp. 1495-1498, 1997.

[45] P.V. Braun, P. Osenar, V. Tohver, S.B. Kennedy, S.I. Stupp, " Nanostructure Templating in Inorganic Solids with Organic Lytotropic Liquid Crystals" J.Am. Chem.Soc., vol. 121, pp. 7302-7309, 1999.

[46] H. Yang, R. Guo, H. Wang, "Lubricationof the Mixed system of Triton X-100/n-$C_{10}H_{21}OH$/ H_2O Lamellar Liquid Crystal and ZnS Nanoparticles", Colloids and Surfaces A, vol. 180, pp. 243-251, 2001.

[47] X. Jiang, "Simultaneous In Situ Formation of ZnS Nanowires in a Liquid Crystal Template by γ–Irradiation", Chem.Mater., vol. 13, pp. 1213- 1218, 2001.

[48] G. S. Attard, C. G. Goltner, J. M. Corker, S. Henke, R.H. Templer, "Liquid Crystal Templates for Nanostructured Metals", Angew.Chem.Int.Ed.Engl., vol. 36, pp. 1315-1317, 1997.

[49]- Ö. Dağ, O. Samarskaya, C. Tura, A. Günay, Ö. Çelik, "Spectroscopic Investigation of Nitrate-Metal and Metal-Surfactant Interactions in the Solid $AgNO_3/C_{12}EO_{10}$ and Liquid-Crystalline $[M(H_2O)_n](NO_3)_2/C_{12}EO_{10}$ Systems" Langmuir, vol.19, pp.3671-3676, 2003.

[50] E. Leontidis, "Hofmeister anion effects on surfactant self-assembly and the formation of mesoporous solids", Current Opinion in Colloid & Interface Science, vol.7, pp.81-91,2002.

[51] G. S. Attard, S. Fuller, G.J.T. Tiddy, "Influence of Added Electrolytes on the Lyotropic Phase Behaviour of Triethylammoniodecyloxycyanobiphenyl Bromide(OCB-$C_{10}NEt_3Br$)," J.Phys.Chem.B, vol. 104, pp. 10426-10436, 2000.

[52] H. Schott, “Effect of Inorganic Additives on Solutions of Nonionic Surfactants.XIV.Effect of Chaotropic Anions on the Cloud Point of Octoxynol 9 (Triton x-100),” J.Coll.Interf.Sci., vol. 189, pp. 117-122,1997.

[53] L. Zhang, P. Somasundaran, C. Maltesh, “Electrolyte Effects on the Surface Tension and Micellization of n-Dodecyl β-D-Maltoside Solutions,” Langmuir, vol. 12, pp. 2371-2373, 1996.

[54] L. D. Charlton, A.P. Doherty, “Electrolyte-Induced Structural Evolution of Triton X-100 Micelles,” J.Phys.Chem.B, vol. 104, pp. 8327-8332, 2000.

[55] C. Washington, “Effect of Electrolytes and Temperatureon the Structures of a Poly(ethylene oxide)-Poly(propylene oxide)-Poly(ethylene oxide) Block Copolymer Adsorbed to a Perfluorocarbon Emulsion,” Langmuir, vol. 13, pp. 4545-4550, 1997.

[56] G. Mao, S. Sukumaran, G. Beaucage, M.L. Saboungi, P.Thiyagarajan, “PEO-PPO-PEO Block Copolymer Micelles in Aqueous Electrolyte Solutions: Effect of Carbonate Anions and Temperature on the Micellar Structure and Interaction,” Macromolecules, vol. 34, pp. 552-558, 2001.

[57] F. Hofmeister, Arch. Exp. Pathol. Pharmakol., vol. 24, p 247, 1888.

[58] M. Kahlweit, E. Lessner, R. Strey, “Phase Behaviour of Quaternary Systems of the Type H_2O-Oil-Nonionic Surfactant-Inorganic Electrolyte”, J.Phys.Chem., vol. 88, pp. 1937-1944, 1984.

[59] H. J. Schneider, A.K. Yatsimirsky, Principles and Methods inSupramolecular Chemistry, John Wiley & Sons: Chichester, 2000.

[60] A.B.P. Lever, Inorganic Electronic Spectroscopy, 2nd ed.;Elsevier: New York, 1984; pp 479-490.

[61] Ö. Dağ, S. Alayoğlu, C. Tura, Ö. Çelik, **“**Lyotropic Liquid-Crystalline Phase of Oligo(ethylene oxide) Surfactant/Transition Metal Salt and the Synthesis of Mesostructured Cadmium Sulfide”, Chem. Mater.,vol.15,pp.2711-2716, 2003.

[62] C.Y. Chen, H.X. Li, M.E. Davis, “Studies on mesoporous materials: Synthesis and characterization of MCM-41”, Microporous Mater., vol.2, pp.17, 1993.

[63] J.M. Kim, R. Ryoo, "Disintegration of Mesoporous Structures of MCM-41 and MCM-48 in Water" Bull. Korean Chem. Soc., vol.17, p.66, 1996.

[64] J.M. Kim, J.H. Kwak, S. Jun, R. Ryoo, "Ion Exchange and Thermal Stability of MCM-41", R. J. Phys. Chem., vol.99, p.16742, 1995.

[65] R. Ryoo, S. Jun, "Improvement of Hydrothermal Stability of MCM-41 Using Salt Effects during the Crystallization Process", J. Phys. Chem. B, vol.101, pp.317-320, 1997.

[66] C. Yu, B. Tian, J. Fan, G. D. Stucky, and Dongyuan Zhao, "Nonionic Block Copolymer Synthesis of Large-Pore Cubic Mesoporous Crystals by Use of Inorganic Salts", J. Am. Chem. Soc.,vol.124, pp.4556-4557, 2002.

[67] G. Oyea, J. Sjoblom, M. Stocke, "Synthesis, characterization and potential applications of new materials in the mesoporous range", Advances in Colloid and Interface Science, vol.89-90, pp.439-466, 2001.

[68] O. Samarskaya, Silver Nitrate Oligo(Ethylene Oxide) Surfactant Mesoporous Nanocomposite Films and Monoliths, September 2000.

[69] P. Sakya, J. M. Seddon, R. H. Templer, R. J. Mirkin, and G. J. T. Tiddy, "Micellar Cubic Phases and Their Structural Relationships: The Nonionic Surfactant System $C_{12}EO_{12}$/Water", Langmuir, vol.13, pp.3706-3714, 1997.

[70] K. Nakamoto, "Infrared and Raman Spectra of Inorganic andCoordination Compounds", parts A and B, 5th ed.; John Wiley & Sons: New York, 1997.

[71]P. Alexandridis, U. Olsson, B. Lindman, "Self-Assembly of Amphiphilic Block Copolymers: The $(EO)_{13}(PO)_{30}(EO)_{13}$-Water-p-Xylene System" Macromolecules, vol.28, p.7700, 1995.

[72] P. Alexandridis, D. Zhou, A. Khan, "Lyotropic Liquid Crystallinity in Amphiphilic Block Copolymers: Temperature Effects on Phase Behavior and Structure for Poly(ethylene oxide)-*b*-poly(propylene oxide)-*b*-poly(ethylene oxide) Copolymers of Different Composition", Langmuir, vol.12, p.2690, 1996.

[73] P.Alexandridis, U. Olsson, B. Lindman, "A Record Nine Different Phases (Four Cubic, Two Hexagonal, and One Lamellar Lyotropic Liquid Crystalline and Two Micellar Solutions) in a Ternary Isothermal System of an Amphiphilic Block Copolymer and Selective Solvents (Water and Oil)", Langmuir vol. 14, p.2627, 1998.

[74] G. Schmidt, W.Richtering, P. Lindner, P. Alexandridis, "Shear Orientation of a Hexagonal Lyotropic Triblock Copolymer Phase As Probed by Flow Birefringence and Small-Angle Light and Neutron Scattering**",** Macromolecules, vol.31, p.2293, 1998,

[75] P. Holmqvist, P. Alexandridis, B. Lindman, "Modification of the Microstructure in Block Copolymer-Water-"Oil" Systems by Varying the Copolymer Composition and the "Oil" Type: Small-Angle X-ray Scattering and Deuterium-NMR Investigation" J. Phys. Chem. B,vol.102, p.1149, 1998.

[76] R. Ivanova, B. Lindman, P. Alexandridis, "Effect of Glycols on the Self-Assembly of Amphiphilic Block Copolymers in Water.1. Phase Diagrams and Structure Identification", Langmuir, vol.16, p.3660, 2000.

[77] J. Zipfel, J. Berghausen, G. Schmidt, P. Lindner, P. Alexandridis, W. Richtering, "Influence of Shear on Solvated Amphiphilic Block Copolymers with Lamellar Morphology" Macromolecules, vol.35, p.4064, 2002.

[78] Ö. Dağ, A. Verma, G.A. Ozin, C.T. Kresge, "Salted Mesostructures: Salt-Liquid Crystal Templating of Lithium Triflate-Oligo(ethylene oxide)surfactant-Mesoporous Silica Nanocomposite Films and Monoliths", J.Materials Chemistry, vol. 9, pp. 1475-1482, 1999.

[79] **O.** Samarskaya, Ö. Dag, "Silver Nitrate/Oligo(Ethylene Oxide) Surfactant/Mesoporous Silica Nanocomposite Films and Monoliths", J.Coll.Interf.Sci., vol. 238, pp. 203-207**,**2001.

[80] Ö. Dağ., O. Samarskaya, N. Coombs, G.A. Ozin, "The synthesis of mesostructured silica films and monoliths functionalised by noble metal nanoparticles"**,** J. Mater. Chem., vol.13, p.328, 2003.

[81] E.L. Crepaldi, D. Grosso, G. J. D. A. Soler-Illia, P.A. Albouny, H. Amenitsch, C. Sanchez, "Formation and Stabilization of Mesostructured Vanadium-Oxo-Based Hybrid Thin Films", Chem. Mater., vol.14, p.3316, 2002.